PHENYLETHYNYLARENE BASED DONOR-ACCEPTOR SYSTEMS: DESIGN, SYNTHESIS AND PHOTOPHYSICAL STUDIES

THESIS SUBMITTED TO
COCHIN UNIVERSITY OF SCIENCE AND TECHNOLOGY
FOR THE DEGREE OF
DOCTOR OF PHILOSOPHY
IN CHEMISTRY
UNDER THE FACULTY OF SCIENCE

By

SUNEESH C. V.

UNDER THE SUPERVISION OF

Dr. K. R. GOPIDAS

PHOTOSCIENCES AND PHOTONICS
CHEMICAL SCIENCES AND TECHNOLOGY DIVISION
NATIONAL INSTITUTE FOR INTERDISCIPLINARY SCIENCE AND TECHNOLOGY
COUNCIL OF SCIENTIFIC AND INDUSTRIAL RESEARCH
TRIVANDRUM 695019
KERALA, INDIA

MAY 2010

STATEMENT

I hereby declare that the matter embodied in the thesis entitled, "**Phenylethynylarene Based Donor-Acceptor Systems: Design, Synthesis and Photophysical Studies**" are results of investigations carried out by me at the Photosciences and Photonics Section, Chemical Sciences and Technology Division of the National Institute for Interdisciplinary Science and Technology, Council of Scientific and Industrial Research, Trivandrum, under the supervision of Dr. K. R. Gopidas and the same has not been submitted elsewhere for a degree.

In keeping with the general practice of reporting scientific observations, due acknowledgement has been made wherever the work described is based on the findings of other investigators.

Suneesh C. V.

i

May 3, 2010

CERTIFICATE

This is to certify that the work embodied in the thesis entitled, **"Phenylethynylarene Based Donor-Acceptor Systems: Design, Synthesis and Photophysical Studies"** has been carried out by Mr. Suneesh C. V., under my supervision and the same has not been submitted elsewhere for a degree.

K. R. Gopidas
(Thesis Supervisor)

ii

ACKNOWLEDGEMENTS

Suneesh C. V.

CONTENTS

PREFACE

Photoinduced Electron Transfer (PET) is a thoroughly investigated process in natural as well as artificial systems. PET plays a central role in photo biological processes such as photosynthesis and in various light driven physical and chemical processes. In natural photosynthetic reaction centre, sequential multi step electron transfer takes place from the excited chromophore to the terminal electron acceptor through electron mediators, which are well assembled in a protein matrix to attain a long-lived charge separated (CS) state. The energy stored in the CS state is utilized for the reduction of CO_2 to glucose and in this process water is oxidized to molecular oxygen. Therefore the formation of a long lived CS state is an essential requirement for developing artificial photosynthetic systems and optoelectronic devices based on PET. The work reported in this thesis deals with generation of long-lived CS states in simple molecular systems.

The thesis consists of four chapters. Chapter 1 is a review of the literature about artificial photosynthetic systems. A number of linked electron donor-acceptor (D-A) molecular systems have been developed in the past to mimic the multi-step electron transfer processes in natural photosynthesis. In these multi-component D-A molecules light absorption initiates a series of electron transfer steps leading to the formation of a long-lived CS state. However a lot of time consuming synthetic steps are needed to produce these multi component arrays. In

addition, a significant amount of energy is lost during the multi step electron transfer processes. Hence the design of simple molecular systems that can sustain a long-lived CS state is extremely important. Recently Fukuzumi and coworkers have claimed long-lived charge separation in a few simple molecular dyads. ΔG^0 for back electron transfer (BET) in these systems fall deep in the inverted region and the authors attribute the long CS state lifetimes observed to inverted region effects. In this chapter we also review the controversy related to Fukuzumi's claim. In this section we also outline a new strategy for the generation of long-lived CS states in molecular dyads. Our strategy involved the use of a sensitizer that has very high singlet quantum yield and negligible inter system crossing efficiency. The quenchers are selected in such a way that their singlet and triplet levels are above the singlet level of the sensitizer and the ΔG_{BET} falls in the deep inverted region. Our hypothesis is that because of the poor ISC rate and large $-\Delta G_{BET}$, BET rates will be very low in such systems. In subsequent chapters this hypothesis is examined using selected molecules.

Chapter 2 of the thesis deals with the synthesis and study of PET processes in dyad systems where bis(phenylethynyl)anthracene (**BPEA**) act as the light absorber. We synthesized two systems (**BPEA-PT and BPEA-PT$_2$**) were BPEA acts as acceptor and one or two phenothiazine (PT) units serve as donors. Absorption spectra of the dyads show that there is no interaction between the D-A constituents in the ground state. Fluorescence of BPEA core was efficiently

quenched by the donor moieties, indicating that efficient electron transfer takes place from the **PT** to **BPEA**. Femtosecond transient absorption studies suggested the formation of a charge separated state directly from the singlet excited state of **BPEA**. Nanosecond flash photolysis experiments gave long-lived transient absorptions assignable to phenothiazine radical cation (**PT$^{\bullet+}$**) and bis(phenylethynyl)anthracene radical anion (**BPEA$^{\bullet-}$**). These assignments were confirmed by oxygen quenching studies and secondary electron transfer experiments. Electron transfer in these systems is analyzed in the light of Marcus theory and the slow back electron transfer exhibited is attributed to inverted region effects.

In the third chapter we have investigated the PET processes taking place in two molecular triads both of which had **BPEA** as sensitizer and **PT** as donor. A nitrotoluene moiety was the acceptor in one of the system and a pyromellitimide species was the acceptor in the other. Steady state and time resolved fluorescence spectroscopy showed facile PET taking place in these systems. The radical ions formed in these systems were characterized by picosecond and nanosecond laser flash photolysis. These studies also showed the existence of a long-lived charge separated state in these systems.

In the fourth chapter, PET processes in a closely related dyad system was examined. The dyad possessed 1,6-bis(phenylethynyl)pyrene (**BPEP**) as the sensitizer and **PT** as the donor. Absorption spectra of the dyad showed that there

is no interaction between the constituents in the ground state. PET process in this dyad was investigated using steady state and time-resolved fluorescence techniques. Picosecond and nanosecond laser flash photolysis experiments proved the existence of a long-lived CS state in this case also. These results suggested that the strategy we proposed works well in the systems studied.

....

Note: The Number of the various compounds given in each chapter corresponds to those given under the respective chapters.

Chapter 1

Long-lived Photoinduced Charge Separation in Molecular Systems: An Overview

1.1. Introduction

Energy is one of the most important issues of the twenty-first century. At present the energy needed is supplied mainly by the use of fossil fuels. Estimates indicate that the energy consumption will increase at least two-fold, from our current burn rate of 12.8 TW to 28-35 TW by the year 2050. World reserves of fossil fuels are progressively decreasing[1] and the projected requirements would not be met by fossil fuel sources alone. In addition, continued use of fossil fuels leads to global warming and pollution problems that threatens human health and creates environmental issues. Therefore use of renewable and clean energy resources is definitely required in order to solve the global energy and environmental issues. Solar energy is one of the most important alternate energy sources that can be exploited to meet our future energy demands. Solar energy can be converted into useful energy forms such as heat, electricity or fuels. However, technologies leading to efficient use of solar energy have not yet been fully developed.

Solar energy can be harvested by direct or indirect pathways. Indirect

pathways include processes such as conversion of biomass to biogas or production

of hydrogen by electrolysis of water using electricity from photovoltaics. Direct

pathways include photovoltaics and production of fuels such as hydrogen using

integrated systems. Artificial photosynthesis is an example of direct sunlight

utilization. The basis of artificial photosynthesis is not to copy the photosynthetic

process in the laboratory but to learn from the natural photosynthetic process and

use some of its essential principles to design systems capable of producing energy

or fuels.

Light excitation can induce a variety of chemical reactions. For energy-

conversion purposes, photoinduced electron transfer (PET) is by far the preferred

reaction in nature. It is a thoroughly investigated process in natural and artificial

systems.[2] PET involves the transfer of an electron from a donor molecule (D) to an

acceptor molecule (A) without making or breaking any chemical bonds. Prior to

electron transfer one of the components is excited with light.[3] Understanding the

process of PET helps scientists to design potential systems for artificial

photosynthesis, which ultimately aims in mimicking green plants and other

photosynthetic organisms that are using sunlight to make high-energy chemicals.[4]

PET results in the formation of product ions (donor radical cation $D^{\bullet+}$ and acceptor

radical anion $A^{\bullet-}$) which are at higher energy levels compared to the starting D and

A molecules. The term 'conversion of solar energy into chemical energy' actually

means the generation of a high-energy charge separated (CS) state by way of light

absorption. The CS state generated in PET reactions is generally short-lived and

undergo 'back electron transfer' (BET) to generate the D-A system in their ground

state, thereby leading to wastage of the absorbed energy as shown in Scheme 1.1.
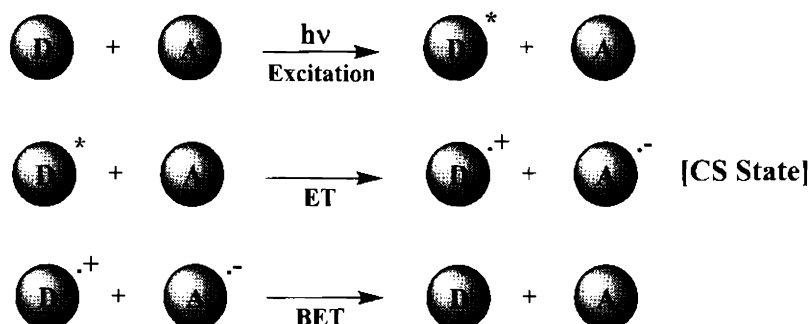
Scheme 1.1. Schematic of PET and BET in intermolecular D-A systems

The D and A units can also be linked by covalent bonds or non-covalent

interactions, as shown in Scheme 1.2. Upon excitation, intramolecular electron

transfer takes place from D to A leading to the formation of a CS state. Possibility

of fast energy wasting BET exists in these cases also.
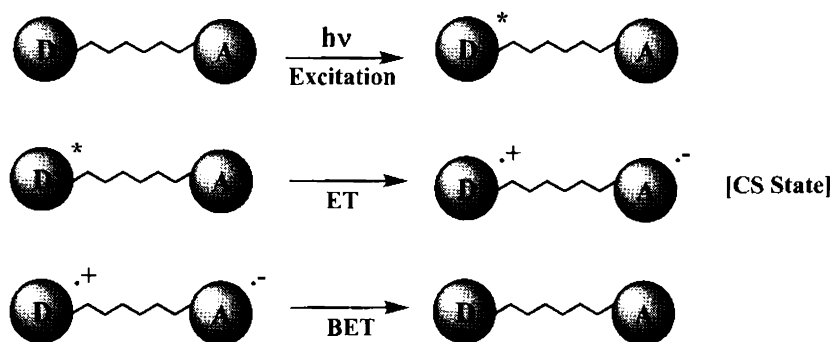
Scheme 1.2. Schematic of PET and BET in covalently linked D-A systems

In Schemes 1.1 and 1.2, BET represents the energy wasting back electron transfer reaction. In simple donor-acceptor systems, $D^{\bullet+}$ and $A^{\bullet-}$ are formed at close proximity which facilitates the BET reaction. BET reaction reduces the yield and lifetime of the CS state. This energy wasting step is a serious limitation of PET reactions in simple D-A systems. A large number of D-A systems have been studied in order to elucidate the charge separation and recombination mechanisms and also to assess the efficiency and practical applicability of such molecular systems. These studies have led to important advances in the theory and practice of electron-transfer reactions.[4] Studies on the photophysical and photochemical processes involved in the natural photosynthetic reaction center also have guided the efforts in this direction.

The photosynthetic apparatus in both bacteria and plants consists of two distinct units called antennae and the reaction centre. Antennae are the light gathering complexes consisting of chlorophyllous pigments as well as carotenoids arranged in the protein matrix. These pigment-protein complexes absorb light and efficiently transfer the excitation to the reaction centre. The reaction centre consists mainly of organic donor and acceptor molecules embedded within a protein matrix. The photosynthetic reaction centre of purple bacteria *Rhodospeudomonas virdis* comprises of four bacteriochlorophylls (**BCl**), two bacteriopheophytins (**BPh**), two quinones, namely ubiquinone and menaquinone, and a non-heme iron atom.[5] The spatial arrangement of these components within

the reaction centre is shown in Figure 1.1. It may be noted that with the exception

of the iron atom, the constituents occur in pairs and the reaction centre has

approximate C_2 symmetry. The right side of the C_2-axis is known as the **L** side and

the left side is termed **M** side. Of the four **BCl** molecules, two are positioned very

close. Hence they are strongly coupled electronically and are termed "special pair"

of **BCls**.

The photosynthetic process within the reaction centre begins with the

excitation of the special pair **BCls** by excitation transfer from the antennae units.

The singlet excited state of the special pair transfers an electron to the **BPh** on the

L side of the branch within 3 ps leading to the formation of special pair radical

cation and **BPh** radical anion.[6] It is believed that **BCl** monomer on the **L** side plays

a role in this electron transfer reaction. The **M** branch of the reaction centre is

almost inactive in the electron transfer process. The **BPh** radical anion decays in

200 ps moving the electron to the menaquinone from where it is further transported

to the ubiquinone in about 100 μs. The positive charge remaining on the special

pair is quenched by electron transfer from an iron porphyrin on the outer side of

the membrane. The net result of this multistep electron transfer is the generation of

a trans-membrane CS state with a quantum yield of near unity. Since the positive

and negative charges are separated by the thickness of the lipid bilayer, BET,

which leads to the wastage of stored energy, is precluded.
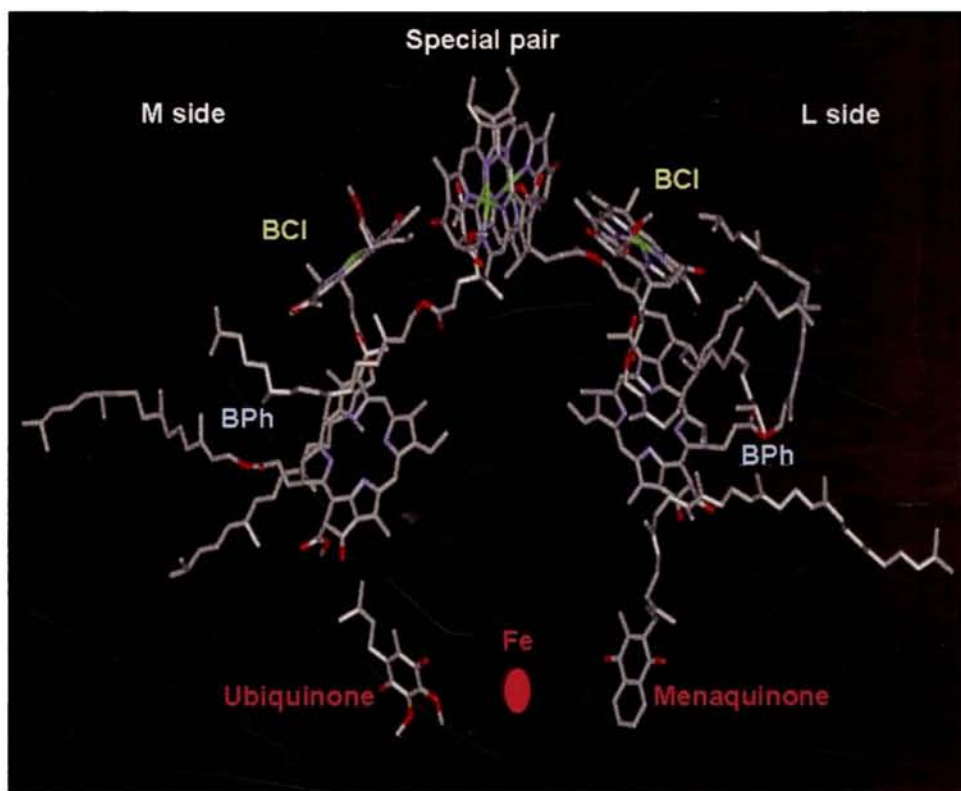
Figure 1.1. Arrangement of the chromophores, electron donors and electron acceptors in the bacterial reaction centre of *Rhodospeudomonas virdis*

The importance and complexity of electron-transfer reactions in nature has led many researchers to look for ways to duplicate the fundamental features of these reactions in simplified chemical systems. Extremely high quantum yield of the PET processes in the natural systems is attributed to the high degree of organization of the donors and acceptors in the reaction centre. It was believed that some degree of organization could be achieved by covalently linking the donor and acceptor molecules. Considerable effort has been devoted to mimick the natural photosynthetic process in the laboratory by constructing covalently connected D-A systems and investigating the photoinduced processes in those systems. As is the

case in photosynthetic reaction center, multi-component donor-acceptor arrays that carry out multistep charge separation reactions are found to be very useful for producing long-lived CS states in artificial systems.

1.2. Photoinduced electron transfer in multi-component donor - acceptor systems

It was proposed that efficient and effective charge separation might be achieved by attaching several acceptors to a light-absorbing donor in such a way as to prevent rapid electron return. Suppose three different acceptors A_1, A_2 and A_3 (acceptor strength is in the order $A_1 < A_2 < A_3$) are attached to the donor D, we would have the sequence of reactions shown in Scheme 1.3, following light absorption by D. Electron transfer is initially favored between D* and A_1 since these groups are closest. Electron transfer then occurs from A_1 to A_2 and then from A_2 to A_3. This process is termed sequential electron transfer. As the charge-separation distance between the ions increases, electron return becomes increasingly difficult, resulting ultimately in long-lived charge separation. A large number of donor-acceptor systems were designed in the past and the electron transfer processes taking place in these systems were studied in detail. Some of these systems are described below.
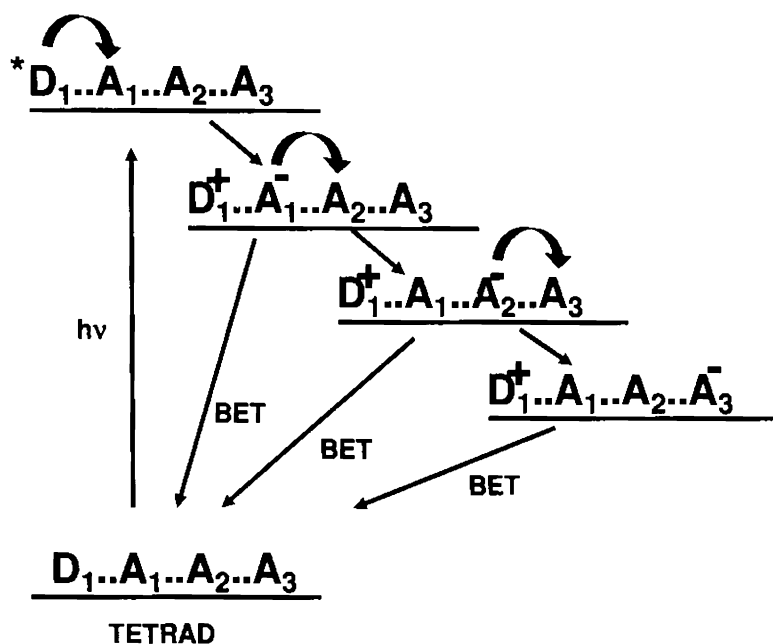
Scheme 1.3. Schematic representation of PET processes in multicomponent D-A array

Mataga and co-workers have investigated the intramolecular PET processes in **1** (Figure 1.2), which consists of a porphyrin connected to two quinones (Q_A and Q_B).[7] The CS state lifetime in **1** was 300 ps, which is nearly three-fold of the CS state lifetime ($\approx$100 ps) observed in a dyad consisting of a porphyrin linked to a quinone by four methylene groups.

1
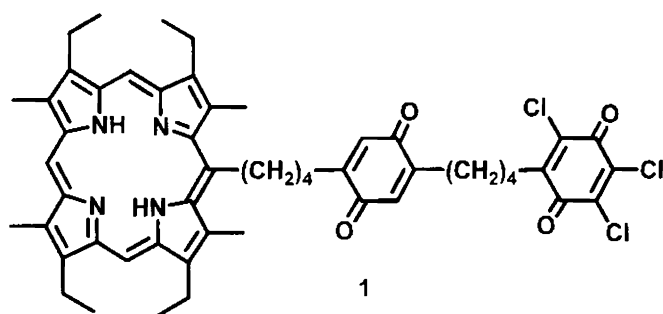
Figure 1.2

In this triad, photoexcitation of the porphyrin is followed by a sequential electron transfer:

$$P\text{-}Q_A\text{-}Q_B \rightarrow {}^1P^*\text{-}Q_A\text{-}Q_B \rightarrow P^{\bullet+}\text{-}Q_A^{\bullet-}\text{-}Q_B \rightarrow P^{\bullet+}\text{-}Q_A\text{-}Q_B^{\bullet-}$$
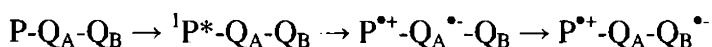
The lifetime of CS state is longer in triad because of the large separation distance between $P^{\bullet+}$ and $Q_B^{\bullet-}$.

Gust, Moore and co-workers are the pioneers in the design of multi-component arrays to mimic natural photosynthesis.[8-10] They have investigated PET processes in several porphyrin (P) - quinone (Q) – carotenoid (C) systems. The C-P-Q triad **2** (Figure 1.3) is one of the earliest examples.[8]

n = 1
n = 2
n = 3
n = 4

2
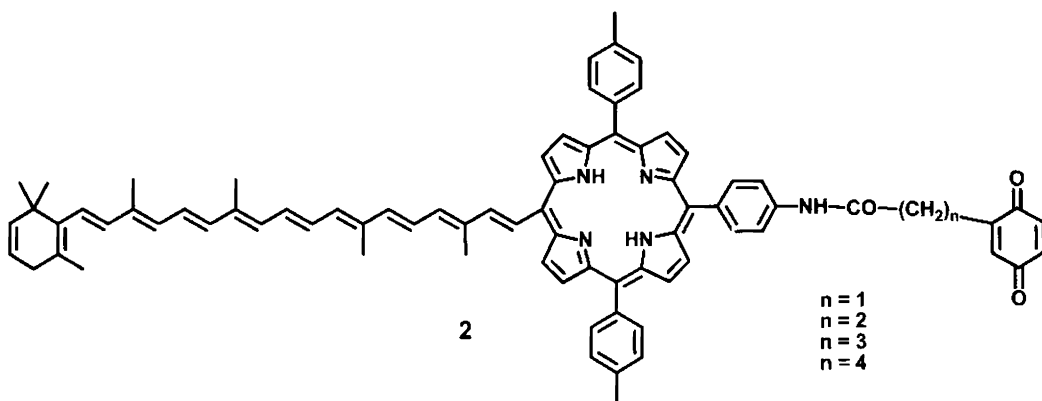
Figure 1.3

On the basis of electrochemical and spectroscopic studies PET pathways as shown in Scheme 1.4 were postulated for **2**. Initially, photoexcitation of the porphyrin produces its singlet excited state. This step is followed by an electron transfer from singlet porphyrin to the quinine acceptor, to generate $C\text{-}P^{\bullet+}\text{-}Q^{\bullet-}$. A second electron

transfer from the carotenoid to the porphyrin moiety then leads to the formation of long-lived $C^{\bullet+}\text{-}P\text{-}Q^{\bullet-}$ state. Using transient absorption spectroscopy the authors identified the carotenoid radical cation absorption at 950 nm, which exhibited a lifetime of few hundred nanoseconds.
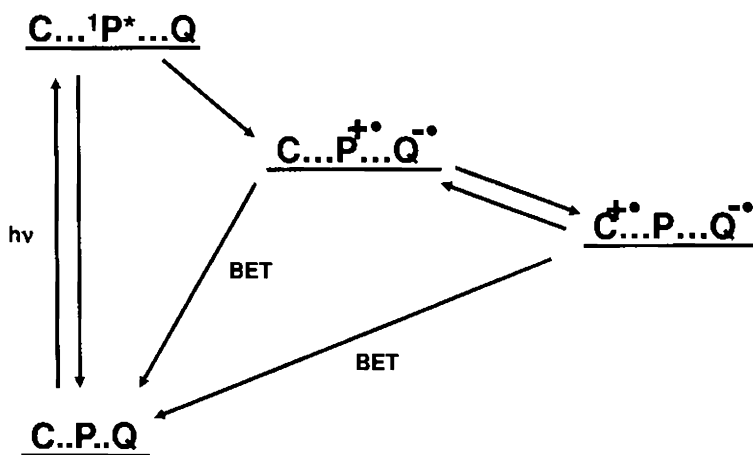
Scheme 1.4. Schematic representation of PET processes in C-P-Q triad

The same authors have extended this work to the molecular tetrad **3** (Figure 1.4).[9]
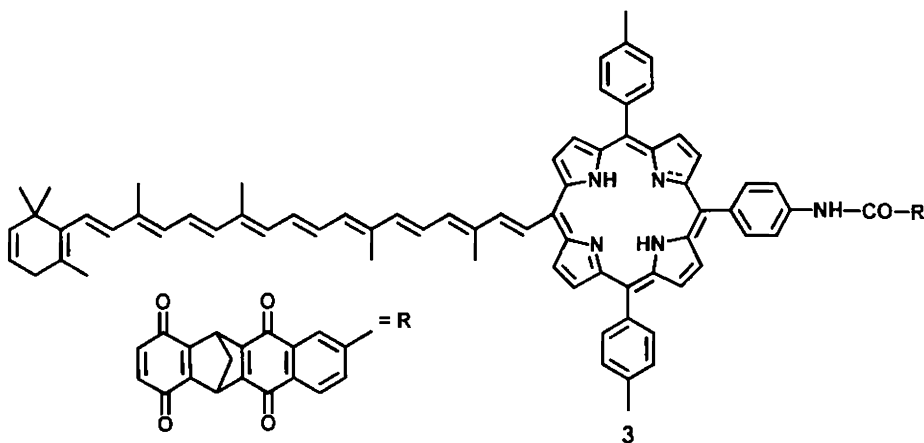
Figure 1.4

The lifetime measured for the final CS state in **3** was 450 ns, which was considerably larger than that observed for **2**. The ET pathways suggested for **3** are shown in Scheme 1.5. The long lifetime of $C^{\bullet+}$-P-Q_A-$Q_B^{\bullet-}$ was ascribed to the large distance separating $C^{\bullet+}$ and $Q_B^{\bullet-}$.
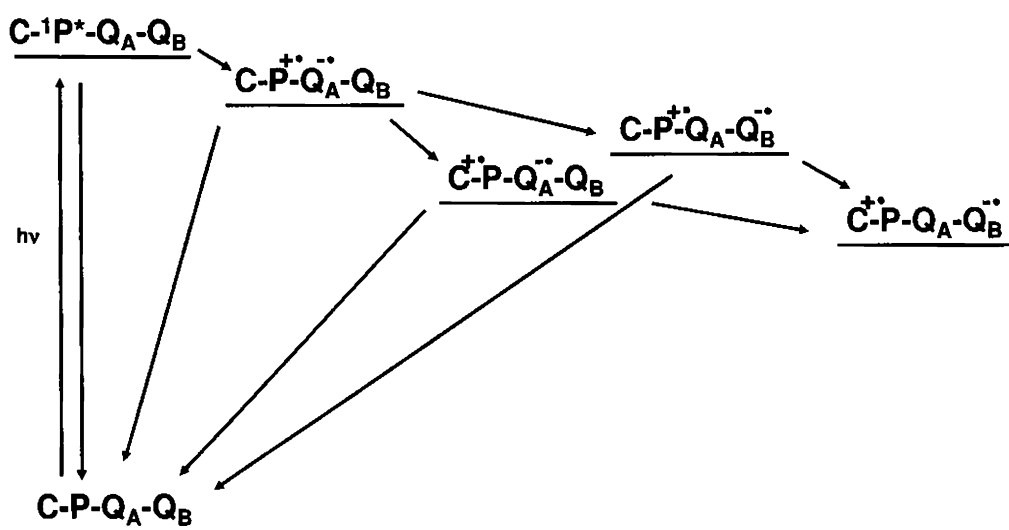
Scheme 1.5. Schematic representation of PET processes in C-P-Q_A-Q_B tetrad

Gust, Moore and co-workers have also investigated the PET processes in the C-P_A-P_B-Q tetrad **4** (Figure 1.5) where P_A stands for a zinc porphyrin and P_B for a free porphyrin and Q is a naphthaquinone. The final charge separated state, $C^{\bullet+}$-P_A-P_B-$Q^{\bullet-}$ was long-lived (2.9 µs) and was identified by its absorption at 980 nm using transient absorption studies.
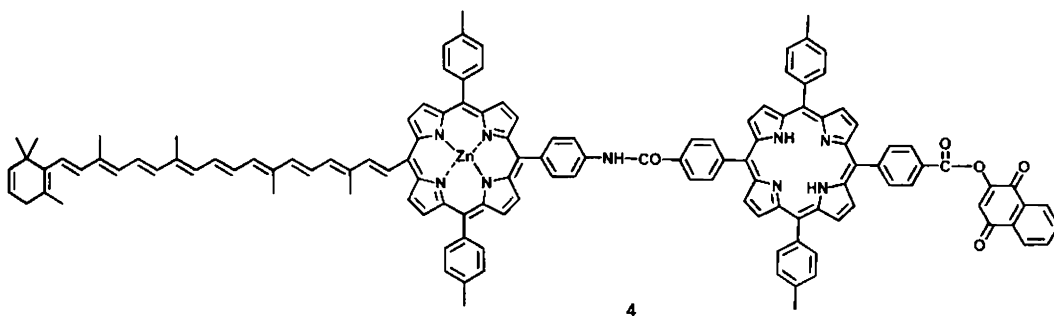
Figure 1.5

The same group has synthesized and studied the electron transfer processes in the molecular pentad C-P_A-P_B-Q_A-Q_B (**5**, Figure 1.6).[10]
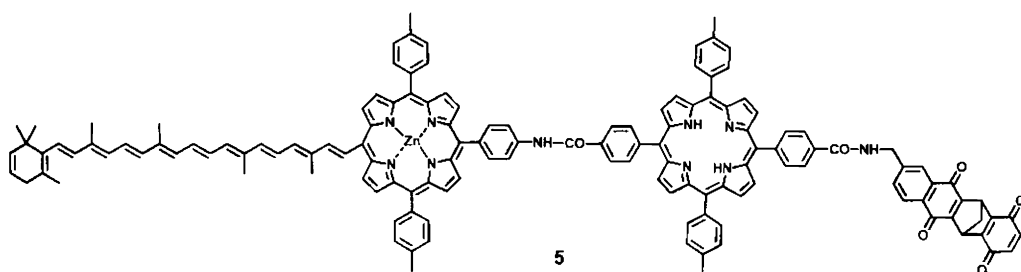
Figure 1.6

Very efficient PET is found to take place in this system. Transient absorption studies revealed that a CS state, C-P_A-P_B-Q_A-Q_B is formed with a lifetime of about 0.55 μs and an overall quantum yield of 0.83 after the series of sequential electron transfer steps shown in Scheme 1.6.
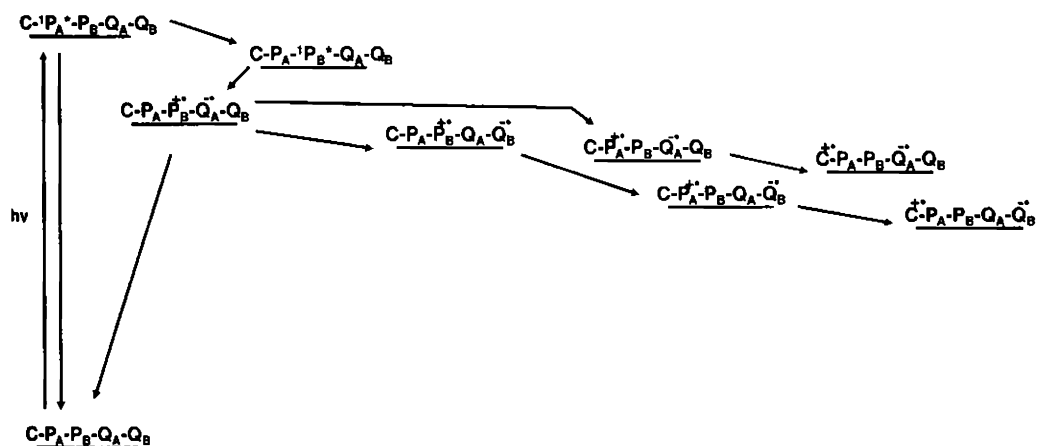
Scheme 1.6. Scheme of PET processes in the C-P_A-P_B-Q_A-Q_B pentad

Several other groups were also engaged in the construction of polyads capable of long-lived charge separation. For example, Wasielewski *et al.*[11] have reported a long-lived CS state in triad **6** (Figure 1.7), consisting of a porphyrin bearing a quinone acceptor and a dimethylaniline-based secondary donor. Here a final CS state is formed in 71% with a lifetime of 2.4 μs.

6
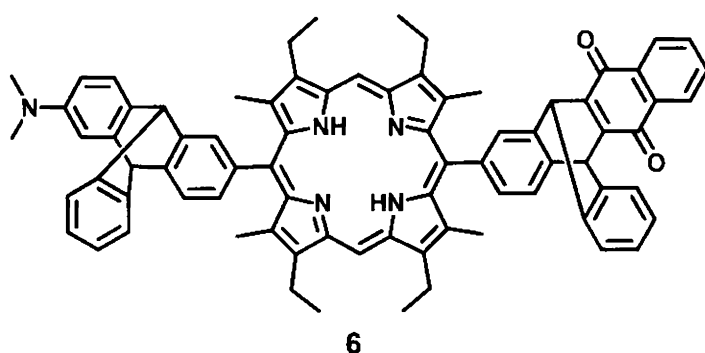
Figure 1.7

Flamigni *et al.* have synthesised and investigated the PET processes in a triad **7** (Figure 1.8), where an Ir (III) bisterpyridine complex connected through an amidophenyl spacer to a triphenylamine electron donor and to a naphthalene bisimide electron acceptor. Steady state and time-resolved optical spectroscopy showed that in this system PET leads to a final CS state with a lifetime of 120 μs.[12] A variety of other successful triads for substantial stabilization of the CS state have been reported in recent years.[13]

7
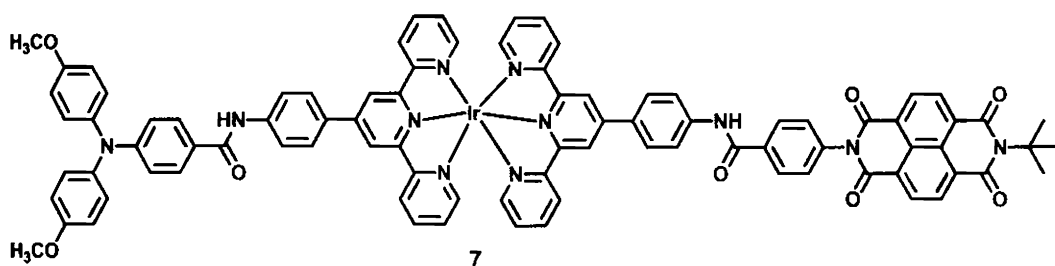
Figure 1.8

Several reports dealing with the construction of higher order tetrads and pentads are available in the literature. Guldi, Imahori and co-workers have achieved extremely long-lived CS states ranging from hundreds of milliseconds to a few seconds in tetrads.[14] For example, tetrad **8** (Fc-ZnP-H$_2$P-C$_{60}$, Figure 1.9) gave the final CS state Fc$^{\bullet+}$-ZnP-H$_2$P-C$_{60}$$^{\bullet-}$, which exhibited a lifetime of 380 ms in benzonitrile solution, with a quantum yield of 0.17.

Figure 1.9

Tetrad, **9** (Figure 1.10) containing Zinc porphyrin (PZn) and methyl viologen (MV^{2+}) as the terminal chromophores and dimethoxynaphthalene (DMN) and naphthaquinone (NQ) as intermediate chromophores studied by Paddon-Row et al.[15] offered very good photoinduced charge separation. **9** exhibited CS state lifetimes of 250-450 ns in different solvents.

Figure 1.10

Although the construction and use of multi-component polyads for photoinduced electron transfer is successful in generating long-lived CS states, the approach suffers from some serious drawbacks. First of all, the synthesis of multi-component systems is very tedious and time consuming. Hence this is a very expensive process. Another important shortcoming is that a significant amount of

energy is lost during each sequential electron transfer step. As shown in Scheme 1.3, each of the forward ET process is exergonic and hence energy stored in the CS state decreases in every step. The final CS state would have much less energy stored in it compared to the initial CS state. Therefore, even though the lifetime of the final CS state is fairly long enough, the energy associated with it (i.e. the energy available to do useful work) would be very low. Thus, it is highly desirable to design and synthesize simple molecular dyads which are capable of fast charge separation but retain long CS state lifetimes without the energy loss.[16]

1.3. Photoinduced electron transfer in simple donor-acceptor dyads

Considerable amount of work is reported in the literature regarding photoinduced electron transfer in covalently linked dyad molecules. Initial systems studied comprised of a porphyrin as both the light absorber and electron donor and a quinone as an electron acceptor.[13a] Other redox components have been proposed, and there now exists a multitude of light active molecular dyads that undergo fast charge separation upon excitation. But almost all such dyads underwent rapid charge recombination, which severely restricted the lifetime of the charge separated state. Indeed, typical lifetimes for the charge separated state in fluid solution are on the order of some hundreds of picoseconds to a few nanoseconds. This range is much too short to carry out useful chemistry with the intermediate

radical ions. Some special approaches are attempted in literature to increase the lifetime of CS ion pairs in simple D-A dyads.

1.3.1. Invoking spin restriction rule for long-lived CS state

One successful approach has been to make the decay of the CS state to the ground state a spin-forbidden process. In particular, this involves the design of dyads in which the CS state has triplet state character (^{3}CS). As will be exemplified below, this allows the creation of CS states with microsecond lifetimes in simple and very compact dyads.

In compact dyads the exchange interaction between D and A in the CS state may be expected to be large enough to allow for discrete singlet and triplet CS states (^{1}CS and ^{3}CS). ^{1}CS can easily be populated when it is energetically below the lowest locally excited singlet state. ^{1}CS can undergo intersystem crossing (ISC) to ^{3}CS. If ^{3}CS is the lowest triplet level in the dyad, then ^{3}CS has to decay eventually to the singlet ground state. This process would be slow because of the spin forbidden nature of this transition, leading to long CS state lifetimes. In general, local triplet states of D and A lie significantly below the ^{1,3}CS states in non-polar solvents. As the solvent polarity increases, local triplet levels are generally unaffected, but ^{1,3}CS state energies decrease considerably. Thus would ultimately lead to a situation in polar solvents, where the ^{3}CS state would be lower in energy compared to the local triplet levels, as shown in Scheme 1.7.

Scheme 1.7. Tuning of a dyad by increasing solvent polarity from a situation in which the CS state is the lowest singlet to one in which the CS state is also the lowest triplet

As shown in Scheme 1.7, few compact dyads can exhibit long-lived charge separation in polar solvents. This approach, however, suffers from two disadvantages. The energy stored in such CS states would be considerably lower compared to the energy absorbed. Secondly, if the ISC efficiency between the singlet and triplet CS states is low, then a considerable fraction of the CS state would be present in the singlet state, which would undergo very fast BET to the ground state. Quantum yield of the CS state would be very low in such a case. Some of the few compact dyads for which long-lived CS has been achieved are

compiled in Figure 1.11, together with quantum yields and lifetimes of their ^{3}CS

states. A more detailed discussion is presented below.

	Φ (%)	τ (μs)
10	26-55	< 2.4 (cyclohexane)
11	~ 100	3.35 (THF) 1.0 (CH$_3$CN)
12	" High"	
13	~ 30	>> 0.02(CH$_3$CN)

Figure 1.11. Structure of D-A dyads which form long-lived ^{3}CS state with quantum yields and lifetimes

While all the systems compiled in Figure 1.11 fulfil the requirement that ^{3}CS is the

lowest excited state, most probably in polar solvents, the mechanism employed to

achieve significant population of ^{3}CS after excitation differs from case to case and

sometimes has not been established beyond doubt.

The simplest mode of population of ^{3}CS would involve ISC from ^{1}CS to ^{3}CS. This spin-forbidden process has to compete with the spin-allowed decay of ^{1}CS to the ground state. Since, the latter process tends to be rather fast in compact dyads quantum yield of ^{3}CS formation is usually low. In fact, the most successful examples of long-lived ^{3}CS states populated via ISC from a short-lived ^{1}CS state are those occurring in metal–organic complexes in which the heavy atom effect of the metal allows for ultrafast ISC.

The first report of detection of a long-lived ^{3}CS state in a fully organic dyad is by Smit and Warman. They observed that **10** (Figure 1.11) gave a long-lived ^{3}CS state.[17] In **10** a carbazole donor and a tetrachlorophthalimide acceptor are linked by a short oligomethylene bridge. Earlier investigations had shown that the ^{1}CS state of these compounds is formed following excitation of the donor or acceptor chromophore.[18] This ^{1}CS state was found to be short-lived (28 ns in cyclohexane falling to 6 ns in 1,4-dioxane), but later investigations revealed the presence of a long-lived ^{3}CS state (lifetime in the microsecond range).[17] The quantum yield of the ^{3}CS state showed strong solvent dependence. Thus, for n = 2, it falls from 52% in cyclohexane to 10% in 1,4-dioxane. This may be taken as evidence that in these systems ^{3}CS is mainly formed via ISC from ^{1}CS. For systems containing a longer spacer, the ^{3}CS quantum yield is less dependent on polarity. Thus for n = 7, ^{3}CS state yield varied from 55% in cyclohexane to 33% in 1,4-dioxane. It is suggested that for longer spacers ^{3}CS can also be formed by ISC

from local singlet to triplet state followed by ET in the triplet manifold. It should

be stressed that these systems are rather unique in the sense that, their ^{3}CS state is

the lowest triplet even in non-polar solvents like cyclohexane. Under these

conditions, the CS state is estimated to lie $\approx$ 2 eV above the ground state. Other

dyads capable of forming long-lived ^{3}CS states (*vide infra*) almost invariably

require a polar solvent to push ^{3}CS below any local triplet states (Scheme 1.7).

Anglos *et al.* described the interesting rigid dyad **11**.[19] Photoexcitation of **11**

in moderate to high polar solvents leads to virtually quantitative population of a

long-lived ^{3}CS state in which an electron is transferred from the strong

diaminobenzene donor to the naphthalenediketone acceptor. Convincing evidence

was presented to show that after excitation of the acceptor, and before charge

separation in the singlet manifold can take place, very fast local ISC (^{1}A* → ^{3}A*)

occurs and is followed by charge separation in the triplet manifold, leading to very

high yield of the ^{3}CS state. Subsequently, a few other compact systems, such as the

piperidine-bridged system **12**,[20] and malachite green lactone **13**,[21] have been

reported in which excitation in polar or semipolar solvents leads to population of a

long-lived ^{3}CS state, although in less than quantitative yield. As far as can be

judged from the solvent dependence of the data reported (Figure 1.11), the lifetime

of the ^{3}CS state decreases slightly in more polar solvents and this is attributed to

lowering of the energy gap between ^{3}CS and the ground state.

In short, direct excitation of compact dyads and other compact donor-acceptor systems leads to population of a long-lived ^{3}CS state only in rare cases. It is relatively easy to design systems that meet the requirement of ^{3}CS being below all other excited states. However, it turns out to be difficult to suppress sufficiently, at least in compact systems, all other deactivation processes that occur in the singlet manifold in competition to formation of ^{3}CS.

It was shown recently by Verhoeven *et al.* that this problem can be circumvented by intermolecular triplet sensitization. Thus, on direct excitation via the dimethoxynaphthalene donor chromophore, the rigid dyad **14** (Scheme 1.8) undergoes quantitative charge separation. This yields a ^{1}CS state which decays with a time constant that varies from a few nanoseconds in non-polar media to less than 10 ps in polar solvents without a trace of ^{3}CS formation. Addition of the triplet sensitizer benzophenone (BP), which can be excited at longer wavelength than dimethoxynaphthalene, leads to a situation wherein the ^{3}CS can be reached via the sequence ^{1}BP* → ^{3}BP* → ^{3}D* → ^{3}CS in polar solvents (D stands for the dimethoxynaphthalene donor).[22] The corresponding energy diagram is depicted in Scheme 1.8.

Scheme 1.8. Structure of dyad **14** and pathways for population of its CS states with direct excitation and sensitisation with benzophenone

The lifetime of ^{3}CS is 1.4 µs in acetonitrile, whereas ^{1}CS, as populated by direct excitation, lives for less than 10 ps in the same solvent. This demonstrates that this type of spin control can increase the lifetime of CS states for compact dyads by at least five orders of magnitude without significantly degrading the energy content of the CS state (the energy gap between ^{1}CS and ^{3}CS in **14** was estimated to be of the order of only 0.2 eV = 4.6 kcalmol^{-1}).

While intermolecular sensitization appears to provide a new method to populate ^{3}CS states in compact dyads, the overall quantum yield of this process is limited by the quantum yield of the intermolecular triplet energy-transfer step.

Increasing the latter to unity may require very high dyad concentrations which may not be experimentally accessible. It therefore seems desirable to design compact dyads that incorporate a suitable sensitizer also. The simple system **15** (Scheme 1.9) designed by Verhoeven and co-workers is the first example of such a system.[23] In addition to the dimethylaniline (D) and the nitrobenzene (A) units, **15** contains an aromatic ketone as a triplet sensitizer (S). A relevant energy diagram in polar solvent is shown in Scheme 1.9.

Scheme 1.9. Structure and energy level diagram (in polar solvent) of **15**

From these data it appears that after excitation and ISC of the sensitizer chromophore in a polar solvent, sufficient energy is still available to induce electron transfer from D to A in the triplet manifold. This produces a ^{3}CS state that is lower in energy than all locally excited states. In low-polarity media, this need not be the case. Nanosecond transient absorption spectroscopic studies on **15** in benzene showed no detectable transients. In acetonitrile, however, a long-lived transient was detected that, under deoxygenated conditions, exhibited a lifetime of 0.33 μs. The lifetime was reduced to 56 ns under aerated conditions and hence the transient absorption was attributed to a triplet species. The absorption spectrum of this transient species displayed peaks corresponding to the acceptor radical anion and donor radical cation. Hence **15** was claimed as the first example of a compact dyad that incorporated an intramolecular sensitization step to produce a ^{3}CS state.

1.3.2. Conformational approach for long-lived CS state

Another approach to increase the lifetime of CS state in simple dyads is the conformational approach. This method proposes that specific conformation of donor and acceptor during the PET process may help the molecule to attain a long lifetime in the CS state. Our group has reported the Ru(bpy)$_3^{2+}$-phenothiazine dyad **16** (Figure 1.12) wherein the D and A moieties are linked by an amide bond.[24] Steady state and time resolved spectroscopic techniques showed that the electron transfer rates ($k_{et} > 10^8$ s^{-1}) in **16** were much faster than those previously reported ($k_{et} < 10^7$ s^{-1}) for other linked Ru(bpy)$_3^{2+}$–phenothiazine systems. Nanosecond

laser flash photolysis showed that compared to the previous systems, back electron

transfer rates in these systems were about 100 times slower. Transient absorptions

assignable to $Ru(bpy)^{3+}$ and phenothiazine radical cation, having lifetimes about

30 ns were observed for **16**. The fast electron transfer after the photoexcitation,

was explained by invoking a closed conformation in which one of the bipyridine

ligands or the Ru^{3+} metal centre is spatially very close to the phenothiazine moiety.

Same reason is assigned to the retardation of the BET rate. In this closed

conformation Ru^{2+} and phenothiazine radical cation will be near to each other,

leading to repulsion between the two positive charge centres, which reduce the

BET rate.

16

Figure 1.12

1.3.3. Invoking Marcus inverted region effect for long-lived CS state

Another approach to increase the lifetime of the CS state is to design D-A

dyads for which BET falls in the Marcus inverted region. In order to understand

the conceptual basis of this proposal, a detailed description of the Marcus equation

is required. According to the Marcus theory of electron transfer,[25] the rate constant

of non-adiabatic electron transfer (k_{ET}) is given by eqn (1.1),

$$k_{ET} = (2\pi/\hbar)\, H_{el}{}^2\, (4\pi\lambda k_B T)^{-1/2}\, \exp[-(\lambda + \Delta G_{ET})^2/4\lambda k_B T] \qquad (1.1)$$
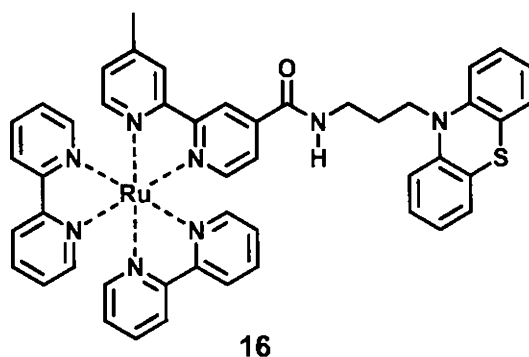
$\hbar$ is the Planck's constant divided by 2π, H_{el} is the electronic coupling matrix

element between the donor and acceptor, λ is the reorganization energy of the

electron transfer, k_B is the Boltzmann constant and T is the absolute temperature.

The reorganization energy of electron transfer (λ) is the energy required to

structurally reorganize the donor, acceptor and their solvation spheres upon

electron transfer. Depending on the relative values of ΔG_{ET} and λ, equation (1)

envisages three typical kinetic regimes for electron-transfer reactions as shown in

Figure 1.13: i) a normal region ($-\Delta G_{ET} < \lambda$) where electron transfer is thermally

activated and is favored by an increase in the driving force, ii) an "activation-less"

regime ($-\Delta G_{ET} = \lambda$) where the rate is maximum, and iii) an "inverted region" for

strongly exergonic reactions ($-\Delta G_{ET} > \lambda$), where the rate actually decreases with

increase in driving force. The existence of an inverted region was the most

important prediction of Marcus theory. Conclusive experimental evidence for the

inverted region was provided in 1984 by Miller *et al.*, almost 25 years after it was

predicted.[26] Although definitive evidence for its existence was lacking for a long

time, the inverted region is now well established in fixed-distance electron-transfer

reactions.[27]
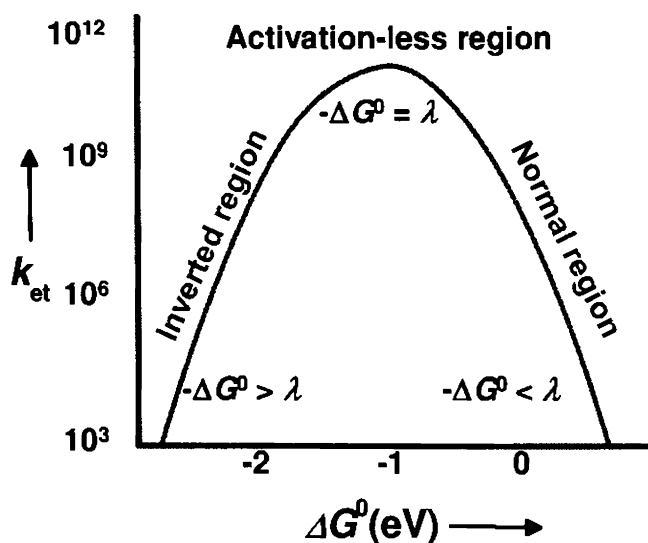
Figure 1.13. Schematic representation of a Marcus parabola

Miller and co-workers had proved the existence of inverted region in covalently connected rigid D-A systems.[26] Our group has established the existence of Marcus inverted region in supramolecular dyads such as hydrogen bonded D-A systems and cyclodextrin-encapsulated systems.[28,29] Our group was able to demonstrate the whole Marcus parabola on the basis of raw fluorescence lifetime data.[29]

It has been suggested that one can design dyads exhibiting long-lived CS states with the aid of the Marcus parabola. One can select D-A systems in such a way that the k_{PET} values lie at the top of the Marcus parabola and k_{BET} values lie deep in the inverted region. In such a case the forward ET would be extremely fast and the BET would be very slow. In such systems k_{PET}/k_{BET} values could be very large ($\geq 10^4$) and it would be possible to observe a long-lived CS state. However,

straight forward demonstration of this "inverted effect" has been very rare. A

general observation is that when $-\Delta G_{BET}$ is very large other deactivation channels

such as jumps to low lying local triplet levels may prevail over charge

recombination to the ground state. Nuclear tunnelling also becomes very important

and it is suggested that the Marcus equation may not adequately describe electron

transfer in the deep inverted region. There are, however, several papers which

claim long-lived CS state formation due to the inverted effect. Since this thesis

deals with long-lived charge separation due to inverted region effects, a detailed

description of these papers is given below.

Our group has studied the PET between anthracene attached to a β-

cyclodextrin (**17**, Figure 1.14) and pyromelliticdiimide (**18**) in aqueous solution.[30]

In aqueous solution **18** would be encapsulated into the β-CD cavity, as confirmed

by UV-Visible absorption, induced circular dichroism, ^{1}H NMR, cyclic

voltammetric and fluorescence studies.

17   **18**
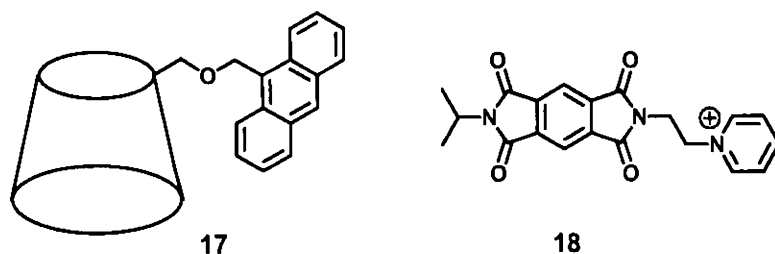
Figure 1.14

Photoinduced electron transfer in the system was studied by fluorescence quenching and laser flash photolysis techniques. At higher concentrations of **17**, it was found that the equilibrium was largely in favour of the supramolecular complex between **17** and **18** and intra-ensemble PET was found to take place. The rate constant for electron transfer within the ensemble from the singlet excited state of anthracene was measured. The experimentally determined rate constant agreed very well with that calculated using the Marcus equation. It was observed that a fraction of the charge separated ion pairs survived for more than 200 µs and this was attributed to inverted region effects.[30]

Inverted region effect was also invoked to explain long-lived charge separation in the covalently linked D-A system **19** (Figure 1.15), studied by Lambert *et al.*[31]
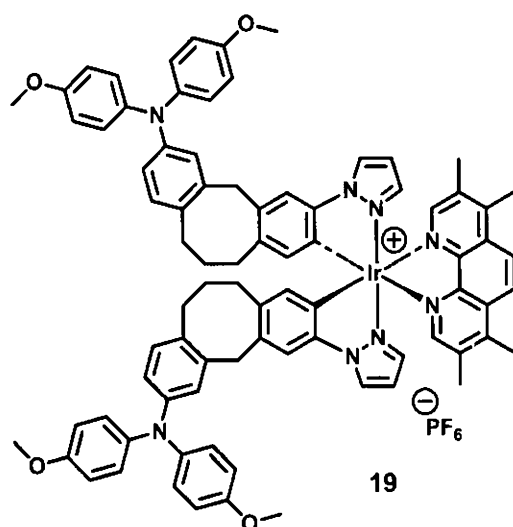
Figure 1.15

Electrochemical and fluorescence studies indicated the possibility of very efficient PET with a quantum yield of near unity. Transient absorption spectroscopy showed that a fraction of the charge separated state has a lifetime of 1.7 μs. It is assumed that both singlet and triplet CS states contribute to the transient absorption. Considering the very low reorganisation energy of the system, BET from both the ^{1}CS and ^{3}CS state would be in the Marcus inverted region. In addition, BET from the ^{3}CS to the singlet ground state would be spin forbidden and slow. It was claimed that the system exhibited a long lifetime for the CS state due to a combination of both inverted region effects and spin-selection rules.

In order to see long-lived charge separation it is essential that the CS state energy be lower than the triplet excited state energies of the donor and acceptor components of the dyad. Otherwise, the CS state would decay rapidly to the triplet excited state rather than to the ground state in the Marcus inverted region. Therefore porphyrin and fullerene derivatives which have local triplet states above the CS state would be ideal components in designing simple molecular dyads capable of long-lived charge separation. Also, the inherently low inner sphere reorganization energy of fullerene and porphyrin/chlorin systems makes the BET process in these dyads to fall in the inverted region.

Fukuzumi and co-workers were among the first to design simple donor acceptor systems based on fullerene and porphyrin/chlorine components which

exhibited long-lived CS states. The system designed (**20**, Figure 1.16) consisted of

zinc chlorin as the donor and fullerene as the acceptor.[32]

20
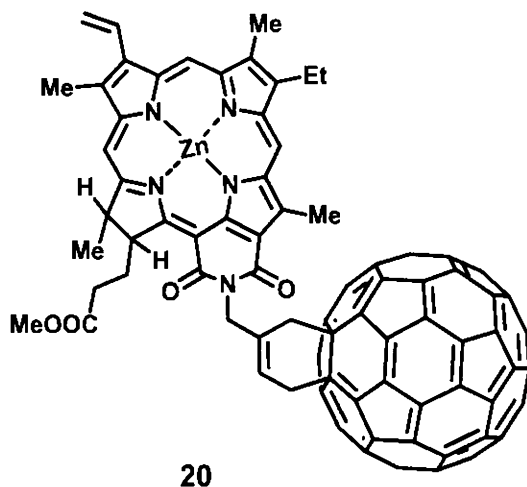
Figure 1.16

Nanosecond laser flash photolysis gave absorptions corresponding to the zinc

chlorin radical cation and fullerene radical anion. The peaks corresponding to the

CS state decayed via first order kinetics with a lifetime of ≈ 110 µs. Formation of

the long-lived CS state is further confirmed by ESR spectroscopy. Irradiation of **20**

in PhCN at 143 K gave two characteristic ESR signals, one of which is attributable

to an organofullerene radical anion (small *g* value) and the other to the chlorin

radical cation (higher *g* value).

Fukuzumi *et al.* have designed another dyad, **21** with zinc-

imidazoporphyrin as the donor and fullerene as the acceptor (Scheme 1.10).[33]
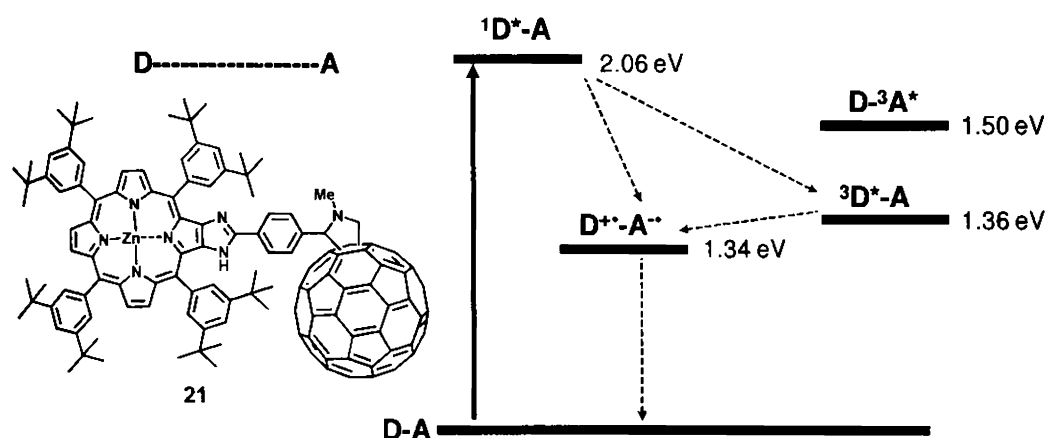
Scheme 1.10. Structure of **21** and its energy level diagram

Excitation of **21** led to the formation of a CS state with 260 μs lifetime at 298 K. At 278 K, the lifetime of the CS state was 310 μs. Energy level diagram (Scheme 1.10) reveals that the CS state (1.34 eV) is lower in energy than the triplet excited state of both C_{60} (1.50 eV) and zinc-imidazoporphyrin (1.36 eV). In this case also long lifetime of the CS state is attributed to the inverted region effect.

Fukuzumi *et al.* designed dyad **22** (Figure 1.17), which is a modification of **20**. Here the zinc chlorin donor is attached to the fullerene acceptor through an extremely short rigid linkage.[34] According to Marcus theory, a smaller distance between the donor and acceptor moieties leads to a reduction in the solvent reorganization energy. Hence the reorganization energy $\lambda \ll -\Delta G^0_{BET}$, and this will push BET in the system deeper into the inverted region. The absorption spectra of the compound indicated that there is no significant electronic interaction between the individual chromophores in the ground-state despite the short linkage

separating them. Fluorescence lifetime of **22** (10 ps) was significantly reduced

compared to that of unlinked zinc chlorine (2.7 ns) as a result of electron transfer

from the singlet excited state of the zinc chlorin to the C_{60} moiety of the dyad. The

rate constant of electron transfer from singlet excited state of the zinc chlorine to

C_{60} was determined as 1.0×10^{11} s^{-1}. Transient absorption spectrum of **22** showed

the formation of fullerene radical cation and zinc chlorin radical anion (Figure

1.17). The quantum yield of the CS state formation was 12%, which is smaller than

the fluorescence quenching efficiency (99.6%). The authors explained this by

invoking a short-lived exciplex state, only a part of which is converted into the

long-lived CS state (Figure 1.10).
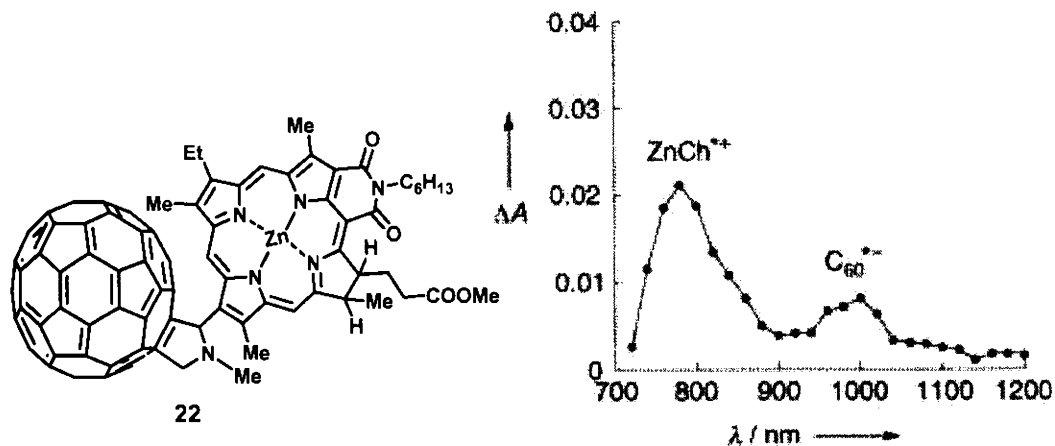
Figure 1.17. Structure of the dyad **22** and its transient absorption spectrum

The CS state decays by back electron transfer to the ground state rather than to

the triplet excited state since the CS state is lower in energy (1.26 eV) than both

the triplet excited states of C_{60} (1.50 eV) and zinc chlorin (1.36 - 1.45 eV). k_{BET}

obtained for **22** was 4.2×10^3 s^{-1}, corresponding to a CS state lifetime of 230 μs at

25 ^{0}C. ESR spectroscopy also gave evidence for the formation of long-lived charge

separation. Lifetime of the CS state showed large temperature dependence

indicating that the BET process belongs to the deep inverted region. The lifetime

of the CS state at -150 ^{0}C is as long as 120 s, which is the longest CS lifetime

reported for linked D-A systems with porphyrin and fullerene derivatives as

components.

A major disadvantage of chlorine-C_{60} systems is the very low energy of the

CS state (1.2 – 1.3 eV). In the case of the porphyrin-C_{60} systems the low triplet

energies of porphyrins have precluded attempts to attain long-lived CS states with

a higher energy than the triplet energies.[35a] In such a case, it is highly desirable to

have a chromophore which has high triplet energy and small reorganization

energy. Acridinium ion is a good candidate for such a purpose, since the

reorganisation energy (0.3 eV) for the electron self-exchange between acridinium

ion and the corresponding one-electron reduced radical is the smallest among

redox active organic compounds.[35b] The triplet energy of acridinium ion is also

very high.[35c]

Fukuzumi *et al.* have designed the dyad, 9-mesityl-10-methylacridinium

ion, (**23**, (Acr$^+$-Mes), Figure 1.18), in which the electron donor moiety (mesityl

group) is directly linked to the 9-position of acridinium ion. Because of the very

short distance between the D and A moieties the solvent reorganization energy for

the electron transfer will be minimized in **23**.[36] The X-ray crystal structure of Acr^+-Mes indicated that the donor and acceptor moieties are perpendicular to each other and that there is no orbital interaction between the two. Indeed, the absorption and fluorescence spectra of Acr^+–Mes are superpositions of the spectra of the components, i.e., mesitylene and 10-methylacridinium ion. The energy of the CS state ($Acr^\bullet$–$Mes^{\bullet+}$) is determined by the redox potentials of the components and the value obtained was 2.37 eV. ΔG^0 for PET in **23** was -0.31 eV.

23
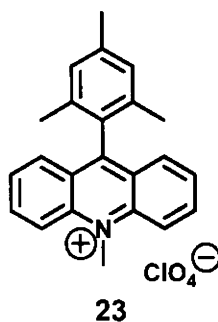
Figure 1.18

Photo-irradiation of a deaerated solution of Acr^+–Mes in acetonitrile by a nanosecond laser light flash at 430 nm resulted in the formation of a transient in 98% yield. Based on several experiments the authors assigned the transient absorption to the CS state $Acr^\bullet$–$Mes^{\bullet+}$, formed as a result of electron transfer from the mesitylene moiety to the singlet excited state of the acridinium ion moiety. The transient was found to be very long-lived with a lifetime of about 2 h at 203 K. BET in the CS state was too slow to compete with the intermolecular BET reaction as evidenced by the decay time profile of $Acr^\bullet$–$Mes^{\bullet+}$, which obeyed second-order

kinetics.[14a] In contrast, the decay of the CS state obeyed first-order kinetics in

benzonitrile at high temperatures. This indicates that the rate of the intramolecular

BET of the CS state becomes much faster than the rate of the intermolecular BET

at higher temperatures because of the larger activation energy of the former than

the latter. When the irradiation was performed at low temperatures, the colour of

the sample changed from green to brown.[37] The resulting solution afforded the

absorption spectrum due to the CS state, which consisted of the absorption bands

of the Acr$^{\bullet}$ and Mes$^{\bullet+}$ moieties. No decay of the absorption due to the CS state was

observed. This observation prompted the authors to claim an almost infinite

lifetime for the CS state Acr$^{\bullet}$–Mes$^{\bullet+}$ at 77 K. EPR experiments also gave evidence

for the formation of long lived CS state. The authors claimed that formation of

such a remarkably stable CS state is made possible by the high energy of the CS

state (2.37 eV), which is located deeply in the Marcus inverted region. It is also

claimed that the CS state could undergo secondary electron transfer experiments

with donors such as anthracene and acceptors such as naphthalenediimide or

methyl viologen.[18c] Because of the long CS state lifetime the authors used **23** as

photoredox catalyst in various applications.[38]

Another simple D-A dyad, **24** (Figure 1.19) reported by the same group

consisted of a formanilide moiety as the donor and anthraquinone moiety as the

light absorber and triplet-state electron acceptor.[39] The one-electron oxidation and

reduction potentials of **24** were determined by cyclic voltammetry and second

harmonic AC votammetry as 1.37 V and -0.87 V vs SCE, respectively. The driving

forces for the PET and BET were calculated to be -0.21 and -2.24 eV, respectively.

Energy of the CS state is found to be less than all local singlet and triplet energies

in **24**.

24
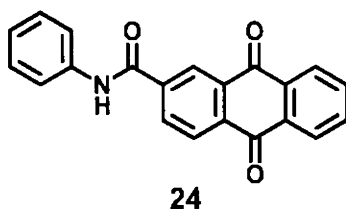
Figure 1.19

Femtosecond transient absorption studies showed that, upon photoexcitation of **24**

in DMSO, electron transfer takes place from the formanilide to the triplet state of

anthraquinone within 1.7 ps. Nanosecond laser flash photolysis gave a transient

with 900 μs lifetime. Based on evidence from secondary electron transfer

experiments the authors assigned the long-lived absorption to the CS state. In this

case also, long lifetime of the CS state was attributed to the inverted region effects.

Harriman, Verhoeven and co-workers have questioned the claims made by

Fukuzumi *et al.* regarding the formation of long-lived CS states in **20**, **21**, **22**, **23**

and **24**.[40] They have reinvestigated the photophysical processes taking place in

these systems and came up with alternate interpretations. According to them the

formation of long-lived CS state due to inverted region effects is not possible in

any of these systems.

According to Harriman, Verhoeven and co-workers the energy level diagram for **22** is as shown in Scheme 1.11. According to them, the energy levels of **22** fulfil the requirements discussed earlier for dyads capable of forming long-lived ^{3}CS state, since no local triplets are situated below the ^{3}CS state. Therefore, an alternative explanation for the reported observations may readily be proposed, at least as far as the behaviour in liquid solution is concerned. According to these authors, the short-lived "exciplex" species that Fukuzumi *et al.* invoked could actually be the ^{1}CS, of which apparently 88% decayed to the ground state and 12% underwent ISC to a longer lived ^{3}CS state. If the CS state has triplet character, inverted region effects need not be invoked and long lifetime of CS state could be attributed to spin restriction factors on charge recombination.

1.76 eV **D-^{1}A*** ━━━━━━
1.70 eV **^{1}D*-A** ━━━━━━

■ ■ ■ ■ ■ ■ ■ **D-^{3}A*** 1.50 eV

■ ■ ■ ■ ■ ■ ■ **^{3}D*-A** 1.36-1.45 eV

1.26 eV **^{1}[D$^+$-A$^-$]** ━━━━━ ------→ ■ ■ ■ ■ ■ ■ ■ **^{3}[D$^+$-A$^-$]**
                                   12%

D-A ━━━━━━━━━━━━━
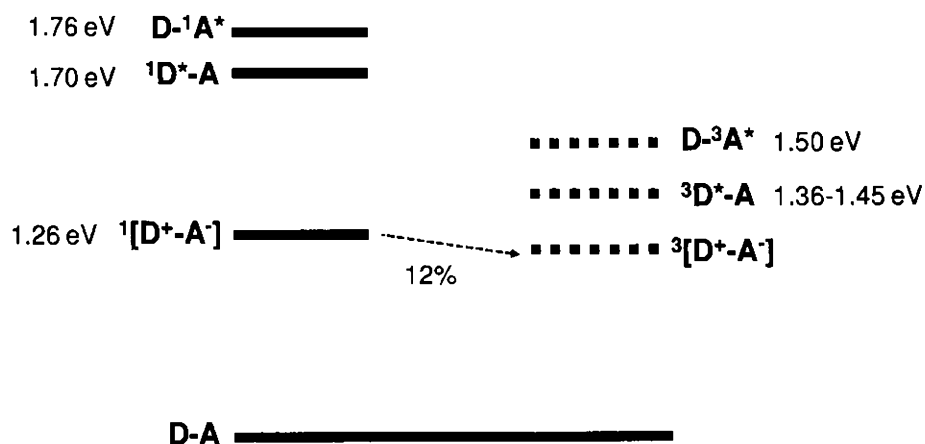
Scheme 1.11. Energy level diagram proposed for dyad **22**

According to Harriman, Verhoeven and co-workers the EPR signal observed in the photo-irradiation of **22** may be resulting from separate radical ions residing on

different molecules. If so, the temperature-dependent EPR lifetime data reported

for **22** can no longer be considered as proof for a strongly temperature dependent

k_{BET}. Harriman, Verhoeven and co-workers thus concluded that the long-lived CS

state formed in 12% yield on the photolysis of **22** in solution is the ^{3}CS state and

there is no need to invoke the inverted region effect to explain the long lifetime.

The same seems to apply to related dyads, **20** and **21**.

Fukuzumi *et al.* have claimed that **23** is even better than the natural

photosynthetic system both in terms of the amount of energy stored and lifetime of

the CS state. They initially estimated the energy of CS state in **23** at 2.37 eV. But

investigations by Harriman, Verhoeven and others suggested that the CS state is at

2.57 eV, which is barely below ^{1}(Acr$^+$)* (2.67 eV). They were also successful in

obtaining the phosphorescence spectrum of **23**, which placed the lowest ^{3}(Acr$^+$)*

energy at 1.94 eV above the ground state. Based on all these observations they

have constructed the energy level diagram of **23** as shown in Scheme 1.12.

Harriman, Verhoeven and co-workers argue that ^{3}(Acr$^+$)* lies below the ^{1,3}CS level

and hence the ^{1,3}CS state would cross over to ^{3}(Acr$^+$)* and the transient that

Fukuzumi *et al.* observed is actually ^{3}(Acr$^+$)*.

^{3}(Acr$^+$)*-Mes ━━━━   2.67 eV

↓ 5 ps

^{1,3}[Acr$^\cdot$-Mes$^{+\cdot}$] ━━━━   2.57 eV

6 ns

^{3}(Acr$^+$)*-Mes ■ ■ ■ ■ ■ ■   1.94 eV

Acr$^+$-Mes ━━━━
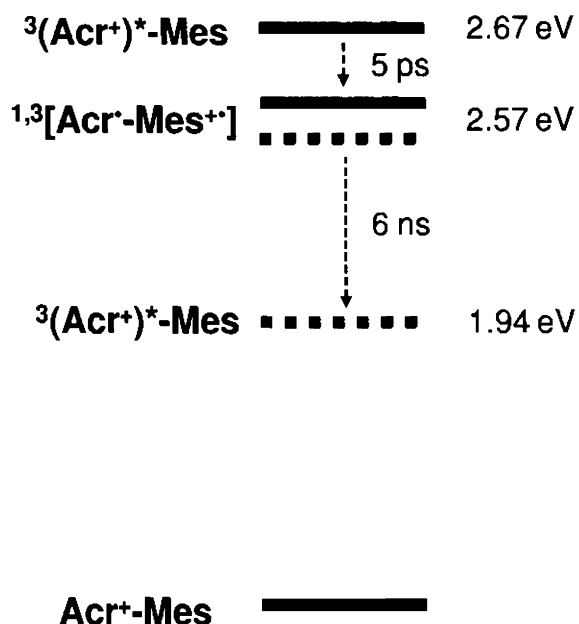
Scheme1.12. Energy level diagram proposed for dyad **23**

According to Harriman and Verhoeven ^{3}(Acr$^+$)* state is a poor reductant and hence incapable of reducing dialkyl naphthalenediimide or viologen dication. These authors attributed the secondary ET reactions of **23** (reported by Fukuzumi *et al.*) to reactions of either ^{3}(Acr$^+$)* or the radicals derived via chemical decomposition of Acr$^\cdot$–Mes$^{\cdot+}$. According to Harriman, Verhoeven and co-workers, the overall photophysics and photochemistry of **23** follow quite usual pathways known for many related systems and certainly do not require the involvement of any excited state with unusual properties. Studies by these authors on **23** indicated that the CS state has a lifetime of only 6 ns at room temperature. During the last five years Fukuzumi *et al.* published several papers supporting long-lived CS state in **23** and

Harriman, Verhoeven and co-workers published several papers opposing this claim. It must be stated here that photoinduced electron transfer in **23** remains a controversial topic even today.

In the case of dyad **24**, the femtosecond laser flash photolysis experiment by Fukuzumi *et al.* showed that this dyad undergoes very fast (τ_{isc} = 0.4 ps) ISC before charge separation occurs. There thus seemed to be no doubt that the CS state in **24** must be born with a triplet spin multiplicity, and it can be assumed that this might be an important factor in slowing down its recombination to the singlet ground state by intramolecular electron transfer. However dyad **24** had been investigated earlier by others who reported no evidence for the formation of a long-lived CS state in this molecule[41]. Harriman, Verhoeven and co-workers therefore synthesized and reinvestigated the PET processes in **24**.[40d] Their study confirmed the earlier reports that no long-lived CS state is formed in common solvents such as acetonitrile or benzonitrile. However, in the DMSO solvent employed by Fukuzumi and co-workers, very long-lived transients were observed with a spectrum closely matching to that of the anthraquinone radical anion. It was suggested that the anthraquinone radical anion was formed as a result of ET between triplet state of anthraquinone moiety and DMSO solvent which acts as a sacrificial electron donor. In fact, several anthraquinone derivatives including 9,10-anthraquinone itself, were capable of photo-oxidizing DMSO. Based on these observations Harriman and Verhoeven dismissed the claims of long-lived CS state

in **24**. In subsequent papers Fukuzumi *et al.* have rebutted all the findings by Harriman, Verhoeven and others and the PET processes in **24** is also an unsettled issue at present.

1.4. Origin of the present work

The most important aspect of Marcus theory was the prediction of an inverted region in electron transfer reactions. This aspect of Marcus theory was controversial from the time the theory was proposed in 1956 until John Miller's group at Argonne National Laboratory found experimental proof for it in 1986. Though long controversial, the presence of inverted region kinetics is now well established in a large number of charge shift and charge recombination reactions. In these examples, the forward PET reaction was generally restricted to the normal region and BET was restricted to the inverted region. Our group were among the first to establish the occurrence of the inverted region in PET reactions and considerable amount of work was carried out previously in our research group in this area.[28-30]

As mentioned earlier the presence of the inverted region is firmly established in several BET reactions.[13(a),42] In almost all these cases, however, the slowest rate observed in the inverted region was $\geq 10^8$ s^{-1}. In the light of these observations claims of $k_{BET} < 10^4$ s^{-1} from the Fukuzumi group is to be viewed with suspicion. It has been suggested that when $-\Delta G_{BET}$ is very large other deactivation

channels such as jumps to low lying local triplet levels may prevail over charge recombination to the ground state.[23] Nuclear tunneling also may become very important and it is suggested that equation 1.1 may not adequately describe electron transfer in the deep inverted region.[43] When viewed from this angle, the arguments of Harriman and Verhoeven seem reasonable.

The concept of designing dyads capable of long-lived charge separation due to the inverted region effects, however, seems very attractive. Theoretically, such a finding would reaffirm the existence of the inverted region. From a practical point of view, the time and effort required for the synthesis of complex tetrads, pentads etc can be saved. Loss of energy in sequential electron transfer steps can also be avoided. In this thesis an attempt is made to design dyads capable of long-lived charge separation. It is clear from the discussion in section 1.3 that most compact dyads would possess low lying local triplets below the CS state and this aspect is responsible for the absence of long-lived charge separation in dyads. We reasoned that if we choose chromophores with extremely high fluorescence quantum yield (or extremely low ISC efficiency), then we might be able to circumvent this difficulty. In these systems ISC to low lying local triplet levels would be slow or absent leading to long lifetimes for the CS state due to inverted region effects. In the remaining chapters of this thesis this idea is demonstrated and discussed in detail.

1.5. References

1. (a) Eisenberg, R.; Nocera, D. G. *Inorg. Chem.* **2005**, *44*, 6799-6801. (b) Gratzel, M. *Nature* **2001**, *414*, 338-344. (c) Armaroli, N.; Balzani, V. *Angew. Chem. Int. Ed.* **2006**, *46*, 52-66.

2. (a) *Electron Transfer in Chemistry*, Balzani, V. (Ed.), *Vol. 1-5*, Wiley-VCH, Weinheim, 2001. (b) Kuznetsov, A. M.; Ulstrup, J. *Electron Transfer in Chemistry and Biology*, Wiley, New York, 1998. (c) *Electron Transfer*, Wishart, J. F.; Nocera, D. G. (Eds.), ACS, Washington DC, 1998. (d) *Electron Transfer Reactions: Inorganic, Organometallic, and Biological Applications*, Isied, S. S. (Ed.), ACS, Washington DC, 1997.

3. (a) Kavarnos, G. J. *Fundamentals of Photoinduced Electron Transfer*, VCH, New York, 1993. (b) *Photoinduced Electron Transfer*, Fox, M. A.; Chanon, M. (Eds), *Parts A-D*, Elsevier, Amsterdam, 1988. (c) *Photoinduced Electron Transfer*, Mattay, J. (Ed.), *Parts I-IV*, Springer Verlag, Heidelberg, 1990.

4. (a) Julliard, M.; Chanon, M. *Chem. Rev.* **1983**, *83*, 425-506. (b) Kavarnos, G. J.; Turro, N. J. *Chem. Rev.* **1986**, *86*, 401-449. (c) Mikkelsen, K. V.; Ratner, M. A. *Chem. Rev.* **1987**, *87*, 113-153. (d) Andrieux, C. P.; Hapiot, P.; Saveant, J. M. *Chem. Rev.* **1990**, *90*, 723-738. (e) Evans, D. H. *Chem. Rev.* **1990**, *90*, 739-751. (f) Blondin, G.; Girerd, J. J. *Chem. Rev.* **1990**, *90*, 1359-1376. (g) Newton, M. D. *Chem. Rev.* **1991**, *91*, 767-792.

5.   (a) Deisenhofer, J.; Epp, O.; Miki, K.; Huber, R.; Michel, H. *J. Mol. Biol.* **1984**, *180*, 385-398. (b) Reimers, J. R.; Hutter, M. C.; Hughes, J. M.; Hush, N. S. *Int. J. Quant. Chem.* **2000**, *80*, 1224-1243. (c) Hutter, M. C.; Hughes, J. M.; Reimers, J. R.; Hush, N. S. *J. Phys. Chem. B* **1999**, *103*, 4906-4915.

6.   (a) Breton, J.; Martin, J.-L.; Migus, A.; Antonetti, A.; Orszag, A. *Proc. Natl. Acad. Sci. USA* **1986**, *83*, 5121-5125. (b) Wasielewski, M. R.; Tiede, D. M. *FEBS Lett.* **1986**, *204*, 368-372. (c) Woodbury, N. W.; Becker, M.; Middendorf, D.; Parson, W. W. *Biochemistry* **1985**, *24*, 7516-7521. (d) Martin, J.-L.; Breton, J.; Hoff, A. J.; Migus, A.; Antonetti, A. *Proc. Natl. Acad. Sci. USA* **1986**, *83*, 957-961.

7.   Mataga, N.; Karen, A.; Okada, T.; Nishitani, S.; Kurata, N.; Sakara, Y.; Misumi, S. *J. Phys. Chem.* **1984**, *88*, 5138-5141.

8.   (a) Moore, T. A.; Gust, D.; Mathis, P.; Mialocq, J. C.; Chachaty, C.; Bensassons, R. V.; Land, E. J.; Doizi, D.; Lidell, P. A.; Lehman, W. R.; Nemeth, G. A.; Moore, A. L. *Nature* **1984**, *307*, 630-632. (b) Gust, D.; Moore, T. A.; Bensasson, R. V.; Mathis, P.; Land, J. L.; Chachaty, C.; Moore, A. L.; Liddell, P. A.; Nemeth, G. A. *J. Am. Chem. Soc.* **1985**, *107*, 3631-3640. (c) Gust, D.; Moore, T. A.; Liddell, P. A.; Nemeth, G. A.; Makings, L. R.; Moore, A. L.; Barrett, D.; Pessiki, P. J.; Bensasson, R. V.;

Rougee, M.; Chachaty, C.; De Schryver, F. C.; Van der Auweraer, M.; Holzwarth, A. R.; Connolly, J.S. *J. Am. Chem. Soc.* **1987**, *109*, 846-856.

9. (a) Gust, D.; Moore, T. A.; Moore, A. L.; Barrett, D.; Harding, L. O.; Makings, L. R.; Liddell, P. A.; De Schryver, F. C.; Van der Auweraer, M. *J. Am. Chem. Soc.* **1988**, *110*, 321-323. (b) Gust, D.; Moore, T. A.; Moore, A. L.; Makings, L. R.; Seely, G. R.; Ma, X.; Trier, T. T.; Gao, F. *J. Am. Chem. Soc.* **1988**, *110*, 7567-7569. (c) Gust, D.; Moore, T. A. *Science* **1989**, *244*, 35-41.

10. Gust, D.; Moore, T. A.; Moore. A. L.; Lee, S. J.; Bittersmann, E.; Luttrull, D. K.; Rehms, A. A.; De Graziano, J. M.; Ma, X. C.; Gao, F.; Belford, R. E.; Trier, T. T. *Science* **1990**, *248*, 199-201.

11. Wasielewski, M. R.; Niemczyk, M. P.; Svec, W. A.; Pewitt, E. B. *J. Am. Chem. Soc.* **1985**, *107*, 5562-5563.

12. Flamigni, L.; Baranoff, E.; Collin, J. P.; Sauvage, J. P. *Chem. Eur. J.* **2006**, *12*, 6592-6606.

13. (a) Wasielewski, M. R. *Chem. Rev.* **1992**, *92*, 435-461. (b) Gust, D.; Moore, T. A. *Adv. Photochem.* **1991**, *16*, 1-65. (c) Gust, D.; Moore, T. A. *Top. Curr. Chem.* **1991**, *159*, 103-151.

14. (a) Imahori, H.; Guldi, D. M.; Tamaki, K.; Yoshida, Y.; Luo, C.; Sakata, Y.;

     Fukuzumi, S. *J. Am. Chem. Soc.* **2001**, *123*, 6617-6628. (b) Guldi, D. M.;

     Imahori, H.; Tamaki, K.; Kashiwagi, Y.; Yamada, H.; Sakata, Y.; Fukuzumi,

     S. *J. Phys. Chem. A* **2004**, *108*, 541-548.

15. (a) Jolliffe, K. A.; Langford, S. J.; Ranasinghe, M. G.; Shephard, M. J.;

     Paddon-Row, M. N. *J. Org. Chem.* **1999**, *64*, 1238-1246. (b) Jolliffe, K. A.;

     Bell, T. D. M.; Ghiggino, K. P.; Langford, S. J.; Paddon-Row, M. N. *Angew.*

     Chem. Int. Ed. Engl. **1998**, *37*, 916-919. (c) Jolliffe, K. A.; Langford, S. J.;

     Oliver, A. M.; Shephard, M. J.; Paddon-Row, M. N. *Chem. Eur. J.* **1999**, *5*,

     2518-2530.

16. (a) Harriman, A. *Angew. Chem. Int. Ed.* **2004**, *43*, 4985-4987. (b) Fukuzumi,

     S. *Bull. Chem. Soc. Jpn.* **2006**, *79*, 177-195. (c) Fukuzumi, S. *Phys. Chem.*

     Chem. Phys. **2008**, *10*, 2283-2297.

17. Smit, K. J.; Warman, J. M. *J. Lumin.* **1988**, *42*, 149-154.

18. Borkent, J. H.; de Jong, A. W. J.; Verhoeven, J. W.; deBoer, T. J. *Chem.*

     Phys. Lett. **1978**, *57*, 530-534.

19. Anglos, D.; Bindra, V.; Kuki, A. *J. Chem. Soc. Chem. Commun.* **1994**, *2*,

     213-215.

20. van Dijk, S. I.; Groen, C. P.; Hartl, F.; Brouwer, A. M.; Verhoeven, J. W. *J. Am. Chem. Soc.* **1996**, *118*, 8425-8432.

21. Karpiuk, J. *Phys. Chem. Chem. Phys.* **2003**, *5*, 1078-1096.

22. (a) Hviid, L.; Brouwer, A. M.; Paddon-Row, M. N.; Verhoeven, J. W. *Chem. Phys. Chem.* **2001**, *2*, 232-235. (b) Hviid, L.; Bouwman, W. G.; Paddon-Row, M. N.; Verhoeven, J. W.; van Ramesdonk, H. J.; Brouwer, A. M. *Photochem. Photobiol. Sci.* **2003**, *2*, 995-1001. (c) Hviid, L.; Verhoeven, J. W.; Brouwer, A. M.; Paddon-Row, M. N.; Yang, J.; George, M. W. *Photochem. Photobiol. Sci.* **2004**, *3*, 246-251.

23. Verhoeven, J. W.; van Ramesdonk, H. J.; Groeneveld, M. M.; Benniston, A. C.; Harriman, A. ChemPhysChem. **2005**, *6*, 2251-2260.

24. Ajayakumar, G.; Gopidas, K. R. *Photochem. Photobiol. Sci.* **2008**, *7*, 826-833.

25. (a) Marcus, R. A.; Sutin, N. *Biochim. Biophys. Acta* **1985**, *811*, 265-322 (b) Marcus, R. A. *Angew. Chem., Int. Ed.* **1993**, *32*, 1111-1121.

26. (a) Miller, J. R.; Calcaterra, L. T.; Closs, G. L. *J. Am. Chem. Soc.* **1984**, *106*, 3047-3049. (b) Closs, G. L.; Miller, J. R. *Science*, **1988**, *240*, 440-447.

27. Suppan, P. *Top. Curr. Chem.* **1992**, *163*, 95-130 and references cited therein.

28. (a) Prasad, E.; Gopidas. K. R.; *J. Am. Chem. Soc.* **2000**, *122*, 3191-3196. (b) Smitha, M. A.; Prasad, E.; Gopidas. K. R.. *J. Am. Chem. Soc.* **2001**, 123, 1159-1165.

29. Balan, B.; Gopidas. K. R. *Chem. Eur. J.* **2006**, *12*, 6701-6710.

30. Balan, B.; Gopidas. K. R. *Chem. Eur. J.* **2007**, *13*, 5173-5185.

31. Geiss, B.; Lambert, C. *Chem. Commun.* **2009**, 1670-1672.

32. Ohkubo, K.; Imahori, H.; Shao, J.; Ou, Z.; Kadish, K. M.; Chen, Y.; Zheng, G.; Pandey, R. K.; Fujitsuka, M.; Ito O.; Fukuzumi, S. *J. Phys. Chem. A* **2002**, *106*, 10991-10998.

33. Kashiwagi, Y.; Ohkubo, K.; McDonald, J. A.; Blake, I. M.; Crossley, M. J.; Araki, Y.; Ito, O.; Imahori, H.; Fukuzumi, S. *Org. Lett.* **2003**, *5*, 2719-2721.

34. Ohkubo, K.; Kotani, H.; Shao, J.; Ou, Z.; Kadish, K. M.; Li, G.; Pandey, R. K.; Fujitsuka, M.; Ito, O.; Imahori, H.; Fukuzumi, S. *Angew. Chem. Int. Ed.* **2004**, *43*, 853-856.

35. (a) Imahori, H.; El-Khouly, M. E.; Fujitsuka, M.; Ito, O.; Sakata, Y.; Fukuzumi, S. *J. Phys. Chem. A* **2001**, *105*, 325-332. (b) Fukuzumi, S.; Ohkubo, K.; Suenobu, T.; Kato, K.; Fujitsuka, M.; Ito, O. *J. Am. Chem. Soc.* **2001**, *123*, 8459-8467. (c) Kikuchi, K.; Sato, C.; Watabe, M.; Ikeda, H.; Takahashi, Y.; Miyashi, T. *J. Am. Chem. Soc.* **1993**, *115*, 5180-5184.

36. Fukuzumi, S.; Kotani, H.; Ohkubo, K.; Ogo, S.; Tkachenko, N. V.; Lemmetyinen, H. *J. Am. Chem. Soc.* **2004**, *126*, 1600-1601.

37. Kotani, H.; Ohkubo, K.; Fukuzumi, S. *Chem. Commun.* **2005**, 4520-4522.

38. Hasobe, T.; Hattori, S.; Kotani, H.; Ohkubo, K.; Hosomizu, K.; Imahori, H.; P.V. Kamat, P.V.; Fukuzumi, S. *Org. Lett.* **2004**, *6*, 3103-3106. (b) Kotani, H.; K. Ohkubo, K.; S. Fukuzumi, S. *J. Am. Chem. Soc.* **2004**, *126*, 15999-16006. (c) Hasobe, T.; Hattori, S.; Kamat, P.V.; Wada, Y.; Fukuzumi, S. *J. Mater. Chem.* **2005**, *15*, 372-380. (d) Ohkubo, K.; Nanjo, T.; Fukuzumi, S. *Org. Lett.* **2005**, *7*, 4265-4268.

39. Okamoto, K. ; Hasobe, T. ; Tkachenko, N. V. ; Lemmetyinen, H. ; Kamat, P. V. ; Fukuzumi, S. *J. Phys. Chem. A* **2005**, *109*, 4662-4670.

40. (a) Benniston, A. C.; Harriman, A.; Li, P.; Rostron, J. P.; Verhoeven, J. W. *Chem. Commun.* **2005**, 2701-2703. (b) Benniston, A. C., Harriman, A.; Li, P.; Rostron, J. P.; Ramesdonk, H. J.; Groeneveld, M. M.; Zhang, H.; Verhoeven, J. W. *J* . *Am. Chem. Soc.* **2005**, *127*, 16054-16064. (c) Verhoeven, J.; van Ramesdonk, H. J.; Zhang, H.; Groeneveld, M. M.; Benniston, A. C.; Harriman, A. *Int. J. Photoenergy* **2005**, *7*, 103-108. (d) van Ramesdonk, H. J.; Bakker, B. H.; Groeneveld, M. M.; Verhoeven, J. W.; Allen, B. D.; Rostron, J. P.; Harriman, A. *J. Phys. Chem. A* **2006**, *110*, 13145-13150. (e) Benniston, A. C.; Harriman, A.; Verhoeven, J. W. *Phys.*

Chem. Chem. Phys. **2008**, *10*, 5156-5158. (f) Verhoeven, J. W.; van Ramesdonk, H. J.; Groeneveld, M. M.; Benniston, A. C.; Harriman, A. *ChemPhysChem.* **2005**, *6*, 2251-2260. (g) Verhoeven, J. W. *J. Photochem. Photobiol. C* **2006**, *7*, 40-60.

41. (a) Hamanoue, K.; Nakayama, T.; Nanshow, H.; Hanada, T.; Naruta, Y.; Kodo, T.; Maruyama, K. *J. Chem. Soc. Faraday Trans.* **1993**, *89*, 3243-3250. (b) Allen, N.S.; Pullen, G.; Shah, M.; Edge, M.; Holdsworth, D.; Weddell, I.; Swart, R.; Catalina, F. *J. Photochem. Photobiol. A: Chem.* **1995**, *91*, 73-79.

42. (a) Suppan, P. In *Topics in Current Chemistry*, Mattay, J. Ed.; Springer Verlag: Berlin, 1992, Vol. 163, pp 95-130. (b) Gould, I.; Farid, S. *Acc. Chem. Res.* **1996**, *29*, 522-528.

43. (a) Smit, K. J.; Warman, J. M.; de Haas, M. P.; Paddan-Row, M. N.; Oliver, A. M. *Chem. Phys. Lett.* **1988**, *152*, 177-182. (b) Liang, N.; Miller, J. R.; Closs, G. L. *J. Am. Chem. Soc.* **1990**, *112*, 5353-5354.

Long-lived Photoinduced Charge Separation in Flexible 9,10-Bis(phenylethynyl)anthracene – Phenothiazine Dyads

2.1. Abstract

Photoinduced electron transfer in linked donor-acceptor dyads with bis(phenylethynyl)anthracene as light absorber and acceptor and one or two phenothiazine units as donors was investigated. Absorption spectra of the dyads can be obtained by adding contributions due to the donor and acceptor moieties indicating that the constituents do not interact in the ground state. Fluorescence of bis(phenylethynyl)anthracene core was efficiently quenched by the donor moieties and this was attributed to electron transfer from the phenothiazine to bis(phenylethynyl)anthracene. Femtosecond transient absorption studies suggested formation of a charge separated state directly from the singlet excited state of bis(phenylethynyl)anthracene. Nanosecond flash photolysis experiments gave long-lived transient absorptions assignable to phenothiazine radical cation and bis(phenylethynyl)anthracene radical anion. These assignments were confirmed by oxygen quenching studies and secondary electron transfer experiments. Electron

transfer in these systems is analyzed in the light of Marcus theory and the slow

back electron transfer exhibited is attributed to inverted region effects.

2.2. Introduction

Formation of a long-lived CS state in simple D-A molecular dyads is an essential requirement for developing efficient artificial photosynthetic systems and optoelectronic devices.[1] In simple D-A systems excitation leads to electron transfer (ET) followed by rapid back electron transfer (BET) which results in extremely short lifetimes and low yields of the CS states. Several approaches like spin restriction rules,[2] conformational gating,[3] applied magnetic fields[4] and orientation effects[5] have been suggested to enhance the lifetimes and quantum yields of CS states in dyads. Design of dyads for which BET fall in the Marcus inverted region is another important suggestion. According to Marcus theory the rate of ET is expected to decrease in the strongly exergonic region where the driving force ($-\Delta G^0$) is much larger than the reorganization energy (λ).[6] This exergonic regime is known as the Marcus inverted region and a few D-A dyads exhibiting long-lived CS states presumably due to the inverted region effect are reported in the literature by Fukuzumi and coworkers.[7] Some of these systems have a fullerene acceptor directly linked to a porphyrin or chlorin donors. The inherently low inner sphere reorganization energy of fullerene and porphyrin / chlorin systems and the short D-A distance contribute to the low λ values in these systems. They have also reported the formation of long-lived CS states in substituted methylacridinium and

anthraquinone derivatives.[8] Verhoeven, Harriman and co-workers have questioned the results obtained in these systems. According to them, usually there will be some triplet excited states which is lower in energy than singlet CS state. Therefore these states can be easily populated, hence reducing the lifetime of the charge separated state.[9] If we can somehow prevent the formation of these triplet state, then we will be able to generate long-lived CS state which will solely depend on the Marcus inverted region effect only. In this work we are using 9,10-bis(phenylethynyl)anthracene which has high fluorescence quantum yield and hence low intersystem crossing ability, as the sensitizer.

In this chapter we report the formation of long-lived CS state in two dyads, wherein the donor and acceptor are linked through a flexible alkyl chain. The acceptor in this study is bis(phenylethynyl)anthracene (**BPEA**, Figure 2.1), which also acts as the light absorbing unit. Due to their high fluorescence quantum yields and conductance properties, **BPEA** derivatives find applications as emitters in chemiluminescent light sources[10] and as molecular probes.[11] They are also used in solar cells,[12] OLED[13] and PLED[14] devices. Albinsson et al. have extensively studied the photoinduced electron transfer processes in bridged donor-acceptor systems containing **BPEA** unit as electron transporting bridge.[15] The donor moiety in our study is phenothiazine (**PT**). We have used **PT** as donor because the triplet energy of it is higher than all other energy states of the molecule. Several studies where **PT** acts as donor are available and the **PT** radical cation is well

characterized by spectroscopic methods.[16] Structures of the two dyads we have

studied (**BPEA-PT** and **BPEA-PT₂**) are shown in Figure 2.1 along with the model

BPEA (R=OCH₃) system. We have probed the photoinduced charge separation in

the **BPEA-PT** dyads using fluorescence lifetime measurements and femtosecond

and nanosecond laser flash photolysis techniques and confirmed formation of a

long-lived CS state. In previous claims of long-lived CS in dyads, the donor and

acceptor residues were directly linked and the small outer sphere reorganization

energy (λ_o) resulting from the short center-to-center distance (d_{cc}) between the D

and A units was claimed as a major reason for long CS state lifetime.[7(b)] In the

work reported here $d_{cc} > 10$ Å suggesting that a small d_{cc} value is not a crucial

factor in stabilizing the CS state. Minimum energy conformation of **BPEA-PT₂**

obtained by AM1 calculation using Gaussian 03 (Revision-D.01) is also shown in

Figure 2.1, which gave $d_{cc} = 14.2$ Å.
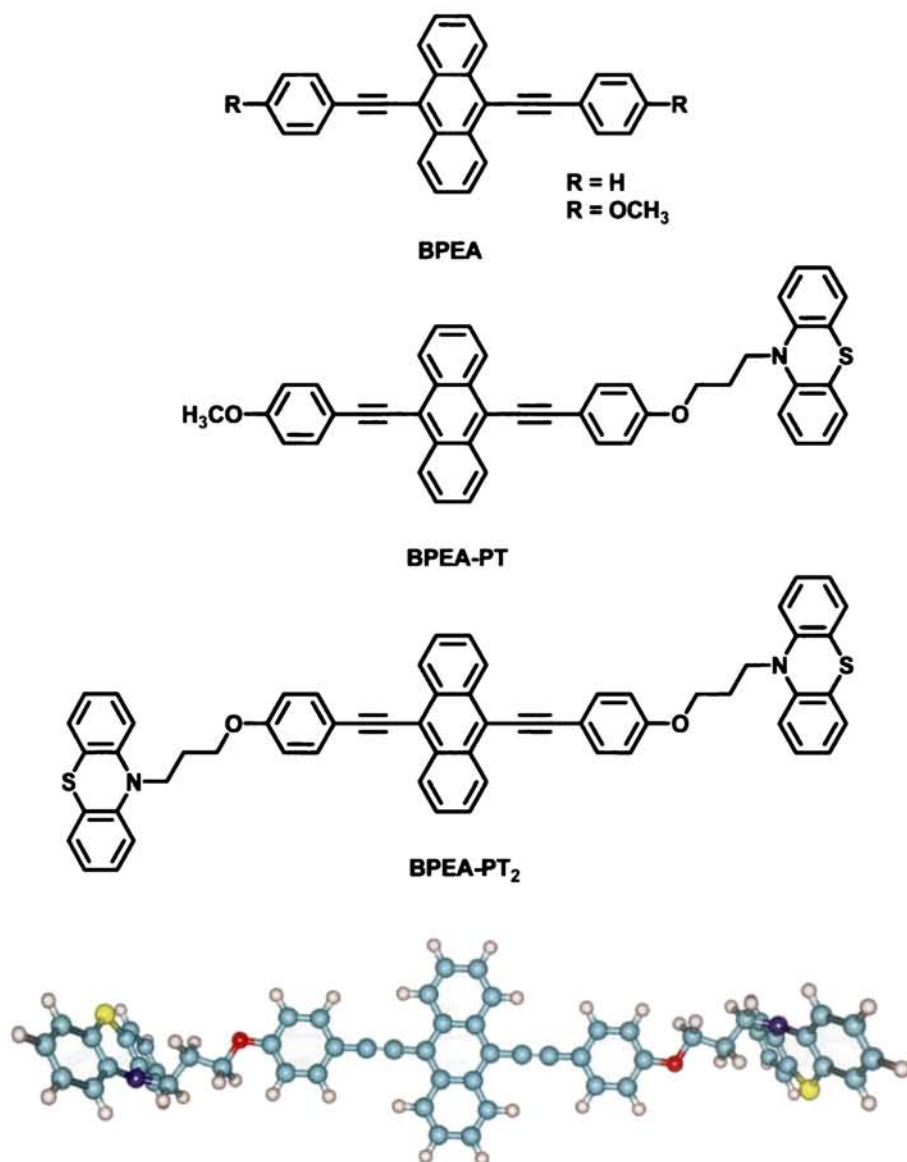
Figure 2.1. Structures of compounds used in this study and optimized structure of **BPEA-PT₂**

2.3. Results and discussion

2.3.1. Synthesis and characterisation of BPEA, BPEA-PT and

BPEA-PT$_2$

BPEA (R=OCH$_3$) was synthesized as shown in scheme 2.1.[17] 4-iodo

anisole, **1** was first converted to **2**, by the reaction with trimethylsilylacetylene

under   Sonogashira   coupling   condition.   **2**   on   deprotection   with

tetrabutylammonium fluoride in THF gave 4-ethynyl anisole, **3**. Two equivalence

of **3** on reaction with 9,10-dibromoanthracene, **4** under palladium catalysed

reaction condition gave the **BPEA**.
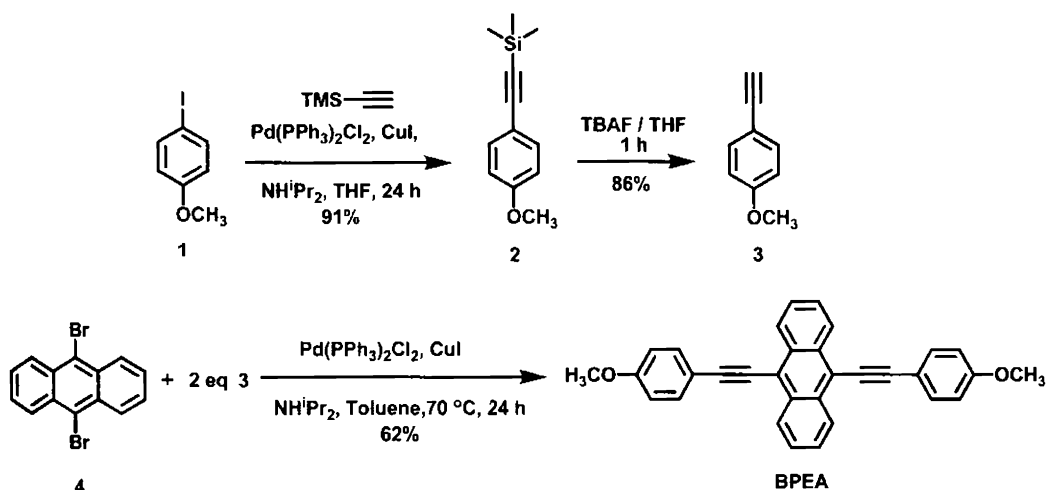
Scheme 2.1. Scheme for the synthesis of BPEA

Compound **8** is required for the synthesis of **BPEA-PT** and **BPEA-PT$_2$**. The

synthesis of **8** is shown in scheme 2.2. **8** was prepared starting from **5**, which on

reaction with 4-iodoanisole gave **6**. **6** on reaction with trimethylsilylacetylene

under Sonogashira coupling condition gave **7**, which was converted to **8**, by the

deprotection with tertrabutylammoniun fluoride in THF.

Scheme 2.2. Scheme for the synthesis of **8**

BPEA-PT₂ was prepared as per Scheme 2.3. Two equivalents of **8** on reaction

with 9,10-dibromoanthracene under palladium catalysed reaction condition gave

BPEA-PT₂ in 49% yield. Along with this 29% of **9** was also formed.
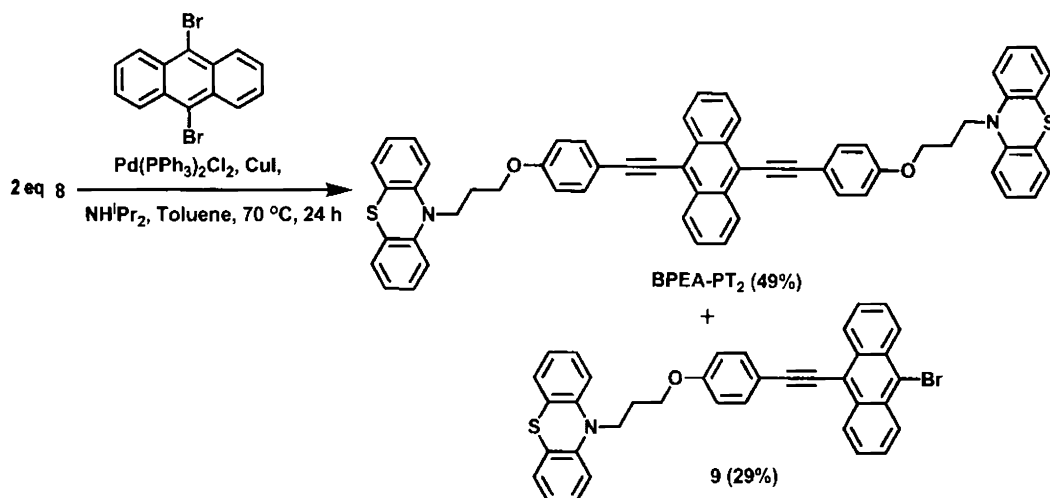
Scheme 2.3. Scheme for the synthesis of **BPEA-PT₂**

The synthesis of **BPEA-PT** is shown in scheme 2.4. Sonogashira coupling reaction

of compound 9 with 4-ethynylanisole gave BPEA-PT in 59% yield.
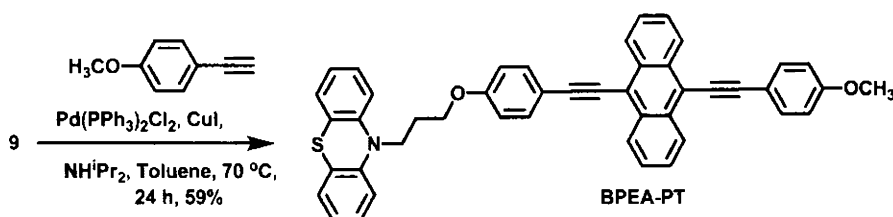
Scheme 2.4. Scheme for the synthesis of **BPEA-PT**

Details of the synthetic procedures are given in the experimental section. The

various intermediates and final products were characterized by analytical and

spectroscopic techniques.

2.3.2. Photophysical and electrochemical studies

The long wavelength absorption due to **BPEA** (R=OCH$_3$) in

dichloromethane (DCM) occurs in the 400-500 nm region (Figure 2.2). Previous

studies suggested that the lowest energy transition in **BPEA** (R=H) is polarized

along the long axis of the molecule.[18] Since the triple bond has cylindrical

symmetry, free rotation about the alkyne-aryl single bond is allowed and results in

the existence of co-planar and twisted structures in equilibrium in solution.[18(c)]

Attaching the **PT** as in **BPEA-PT** and **BPEA-PT$_2$** did not lead to any changes in

the long wavelength absorption band (Figure 2.2). The absorption due to the **PT**

moieties appeared at 250 and 300 nm. Absorption spectra of **BPEA-PT** and

BPEA-PT$_2$ can be obtained by adding the contributions due to the **BPEA** and **PT**

moieties and this suggests that the two chromophores do not interact in the ground state in these molecules. This is also clear from the fact that the long wavelength absorption band is identical for all the three systems and we assume that excitation above 350 nm populates only the **BPEA** excited states.
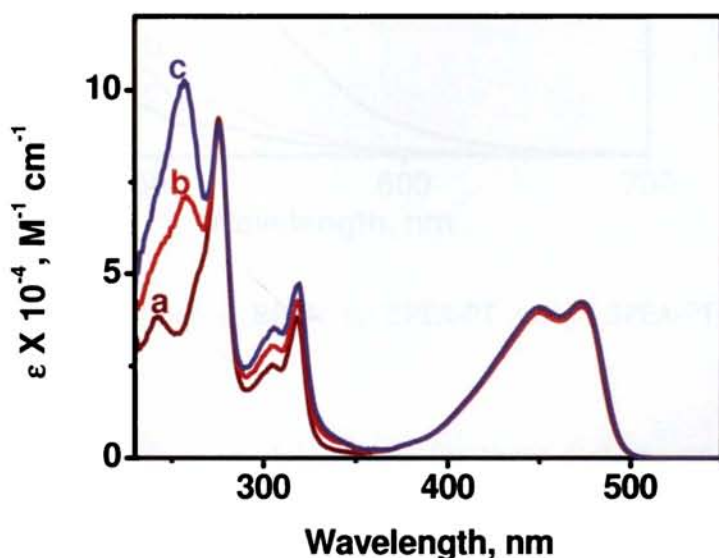
Figure 2.2. Absorption spectra of (a) **BPEA**, (b) **BPEA-PT** and (c) **BPEA-PT₂** in DCM

Fluorescence spectrum of **BPEA** (R=OCH$_3$) is shown in Figure 2.3a. The emission maximum occurs at 490 nm. The Stokes shift observed is very small (775 cm^{-1}) suggesting similar geometry for the S_0 and S_1 states. Using the absorption and emission spectra, the excitation energy (E_{00}) was calculated and the value obtained was 2.57 eV. Substitution of **PT** leads to considerable quenching of the fluorescence intensity as is evident from a comparison of the fluorescence spectra of **BPEA** (R=OCH$_3$), **BPEA-PT** and **BPEA-PT$_2$** shown in Figure 2.3b,c.
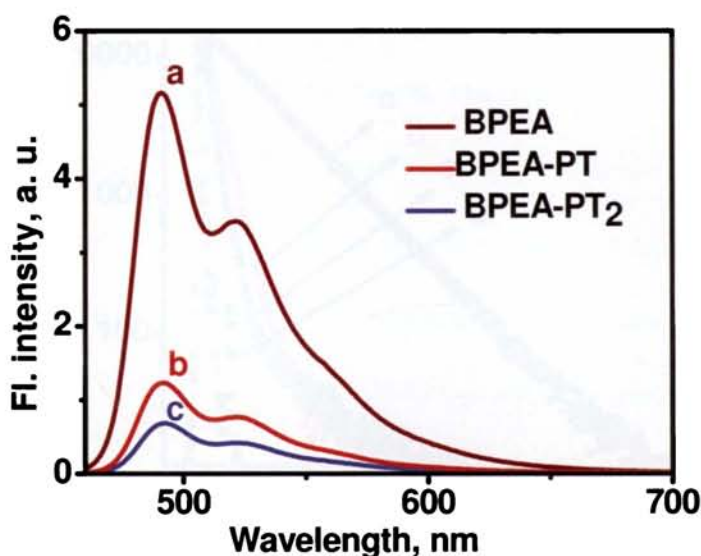
Figure 2.3. Fluorescence spectra of (a) **BPEA**, (b) **BPEA-PT** and (c) **BPEA-PT₂** in DCM. Excitation was at 440 nm

Fluorescence quantum yields were determined for these systems and the values obtained were 0.66, 0.15 and 0.08, respectively, for **BPEA**, **BPEA-PT** and **BPEA-PT₂**. Fluorescence lifetimes were determined using single photon counting technique and the decay profiles obtained are shown in Figure 2.4. For **BPEA** (R=OCH₃), the decay was mono-exponential with a lifetime (τ_0) of 3.04 ns. For **BPEA-PT**, the decay was bi-exponential with $\tau_1 = 0.64$ ns (97%) and $\tau_2 = 3.17$ ns (3%). **BPEA-PT₂** also exhibited bi-exponential decay with $\tau_1 = 0.37$ ns (94%) and $\tau_2 = 3.37$ ns (6%).
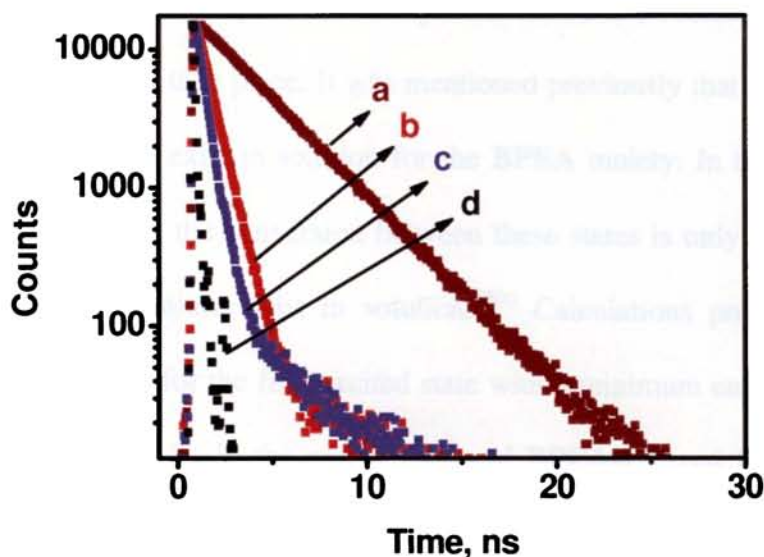
Figure 2.4. Fluorescence decay profiles of (a) **BPEA** (R=OCH₃), (b) **BPEA-PT** and (c) **BPEA-PT₂** in DCM. (d) Lamp profile. Excitation was at 440 nm

It is obvious from Figures 2.3 and 2.4 that **PT** is an efficient quencher of **BPEA** fluorescence. Since the absorption due to **PT** occurs at higher energy compared to **BPEA**, quenching of **BPEA** fluorescence by energy transfer to **PT** is not possible and we can safely assume an electron transfer mechanism for the quenching. The fast decay component τ_1 in **BPEA-PT** and **BPEA-PT₂** arises due to facile electron transfer from **PT** to **BPEA**. The slow decay component τ_2 in these systems is similar to the unquenched fluorescence in **BPEA**, and could arise from a small percentage of **BPEA** present as an impurity. This possibility, however, is ruled out because repeated sample purification using HPLC gave reproducible decay profiles. Also synthesis of **BPEA-PT** and **BPEA-PT₂** did not involve **BPEA** (see synthetic schemes in the experimental section) in any of the steps either as starting material or as product and hence the presence of **BPEA** as impurity is improbable.

The small percentage of unquenched decay is attributed to a conformational isomer in which PET did not take place. It was mentioned previously that twisted and co-planar conformations exist in solution for the **BPEA** moiety. In the ground state the energy barrier for the conversion between these states is only 1.4 kJ M^{-1} and hence both conformations exist in solution.[18(c)] Calculations predicted a much deeper potential well for the first excited state with a minimum energy for the co-planar conformation. So in the excited state of **BPEA-PT** and **BPEA-PT$_2$**, the **BPEA** moiety would be planar and conformational isomers will most probably arise due to flexibility of the alkyl linker which would place the **PT** moiety at different locations with respect to the **BPEA** unit. In the optimized structure of **BPEA-PT$_2$** shown in Figure 2.1, the aryl rings in the **PT** are symmetrically placed on both sides with respect to the **BPEA** plane, with the *N* atoms in the plane. The interaction between the donor and acceptor units would be maximum in such a configuration. Studies with molecular models show that extreme conformations in which the **PT** unit is placed on one side of the plane, are also probable. A small fraction of such conformations may be responsible for the bi-exponential decay. Bi-exponential decays due to the presence of conformers were proposed in several D-A systems earlier.[19]

Redox potentials of the compounds (vs SCE) were measured in DCM using square wave voltammetry. **BPEA** (R=OCH$_3$) exhibited oxidation peak at 0.96 V and reduction peak at -1.46 V. Linking **PT** moieties did not change the **BPEA**

centered redox potentials but a new peak corresponding to **PT/PT$^{\bullet+}$** oxidation

appeared at 0.75 V for **BPEA-PT** and at 0.72 V for **BPEA-PT$_2$** (Figure 2.5).

Thus in the dyads studied here the **BPEA** chromophore acts as the excited state

electron acceptor and the **PT** acts as the ground state electron donor. The free

energy change associated with the PET process can be calculated using the Weller

equation.[20]

$$\Delta G_{PET} = F(E_{ox} - E_{red}) - E_{00} - e^2/\varepsilon_s\, d_{cc} \qquad (2.1)$$

F is the Faraday constant, E_{ox} is the oxidation potential of **PT**, E_{red} is the **BPEA**

centred reduction potential and ε_s is the solvent dielectric constant. Since the value

of d_{cc} is very large, the last term in equation 2.1 was neglected and we obtained

ΔG_{PET} values of -0.36 eV for **BPEA-PT** and -0.39 eV for **BPEA-PT$_2$**. Thus PET is

exergonic in the **BPEA-PT** systems and upon excitation in the lowest energy band

we expect the following processes to take place.

$$\text{BPEA–PT} \xrightarrow{\quad h\nu > 350\ nm \quad} {}^1\text{BPEA}^*\text{–PT} \qquad (2.2)$$

$${}^1\text{BPEA}^*\text{–PT} \xrightarrow{\quad ET \quad} {}^{\bullet-}\text{BPEA–PT}^{\bullet+} \qquad (2.3)$$

$${}^{\bullet-}\text{BPEA–PT}^{\bullet+} \xrightarrow{\quad BET \quad} \text{BPEA–PT} \qquad (2.4)$$
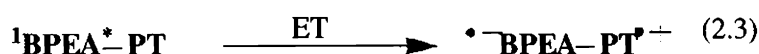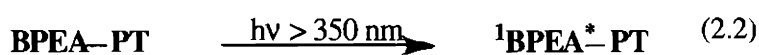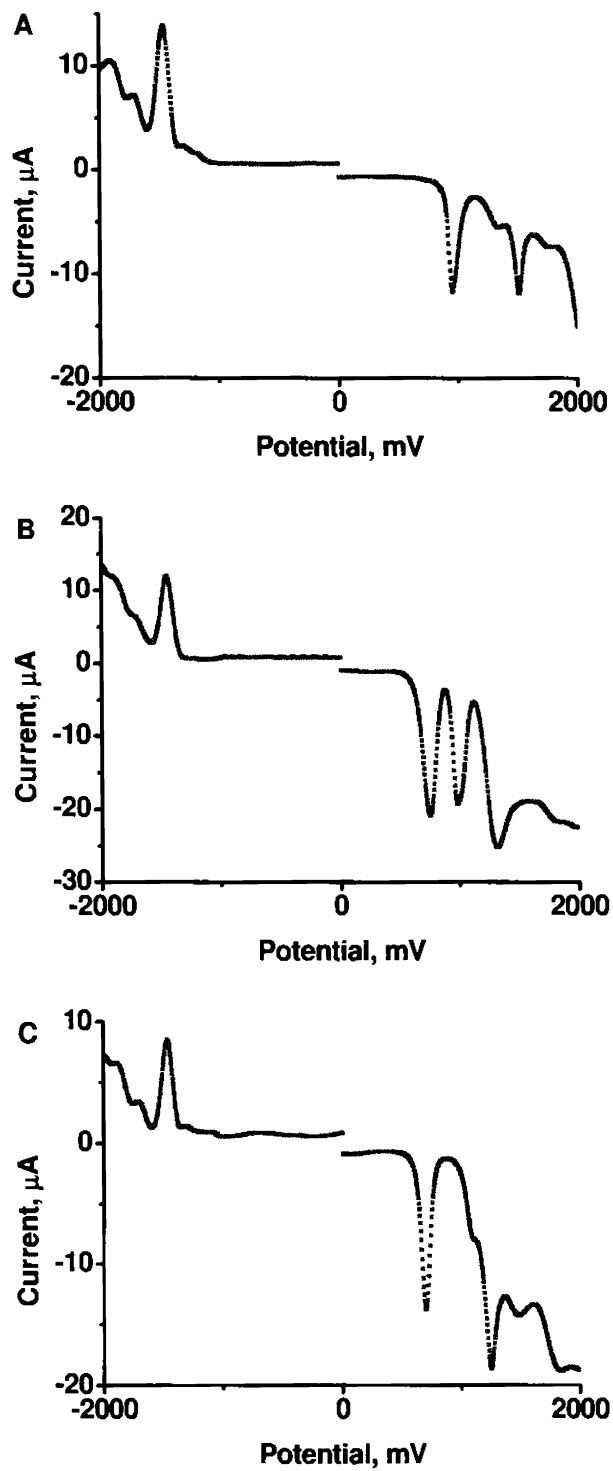
Figure 2.5. S wave voltammogram of (A) **BPEA**, (B) **BPEA-PT** and (C) **BPEA-PT₂** in DCM

The rate constant for the PET reaction can be calculated from the fluorescence quantum yields using equation 2.5.

$$k_{PET} = \frac{1}{\tau_0}\left(\frac{\Phi_{BPEA}}{\Phi_{DYAD}} - 1\right) \qquad (2.5)$$

We obtained k_{PET} values of 1.12×10^9 s^{-1} and 2.38×10^9 s^{-1}, respectively, for **BPEA-PT** and **BPEA-PT$_2$**. k_{PET} values can also be calculated from the fluorescence lifetime data using equation 2.6.

$$k_{PET} = \frac{1}{\tau_f} - \frac{1}{\tau_0} \qquad (2.6)$$

Using equation 2.6 we obtained k_{PET} values of 1.23×10^9 s^{-1} and 2.37×10^9 s^{-1}, respectively, for **BPEA-PT** and **BPEA-PT$_2$**. k_{PET} values calculated using the two expressions agree very well. It is to be noted that k_{PET} value doubles when the number of **PT** moieties increases from one to two. Quantum yield for PET was calculated using the k_{et} values ($\Phi_{et} = k_{et}\tau$) and we obtained values of 0.79 and 0.88 for **BPEA-PT** and **BPEA-PT$_2$**, respectively (the fast decay component was used for this calculation), which indicated that PET is very efficient in these systems.

2.3.3. Femtosecond flash photolysis studies

In order to gain a deeper understanding of the excited state processes all the **BPEA** systems were subjected to femtosecond flash photolysis studies in deaerated DCM solution. The transient absorption spectra obtained in the case of **BPEA** (Figure 2.6) exhibited bleaching below 520 nm and absorption maximum at

570 nm. Decay time of the transient (inset in Figure 2.6) was the same as the fluorescence lifetime of **BPEA** and hence we safely assign the transient to the $S_1 \rightarrow$ S_n absorption of **BPEA**. It is to be noted that the transient exhibited a monotonous decay at all wavelengths and growth components indicating formation of a triplet excited state is absent in the transient spectrum.
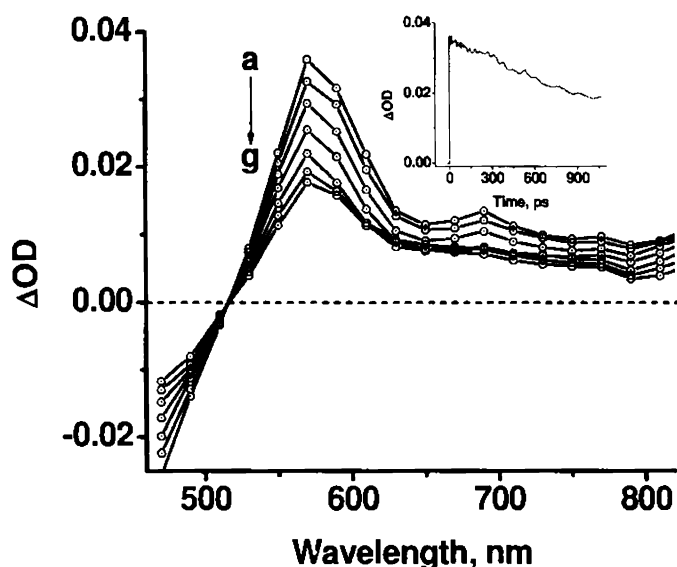
Figure 2.6. Femtosecond transient absorption spectra obtained in flash photolysis of **BPEA** in DCM (a) 50ps, (b) 100 ps, (c) 200 ps, (d) 400 ps, (e) 600 ps, (f) 800 ps and (g) 1 ns. Inset shows decay of the transient at 570 nm

Figure 2.7 shows the transient absorption spectra obtained in the femtosecond flash photolysis of **BPEA-PT** and **BPEA-PT₂** systems. In the case of **BPEA-PT**, decay of the $S_1 \rightarrow$ S_n absorption (shown in the inset of Figure 2.7A) was fitted to a single exponential and we obtained a lifetime of 670 ps, which was close to the fast fluorescence decay component (0.64 ns). At higher time scales

formation of a transient absorption at 510 nm and also around 640 nm is indicated.

In the case of **BPEA-PT$_2$** decay of the $S_1 \rightarrow S_n$ absorption at 570 nm (shown in the

inset of Figure 2.7B) occurs at a time scale matching the fast fluorescence decay

component. The transient exhibits bleaching below 530 nm at very short time

scales but formation of a transient with absorption at 510 nm and isosbestic point

at 530 nm is observed. In the 620-700 nm region the transient absorption intensity

showed relatively minor change. The $S_1 \rightarrow S_n$ absorption has reasonably good

intensity in this region and the relatively small intensity change suggests that a new

transient is forming in this region at a rate nearly matching with the decay of the

singlet state. In the case of **BPEA-PT$_2$** the sub-nanosecond transient absorption

spectra suggest decay of the singlet and concomitant growth of transient

absorptions at 510 and 660 nm. In the case of **BPEA-PT** also, growth of transients

are indicated in 510 and 660 nm regions, but the growth is not complete most

probably due to the comparatively low k_{PET} value in this case.
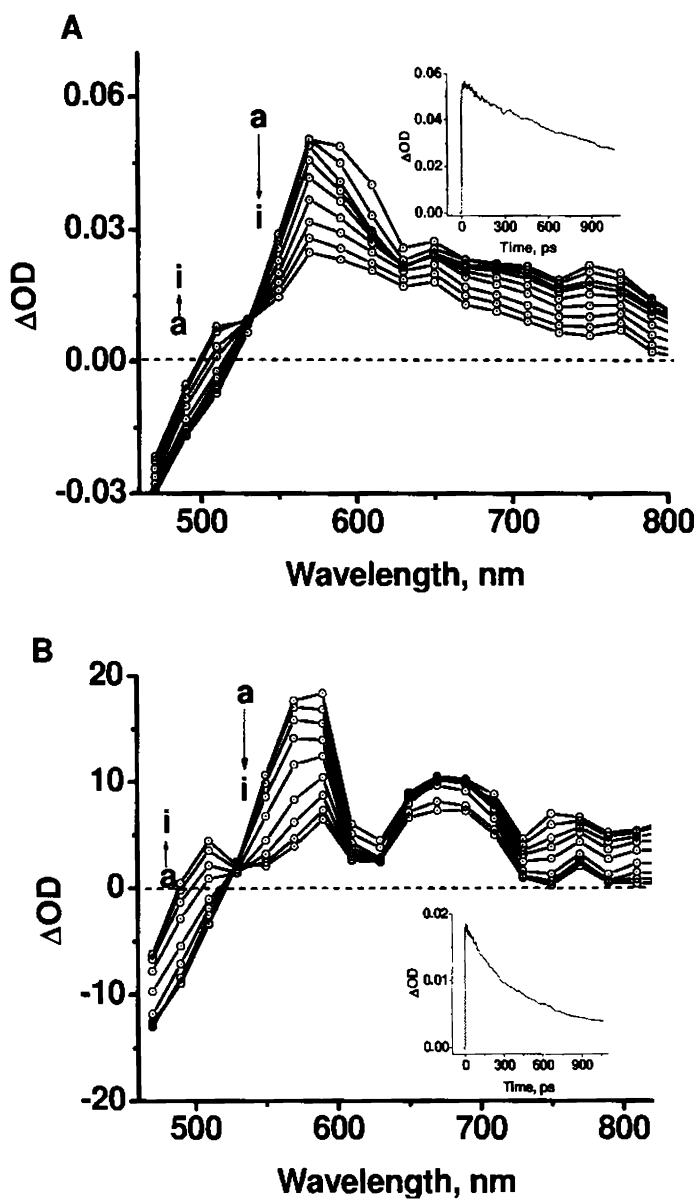
Figure 2.7. Sub-nanosecond transient absorption spectra obtained in the flash photolysis of (A) **BPEA-PT** and (B) **BPEA-PT₂** systems in DCM (a) 10 ps, (b) 20 ps, (c) 50 ps, (d) 100 ps, (e) 200 ps, (f) 400 ps, (g) 600 ps, (h) 800 ps and (i) 1 ns after the excitation. Insets show decays of the transients at 570 nm

2.3.4. Nanosecond flash photolysis studies

Nanosecond transient absorption measurements were performed on all three

substrates in deaerated DCM solution. Upon excitation using 355 (Nd-YAG, 3rd

harmonic) or 426 nm (Nd-YAG laser pumped dye laser), **BPEA** did not exhibit

any transient absorption in the nanosecond time scale. The fluorescence quantum

yield of **BPEA** ($R=OCH_3$) is 0.66. Since no transient absorption is observed it is

assumed that the remaining fraction of **BPEA** S_1 states undergo non-radiative

decay to the ground state and the propensity for intersystem crossing to the triplet

is very low. This is in accordance with the results obtained by Levitus and Garcia-

Garibay, who concluded that intersystem crossing does not play a significant role

in the photophysics of **BPEA** ($R=H$).[18(a)] Although the triplet of **BPEA** could not

be obtained by direct excitation, it could be generated through sensitization

experiments.[21] Figure 2.8 shows the transient absorption spectrum obtained upon

excitation of benzophenone in the presence of **BPEA** ($R=OCH_3$) in DCM. Under

the experimental conditions most of the light is absorbed by benzophenone to form

its triplet state which undergo energy transfer to generate the **BPEA** triplet state.

The absorption band at short time in Figure 2.8 corresponds to benzophenone

triplet state and the spectrum obtained at long time scales are assigned to **BPEA**

triplet. The **BPEA** triplet so generated exhibited absorption maximum at 490 nm

and decayed with lifetime of 10 μs.
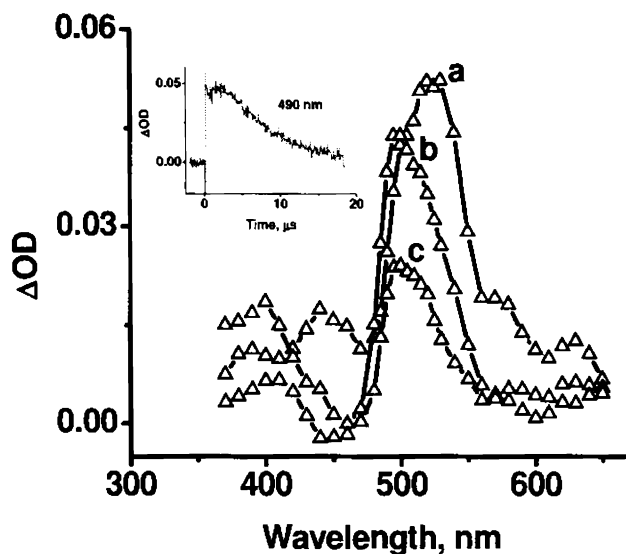
Figure 2.8. Transient absorption spectra obtained upon excitation of benzophenone (5 × 10⁻³ M) in the presence of **BPEA** (5 × 10⁻⁵ M) (a) 200 ns (b) 3 μs and (c) 7 μs after the laser pulse. Inset shows the kinetic trace at 490 nm

In contrast to **BPEA**, **BPEA-PT** and **BPEA-PT₂** exhibited long-lived transient absorptions in the nanosecond timescale (Figure 2.9). In both cases the transient absorption spectra exhibited maxima at 515 and 640 nm. Under deaerated conditions decays of both the absorptions were similar and exhibited a lifetime of 36 μs. According to equations 2.2 and 2.3, excitation of **BPEA-PT** leads to electron transfer to generate the CS state and one can assign the transient absorption spectra to the CS state. In fact femtosecond transient absorption studies indicated formation of these two transient absorptions directly from the singlet excited state of the **BPEA** moiety. A large number of studies are available with **PT** as electron donor and the **PT•⁺** is known to have absorption maxima in the 510-520

nm region.[16] Albinsson and co-workers have used **BPEA** as an acceptor component in PET reactions and observed **BPEA**$^{\bullet-}$ around 600-650 nm.[15(c)] They also generated **BPEA**$^{\bullet-}$ spectroelectrochemically in DMF and observed an absorption band centered around 630 nm. Based on these literature reports we assign the absorption at 515 nm to **PT**$^{\bullet+}$ and the 640 nm absorption to **BPEA**$^{\bullet-}$. These absorptions are very long-lived ($\tau = 36$ μs) and decay by BET process, for which we obtained a rate constant ($k_{BET} = 1/\tau$) of 2.78×10^4 s^{-1}. Thus the ratio of the forward and reverse electron transfer steps (k_{PET}/k_{BET}) exceeds 10^4 in the **BPEA-PT** systems. Quantum yields of charge separation (Φ_{CS}) were also determined and we obtained values of 0.36 and 0.42 for **BPEA-PT** and **BPEA-PT$_2$**, respectively. Φ_{CS} were nearly 50% of Φ_{et} values indicating that more than 50% of the radical ions formed in the PET reaction underwent fast BET reaction to regenerate the ground state and the remaining fraction survived to give the long-lived CS state. Kinetic traces in Figure 2.9 suggest that a fraction of the transients survived even after 200 μs. We assign this residual absorption to a small fraction (~15%) of extremely long-lived CS state (vide infra).
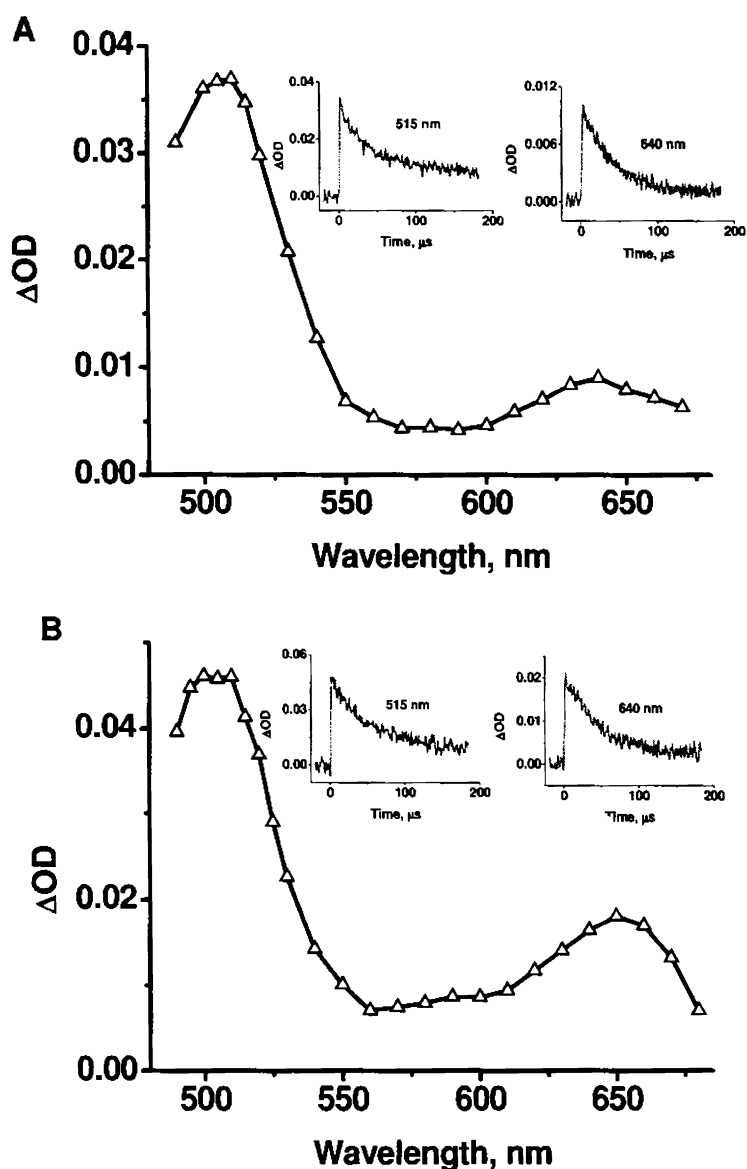
Figure 2.9. Transient absorption spectra of (A) **BPEA-PT** and (B) **BPET-PT₂** systems immediately after the laser pulse. The insets show decay profiles

PET processes in a large number of dyads were studied in the past and typical lifetimes in fluid solution for CS states were found to be of the order of a few hundred picoseconds to few nanoseconds.[9(e),9(f)] In dyad systems the ratio

k_{PET}/k_{BET} rarely exceed 10,000 fold.[9(e)] A few dyads with k_{PET}/k_{BET} >> 10^5 were

reported recently and in all these cases the inverted region effects were proposed as

the reason for the large k_{PET}/k_{BET} values.[7,8] In a series of papers Harriman,

Verhoeven and co-workers have re-examined the claims and reported serious flaws

in some of the interpretations.[9] These authors proposed that a dyad with k_{PET}/k_{BET} >

5000 can be called "unusually long-lived", but suggested several criteria that must

be fulfilled before claiming the status.[9(d)] In the **BPEA-PT** systems we report here

k_{PET}/k_{BET} >> 5000, and hence the CS states in these systems qualify to be named

unusually long-lived. In the light of all the controversy currently existing in the

literature, it appears essential for us to reconfirm the assignments of the long-lived

transient absorptions. In the following section an attempt is made in that direction.

The **BPEA-PT** systems studied here follow most of the criteria put forward

by Harriman and Verhoeven. **PT**[•+] and **BPEA**[•−] were known previously in the

literature and the absorption maxima obtained in the nanosecond flash photolysis

studies are consistent with previous reports. In deaerated solution both the transient

absorptions decayed at the same rate as would be expected for a BET reaction

between **PT**[•+] and **BPEA**[•−]. In the presence of oxygen, decay behaviors of the

transients were different and this is shown in Figure 2.10. It is well known that

radical anions are quenched efficiently by oxygen whereas radical cations are

relatively unaffected. Insets in Figure 2.10 show that in the presence of oxygen the

absorption assigned to **BPEA**[•−] decayed rapidly and decay of the absorption

assigned to **PT$^{\bullet+}$** slowed down considerably. It is very clear that the two absorption

maxima correspond to different chromophores.
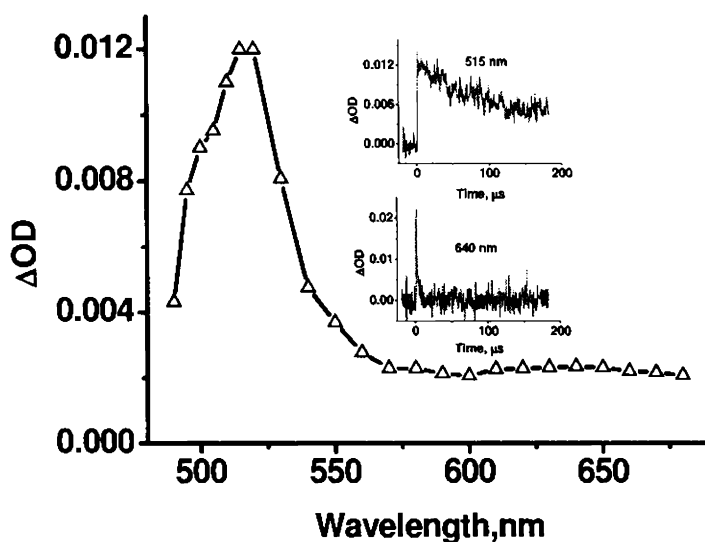
Figure 2.10. Transient absorption spectra of **BPEA-PT$_2$** in the presence of oxygen at 10 µs after the laser pulse. Insets shows decay profiles of transients at 515 and 640 nm

Since the radical ions are long-lived, they can be involved in exergonic

electron transfer reactions with better donors or acceptors. For example tris(4-

methoxyphenyl)amine (**TMPA**, E_{ox} = 0.57 V vs SCE in DCM) is a better electron

donor than **PT** (E_{ox} = 0.72 V vs SCE) and hence ET as shown in equation 2.7 is

feasible with ΔG = -0.15 eV.

$$^{\bullet-}\text{BPEA-PT}^{\bullet+} + \text{TMPA} \xrightarrow{\quad \text{ET} \quad} {}^{\bullet-}\text{BPEA-PT} + \text{TMPA}^{\bullet+} \qquad (2.7)$$

TMPA$^{\bullet+}$ is well characterized in the literature with absorption maximum at 720

nm.[22] Figure 2.11 shows the time dependent transient absorption spectra of **BPEA-**

PT$_2$ in the presence of **TMPA** in deaerated DCM solution. The spectrum at short time scales show absorptions due to **PT$^{\bullet+}$---BPEA$^{\bullet-}$**. At longer time scales decay of the transient at 515 nm assigned to **PT$^{\bullet+}$** along with concomitant formation of a transient at 720 nm assignable to **TMPA$^{\bullet+}$** is observed. Insets in Figure 2.11 show the decay profile of **PT$^{\bullet+}$** at 515 nm and a matching growth profile of **TMPA$^{\bullet+}$** at 720 nm. It is very clear from Figure 2.11 that electron transfer occurs from **TMPA** to **PT$^{\bullet+}$** leading to the formation of **TMPA$^{\bullet+}$**.
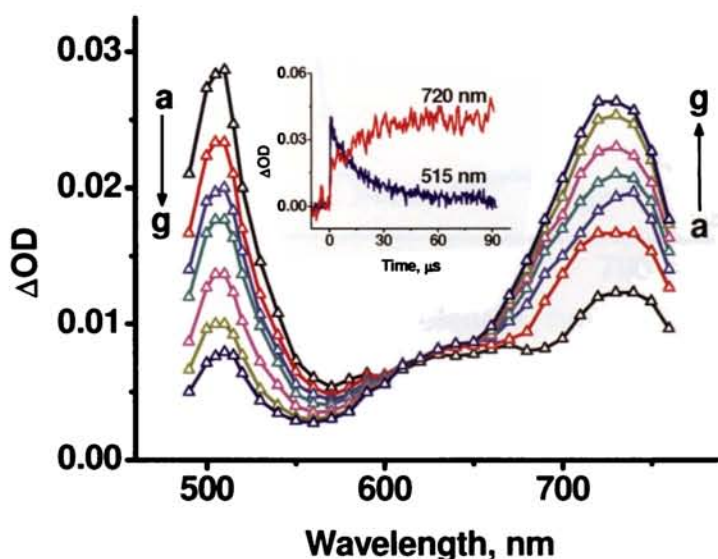
Figure 2.11. Transient absorption spectra of **BPEA-PT$_2$** in the presence of **TMPA** (2×10^{-4} M) in deaerated DCM solution, (a) 5, (b) 10, (c) 15, (d) 20, (e) 30, (f) 40 and (g) 50 µs after excitation

The **BPEA$^{\bullet-}$** side of the CS state can also participate in intermolecular ET reactions. *N,N*-di-*n*-octylpyromellitic diimide (**PI**, E_{red} = -0.86 V vs SCE in DCM) was selected for this purpose. Figure 2.12 shows the transient absorption spectra of **BPEA-PT$_2$** in the presence of **PI** at 5 µs after the laser flash. Absorption due to

PI$^{\bullet-}$ occurs at 720 nm[23] and this is seen in Figure 2.12. Since the absorptions due to

BPEA$^{\bullet-}$ and PI$^{\bullet-}$ occur in nearly the same region, decay and growth profiles were

not as clear as in Figure 2.11. These results suggest secondary electron transfer

taking place as shown in equation 2.8.

$$^{\bullet-}\text{BPEA}\!-\!\text{PT}^{\bullet+} + \text{PI} \xrightarrow{\quad\text{ET}\quad} \text{BPEA}\!-\!\text{PT}^{\bullet+} + \text{PI}^{\bullet-} \qquad (2.8)$$
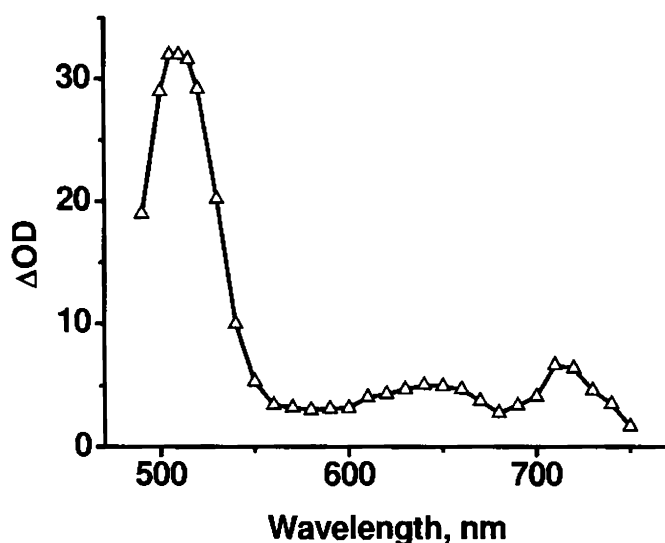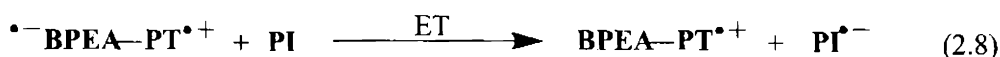
Figure 2.12. Transient absorption spectra of **BPEA-PT₂** in the presence of PI (2 × 10⁻⁴ M) in deaerated DCM solution, 5 μs after excitation

Based on data presented in Figures 2.10-2.12, we reconfirm our assignments and

claim the formation of long-lived CS states in the flash photolysis of **BPEA-PT**

and **BPEA-PT₂**. Previously we attributed the residual absorptions seen in Figure

2.9 to a small fraction of extremely long-lived CS states. Kinetic traces shown in

Figures 2.10 and 2.11 support this assignment. Note that in the presence of oxygen

the transient absorption due to **BPEA$^{\bullet-}$** decays completely (inset of Figure 2.10).

Similarly the absorption due to **PT**•+ at 515 nm decays completely in the presence

of **TMPA** (inset of Figure 2.11). Complete decay of these transients would not

have been possible if permanent products were formed in the photolysis. As

mentioned previously the linkage between **BPEA** and **PT** is very flexible and

several conformations are possible. In those conformations where the ET partners

are close together, PET will be followed by rapid BET. We observed that Φ_{CS} is

only half of Φ_{et}, indicating that BET is very facile in 50% of the excitations.

Likewise we can assume that there are conformations where BET would be

extremely slow due to distance or orientational factors and in these cases

extremely long-lived CS states can result.

We attribute the long lifetime of the CS state to inverted region effects.

According to Marcus theory the rate constant for electron transfer in non-adiabatic

donor-acceptor systems is given by equation 2.9.[6]

$$k_{et} = (2\pi/\hbar)\, H_{el}^2\, (4\pi\lambda k_B T)^{-1/2}\, \exp[-(\lambda + \Delta G^0)^2/4\lambda k_B T] \qquad (2.9)$$

$\hbar$ is the Planck's constant divided by 2π, H_{el} is the electronic coupling matrix

element between the donor and acceptor, k_B is the Boltzmann constant and T is the

temperature. This equation predicts that in the deep inverted region where $-\Delta G^0$

$\gg \lambda$, k_{et} will be very low. For the BET reaction between **BPEA**•- and **PT**•+ the ΔG^0

value is highly negative at -2.18 eV for **BPEA-PT** and -2.23 eV for **BPEA-PT$_2$**.

The reorganization energy λ is the sum of λ_o and λ_i. The outer sphere

reorganization energy λ_o depends on the radii of the donor (r_D) and acceptor (r_A),

the center-to-center distance d_{cc} and the optical (ε_{op}) and static (ε_s) dielectric

constants of the solvent as given in equation 2.10.

$$\lambda_0 = \Delta e^2 \left(\frac{1}{2r_A} + \frac{1}{2r_D} - \frac{1}{d_{cc}} \right) \left(\frac{1}{\varepsilon_{op}} - \frac{1}{\varepsilon_s} \right) \qquad (2.10)$$

Since the donor and acceptor moieties are not spherical, an approximate radius =

½(length × breadth)$^{1/2}$ was assumed. Using these values we obtained λ_0 = 0.88 eV

in DCM. **BPEA** is a very rigid organic molecule for which we can assume a low

value of λ_i = 0.1 eV. In the case of **PT**, oxidation to **PT**$^{\bullet+}$ leads to substantial

conformational changes that involve bending of the ring systems. λ_i values

reported for **PT** → **PT**$^{\bullet+}$ oxidation is in the 0.2 – 0.27 eV range.[24] Using 0.27 eV

we get total λ_i = 0.37 eV. Thus the total reorganization energy for the BET process

would be 1.25 eV, which is approximately 1.0 eV lower than $-\Delta G^0$, pushing the

system into the deep inverted region.

The presence of inverted region kinetics in charge shift and charge

recombination reactions was unequivocally established by several research

groups.[25] In almost all these cases, however, the slowest rate observed in the

inverted region was ≥ 10^8 s^{-1}. A general observation is that when $-\Delta G_{BET}$ is very

large other deactivation channels such as jumps to low lying local triplet levels

may prevail over charge recombination to the ground state.[9(f)] Nuclear tunneling

also becomes very important and it is suggested that equation 2.9 may not

adequately describe electron transfer in the deep inverted region.[26] Hence it is

essential to get a detailed picture of the energy level diagram for the **BPEA-PT** systems. Energies of the lowest excited singlet and CS states of **BPEA-PT** were placed respectively, at 2.56 and 2.18 eV. The triplet energy of **PT** in non-polar solvents is 253 kJ M^{-1} (2.62 eV).[27] For **BPEA** the triplet energy level (E_T) is not known with certainty because the phosphorescence spectrum is not accessible by direct excitation. Using sensitization experiments Fang et al. placed the E_T of **BPEA** between 1.38 – 1.82 eV.[21] Albinsson and co-workers found that ^{3}**BPEA*** can be generated through energy transfer from zinc porphyrin triplet and placed the ^{3}**BPEA*** in the range 1.36 – 1.74 eV.[15(e)] In Figure 2.13 we have presented the energy level diagram for **BPEA-PT** where we placed ^{3}**BPEA*** at 1.74 eV.
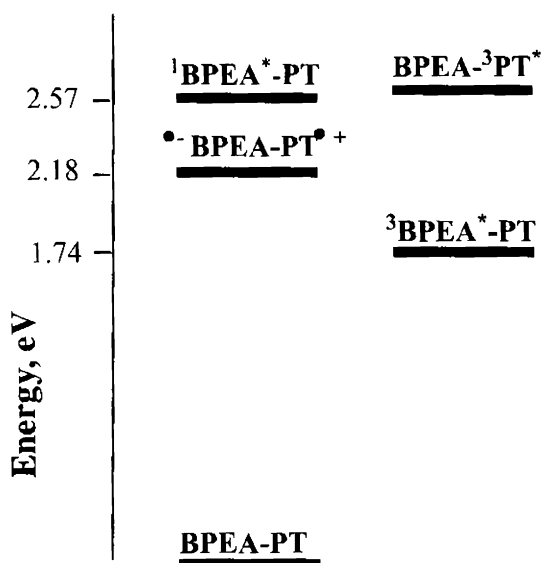
Figure 2.13. Energy level diagram for **BPEA-PT**

^{3}**BPEA*****-PT** is below the CS state and decay of the CS state to local triplet state appear very probable. Hence it can be argued that the short wavelength absorption seen in Figure 2.9 is actually ^{3}**BPEA*****-PT** and not **PT**$^{\bullet+}$. Several arguments can be cited against this assignment. First of all we have presented the T-T absorption spectrum of ^{3}**BPEA*** in Figure 2.8, which does not show the peak at 640 nm present in Figure 2.9. Lifetimes of the transients in Figures 2.8 and 2.9 were also different. Formations of **TMPA**$^{\bullet+}$ and **PI**$^{\bullet-}$ in the flash photolysis experiments in Figures 2.11 and 2.12 also do not support the triplet assignment. If **TMPA**$^{\bullet+}$ and **PI**$^{\bullet-}$ were to form from ^{3}**BPEA***, the following reactions should occur.

$$^3\textbf{BPEA}\text{-- PT} + \textbf{TMPA} \xrightarrow{\quad ET \quad} {}^{\bullet-}\textbf{BPEA-PT} + \textbf{TMPA}^{\bullet+} \qquad (2.11)$$

$$^3\textbf{BPEA}\text{-- PT} + \textbf{PI} \xrightarrow{\quad ET \quad} {}^{\bullet+}\textbf{BPEA-PT} + \textbf{PI}^{\bullet-} \qquad (2.12)$$

ΔG^0 values will be +0.24 and +0.08 eV for reactions 2.11 and 2.12, respectively, if $E_T = 1.74$ eV is used for ^{3}**BPEA***. Note that 1.74 eV is the maximum limit for E_T[15(e)] and ΔG^0 values will be more positive if lower E_T values are used. If these reactions were occurring, additional peaks corresponding to **BPEA**$^{\bullet-}$ would be present in Figures 2.11 and peaks corresponding to **BPEA**$^{\bullet+}$ would be present in Figure 2.12. Such peaks were absent in the above figures. The most convincing evidence against the triplet assignment is the insensitivity of the 515 nm peak (in Figure 2.9) to the presence of oxygen. This peak would have disappeared in the presence of oxygen if it were a triplet. Based on these arguments we rule out the

triplet state assignment to the transients in Figure 2.9. Although we rule out decay

of the CS state to ^{3}**BPEA*-PT** the reason for its absence is not clear to us. The

triplet state of **BPEA** could not be populated by direct excitation, which means that

ISC from ^{1}**BPEA*-PT** to ^{3}**BPEA*-PT** is forbidden. Perhaps the same

forbiddenness may be present in the CS state also.

Verhoeven, Harriman and co-workers attributed the long lifetime of the CS

state in the compact zinc chlorine-C_{60} dyad to triplet character of the CS state.[9(f)] If

the CS state has triplet character, inverted region effects need not be invoked and

long lifetime of CS state can be attributed to spin restriction factors on charge

recombination. Based on this it can be argued that the CS state observed here has

triplet character. This argument, however, is not consistent with the energy level

diagram shown in Figure 2.13. Verhoeven, Harriman and co-workers have

discussed this aspect in detail and they emphasized that a triplet character can be

assigned to a long-lived CS state if and only if this state is the lowest triplet state of

the dyad as a whole.[9(f)] If any local triplet state is available below the ^{3}CS state,

then a spin-allowed (and hence very fast) decay of the ^{3}CS state to the local triplet

state would be observed. According to this paradigm one can put the ^{3}CS state in

the **BPEA-PT** system only below 1.74 eV, which is the energy level for ^{3}**BPEA-**

PT. The ^{1}CS state in **BPEA-PT** is at 2.18 eV and if we place the ^{3}CS state below

1.74 eV, the singlet - triplet splitting in the CS state would be nearly 0.4 eV, which

is a very unrealistic situation. The singlet – triplet splitting within radical ion pairs

is given by the magnitude of the spin-spin exchange interaction $2J$, which actually

is a very small value. Hence we rule out the involvement of ^3CS state in **BPEA-PT**

systems.

Based on the arguments presented above a scheme summarizing the

dynamics and energetics for the **BPEA-PT** system is presented in Figure 2.14.

Excitation of the **BPEA** chromophore leads to ^{1}**BPEA*-PT**, where the excitation

is localized on **BPEA**. The excited chromophore can undergo fluorescence decay

to the ground state or accept an electron from **PT** to generate the ^1CS state,

$^-$**BPEA-PT**$^{\bullet+}$. ^{1}**BPEA*-PT** and **BPEA-**^{3}**PT*** are nearly isoenergetic, but

transitions between the two states are forbidden due to spin restrictions.

Intersystem crossing is very inefficient in **BPEA** systems and hence the ^{3}**BPEA-**

PT state is not populated at all. In principle, $^{\bullet}$**BPEA-PT**$^{\bullet+}$ formed can decay to the

local triplet ^{3}**BPEA-PT**, but this transition does not take place. The only

deactivation pathway available to $^{\bullet}$**BPEA-PT**$^{\bullet+}$ is BET to the ground state and

because of the inverted region effect, this process is very slow. We propose that

the inefficiency of the ^1CS state to undergo intersystem crossing to ^3CS or to local

triplet states most probably is the reason for observing the long-lived CS state in

these systems.
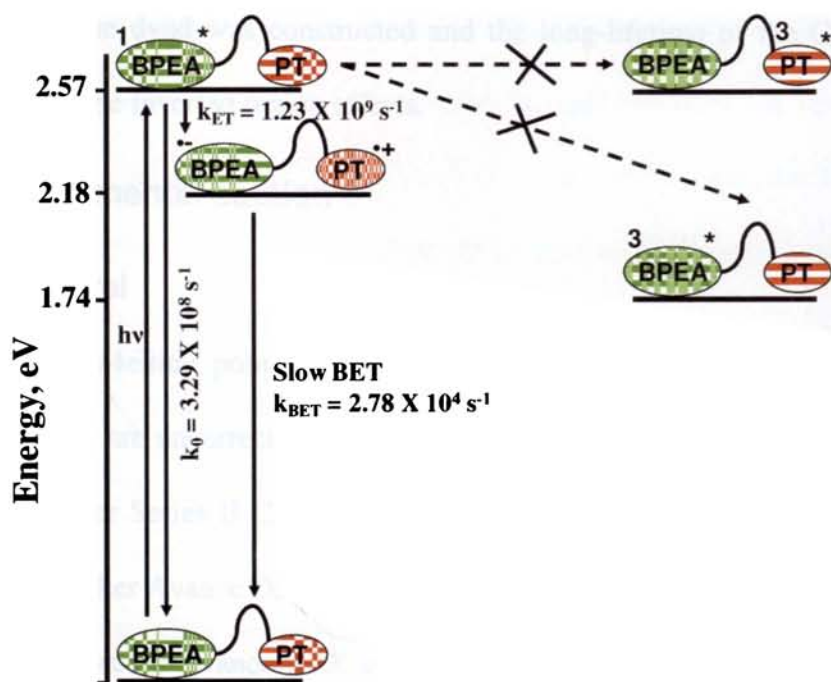
Figure 2.14. Schematic representation of various photophysical processes in **BPEA-PT**

2.4. Conclusions

Here we have investigated the PET processes in two **BPEA-PT** dyads using steady state and time resolved absorption and emission techniques. Absorption spectra of the dyads indicated the absence of any ground state interactions between **BPEA** and **PT** moieties. Fluorescence of the **BPEA** moiety is highly quenched in the dyads due to facile electron transfer from the **PT** unit. The rate constants and quantum yields of the PET process were determined. Femtosecond and nanosecond transient absorption studies suggested formation of long-lived CS states in these dyads. Assignment of the transient spectra to the CS state was confirmed by additional experiments. Based on available data energy level

diagram of the dyad was constructed and the long-lifetime of the CS state was attributed to the inverted region effects.

2.5. Experimental section

2.5.1. General

Melting points were determined on a Mel-Temp II melting point apparatus and are uncorrected. Elemental analysis experiments were performed on a Perkin Elmer Series II CHN analyzer. Proton NMR data were obtained from a 300 MHz Bruker Avance DPX spectrometer. ^{13}C NMR spectra were recorded using a 500 MHz Bruker Avance DPX spectrometer. FT-IR spectra were recorded on a Shimadzu IR Prestige 21 spectrometer. High-resolution mass spectra were obtained by using a JOEL JMS600 mass spectrometer. Absorption spectra were obtained using a Shimadzu 3101PC UV/Vis-NIR scanning spectrophotometer. Steady state fluorescence experiments were performed with a SPEX Fluorolog F112X spectrofluorimeter by using optically dilute solutions. The fluorescence quantum yields in dichloromethane were determined with relative method employing an optically matched solution of **BPEA** in chloroform as reference (Φ_R = 0.64).[28] The following equation was used,

$$\Phi_F = \Phi_R \frac{A \; OD_R \; n^2}{A_R \; OD \; n_R^2} \qquad (2.13)$$

where, the subscript R refers to the reference, OD is the optical density at the excitation wavelength (OD $\approx$ 0.1 at 440 nm for both reference and standard), n is the refractive index of the solvent and A is the area under the fluorescence spectrum. Electrochemical experiments were performed by using a BAS 50W voltammetric analyser. Solutions of the compounds (1 $\times$ 10^{-3} M) in dichloromethane containing 0.1 M tetra-n-butylammonium hexafluorophosphate were thoroughly deaerated and used for CV experiments. Time-resolved fluorescence experiments were performed by using an IBH picosecond single-photon counting system employing a 440 nm Nano-LED excitation source and a Hamamatsu C4878-02 micro channel plate (MCP) detector. Nanosecond laser flash photolysis experiments were performed by using an Applied Photophysics Model LKS-20 laser kinetic spectrometer by using the third harmonic (355 nm) from a GCR-12 series Quanta Ray Nd:YAG laser or by using a Sirah pulsed Dye Laser CBR-P. The compounds were excited at 426 nm using the emission from Exalite 428 dye. The third harmonic (355 nm) from an INDI-40-10-HG Quanta Ray Nd: YAG laser was used to pump the dye laser. The analysing and laser beams were fixed at right angles to each other. Quantum yields of the CS (Φ_{CS}) states were determined by relative actinometry employing a solution of benzophenone (BP) in benzene as reference. The following equation was used,[29]

$$\Phi_M = \Phi_R \ \frac{\Delta OD_M \ \varepsilon_R}{\Delta OD_R \ \varepsilon_M} \qquad (2.14)$$

in which the subscript M refers to the charge separated state and R refers to BP, ΔOD is the end-of-pulse optical density of transients and ε the extinction coefficients of transients. For BP, values of $\Phi_R = 1.0$ and $\varepsilon_R = 7600 \ M^{-1}cm^{-1}$ at 530 nm were used.[30] For the calculation of Φ_{CS}, known extinction coefficients of the phenothiazine radical cation ($\varepsilon_{PTZ^{\bullet+}} = 9200 \ M^{-1} \ cm^{-1}$ at 520 nm)[16(a)] was used. Solutions for laser flash photolysis studies were deaerated by purging with argon for 20 min before experiments. Femtosecond transient absorption studies were carried out with 400 nm laser pulses using a femtosecond pump probe transient absorption spectrometer (1 kHz repetition rate at 800 nm, 70 fs, 300 μJ/pulse). The overall time resolution of the absorption spectrometer is about 120 fs. The temporal profiles recorded using different probe wavelengths were fitted with up to four exponentially decaying or growing components by iterative deconvolution method using a sech^2 type instrument response function with fwhm of 120 fs and were also used for constructing the time-resolved differential absorption spectra. Detailed description of the experimental setup is given elsewhere.[31] Unless stated otherwise, all experiments were performed at 25 °C.

2.5.2. Synthesis and characterization

Synthesis of 2: 4-iodoanisole (5g, 21.36 mmol), dichlorobis(triphenylphosphine) palladium(II) (600 mg, 0.85 mmol) and copper(I) iodide (160 mg, 0.85 mmol) were dissolved in dry THF (50 mL). Dry diisopropylamine (10 mL) and

trimethylsilylacetylene (3.15 g, 32.1 mmol) were added under argon and the mixture stirred for 24 h. Solvent was removed and residue was purified by column chromatography on alumina using chloroform/hexane (1:9) to get **2**. (3.97 g, 91%). Mass (GC-MS): calcd. for $C_{12}H_{16}OSi$: 204; found: 204. ^1H NMR ($CDCl_3$, 300 MHz) δ: 0.27 (s, 9H), 3.58 (s, 3H), 6.62 (d, 2H), 7.19 (d, 2H).

Synthesis of 3: 2 (2 g, 9.8 mmol) was dissolved in THF (20 mL). The solution was cooled to 0 °C and TBAF (1M in THF, 12 mL) added. The mixture was then stirred for 2 h at RT, poured into ice-cold water and extracted with dichloromethane. The solvent was removed and residue was purified over alumina column using chloroform: hexane (1:9) to obtain **3**. (1.1 g, 86%). Mass (GC-MS): calcd. for C_9H_8O: 132; found: 132. ^1H NMR ($CDCl_3$, 300 MHz) δ: 2.99 (s, 1H), 3.76 (s, 3H), 6.83 (d, 2 H), 7.43 (d, 2H).

Synthesis of BPEA: To an argon degassed RB flask, 9,10-dibromoanthracene (500 mg, 1.49 mmol), dichlorobis(triphenylphosphine)palladium(II) (63 mg, 0.09 mmol), copper(I) iodide (17 mg, 0.09 mmol), dry toluene (35 mL) and dry diisopropylamine (10 mL) were added. **3** (413 mg, 3.12 mmol) in dry toluene (10 mL) was added and the reaction mixture stirred for 24 h at 70 °C under argon. Solvent was removed and the residue obtained was purified by column chromatography over silica gel using chloroform: hexane (3:7) to obtain **BPEA**, (400 mg, 62%). mp 244-245 °C. IR (KBr) v_{max}: 532, 555, 636, 764, 833, 1030, 1105, 1178, 1250, 1290, 1462, 1510, 1603, 2193, 2968, 3017, 3055 cm^{-1}. ^1H NMR

(CDCl$_3$, 300 MHz) δ: 3.89 (s, 6H), 6.99 (d, 4H), 7.63 (q, 4H), 7.73 (d, 4H), 8.69

(q, 4H). ^{13}C NMR (CDCl$_3$, 125 MHz) δ: 55.40, 85.37, 102.42, 114.22, 115.61,

118.44, 126.61, 127.30, 131.97, 133.17, 159.97. FAB-MS (M$^+$) calcd. for

C$_{32}$H$_{22}$O$_2$: 438.52; found: 438.55. Anal. calcd. for C$_{32}$H$_{22}$O$_2$: C, 87.65; H, 5.06;

found: C, 87.39; H, 4.93.

Synthesis of 6: 4-iodophenol (1.65 g, 7.5 mmol) was dissolved in dry acetone (20

mL). Potassium carbonate (2.15 g, 15.6 mmol) and **5** (2 g, 6.25 mmol) in dry

acetone (20 mL) were added and the mixture refluxed under argon for 24 h. It was

poured into water and extracted with dichloromethane. The extract was washed

with 20% sodium hydroxide solution and then with water. The organic layer was

dried and evaporated at reduced pressure to get **6**, (2.86 g, 97%). mp 68-69 °C.

Mass (GC-MS): calcd. for C$_{21}$H$_{18}$INOS: 459; found: 459. ^{1}H NMR (CDCl$_3$, 300

MHz) δ: 2.23 (m, 2H), 4.07 (m, 4H), 6.61 (d, 2H), 6.91 (t, 4H), 7.13 (m, 4H), 7.49

(d, 2H).

Synthesis of 7: **6** (2g, 4.36 mmol), dichlorobis(triphenylphosphine)palladium(II)

(123 mg, 0.17 mmol) and copper(I) iodide (83 mg, 0.44 mmol) were dissolved in

dry THF (50 mL). Dry diisopropylamine (10 mL) and trimethylsilylacetylene (555

mg, 5.66 mmol) were added under argon and the mixture stirred for 24 h. Solvent

was removed and residue was purified by column chromatography on alumina

using ethyl acetate/hexane (5:95) to get **7**. (1.8 g, 95%). mp 71-72 °C. Mass (GC-

MS): calcd. for C$_{26}$H$_{27}$NOSSi: 429; found: 429. ^{1}H NMR (CDCl$_3$, 300 MHz) δ:

0.233 (s, 9H), 2.24 (m, 2H), 4.07 (m, 4H), 6.73 (d, 2H), 6.91 (t, 4 H), 7.15 (m, 4H),

7.33 (d, 2H).

Synthesis of 8: 7 (1.8 g, 4.19 mmol) was dissolved in THF (20 mL). The solution

was cooled to 0 °C and TBAF (1M in THF, 4.2 mL) added. The mixture was then

stirred for 2 h at RT, poured into ice-cold water and extracted with

dichloromethane. The solvent was removed and residue was purified over alumina

column using ethyl acetate: hexane (5:95) to obtain **8**. (1.2 g, 81%), mp 100-101

°C. Mass (GC-MS): calcd. for $C_{23}H_{19}NOS$: 357; found: 357. ^{1}H NMR (CDCl$_3$, 300

MHz) δ: 2.23 (m, 2H), 2.94 (s, 1H), 4.05 (m, 4H), 6.73 (d, 2H), 6.89 (t, 4H), 7.12

(m, 4 H), 7.32 (d, 2H).

Synthesis of BPEA-PT$_2$ and 9: To an argon degassed RB flask, 9, 10-

dibromoanthracene (493mg, 1.47 mmol), dichlorobis(triphenylphosphine)

palladium(II) (52 mg, 0.073mmol), copper(I) iodide (28 mg, 0.028 mmol), dry

toluene (40 mL) and dry diisopropylamine (20 mL) were added. A solution of

Compound **8** (1.1 g, 3.1mmol) in dry toluene (15 mL) was added and the mixture

was refluxed for 24 h at 70 °C under argon. The solvent was removed and residue

was purified by column chromatography over silica using chloroform: hexane

(1:1) to obtain **9** as yellow solid, (260 mg, 29%). FAB-MS (M$^+$) calcd. for

$C_{37}H_{26}BrNOS$: 611.09; found: 611.82. ^{1}H NMR (CDCl$_3$, 300 MHz) δ: 2.23 (q,

2H), 4.07 (q, 4H), 6.85 (m, 6H), 7.10 (d, 4H), 7.54 (m, 6H), 8.47 (m, 2H), 8.60 (m,

2H).

Further elution with chloroform: hexane (1:1) gave **BPEA-PT$_2$**, (630 mg, 49%).

mp 217-218 °C, IR (KBr) v_{max}: 752, 829, 1051, 1173, 1246, 1283, 1458, 1506,

1597, 2191, 2843, 2924, 3055 cm^{-1}. ^{1}H NMR (CDCl$_3$, 300 MHz) δ: 2.28 (m, 4 H),

4.14 (m, 8 H), 6.75 (d, 2 H), 6.9 (m, 10 H), 7.15 (m, 8 H), 7.38 (d, 2 H), 7. 63 (q, 6

H), 8.67 (q, 2 H). ^{13}C NMR (CDCl$_3$, 125 MHz) δ: 26.78, 43.81, 65.47, 85.41,

102.49, 114.87, 115.64, 118.47, 122.67, 125.62, 126.61, 127.29, 127.60, 132.00,

133.12, 145.16, 159.26. FAB-MS (M$^+$) calcd. for C$_{60}$H$_{44}$N$_2$O$_2$S$_2$ = 889.13; found:

889.07. Anal. calcd. for C$_{60}$H$_{44}$N$_2$O$_2$S$_2$: C, 81.05; H, 4.99; N, 3.15; found: C,

80.76; H, 4.96; N, 3.41.

Synthesis of BPEA-PT: To an argon degassed RB flask, **9** (200 mg, 0.327 mmol),

dichlorobis(triphenylphosphine)palladium(II) (20 mg, 0.013 mmol), copper(I)

iodide (10 mg, 0.049 mmol), dry toluene (40 mL) and dry diisopropylamine (15

mL) were added. 4-methoxyphenylacetylene (40 mg, 0.39 mmol) in dry toluene

(10 mL) was added and the reaction mixture stirred for 24 h at 70 °C under argon.

Solvent was removed and the residue obtained was purified by column

chromatography over silica gel using chloroform: hexane (3:7) to obtain **BPEA-**

PT, (120 mg, 59%). mp 188-189 °C,. IR (KBr) v_{max}: 752, 833, 1032, 1173, 1246,

1458, 1510, 1601, 2191, 2839, 2938, 3055 cm^{-1}. ^{1}H NMR (CDCl$_3$, 300 MHz) δ =

2.31 (t, 2H), 3.88 (s, 3H), 4.14 (m, 4H), 6.92 (m, 8H), 7.18 (m, 4H), 7.62 (m, 6H),

7.71 (d, 2H), 8.69 (m, 4H). ^{13}C NMR (CDCl$_3$, 125 MHz) δ: 26.72, 43.76, 55.40,

65.43, 85.39, 102.48, 114.23, 114.83, 115.62, 118.45, 122.65, 125.58, 126.61,

127.29, 127.59, 131.97, 133.17, 145.14, 159.22, 159.99. FAB-MS (M^+) calcd. for

$C_{46}H_{33}NO_2S$: 663.82; found: 663.46. Anal. calcd. for $C_{46}H_{33}NO_2S$: C, 83.23; H,

5.01; N, 2.11; found: C, 82.81; H, 5.18; N, 2.41.

2.6. References

1. (a) Harriman, A. *Angew. Chem. Int. Ed.* **2004**, *43*, 4985-4987. (b) Fukuzumi,

   S. *Phys. Chem. Chem. Phys.* **2008**, *10*, 2283-2297. (c) Fukuzumi, S. *Eur. J.*

   Inorg. Chem. **2008**, 1351-1362.

2. (a) Hviid, L.; Brouwer, A. M.; Paddon-Row, M. N.; Verhoeven, J. W. *Chem.*

   Phys. Chem. **2001**, *2*, 232-235. (b) Hviid, L.; Bouwman, W. G.; Paddon-

   Row, M. N.; Verhoeven, J. W.; van Ramesdonk, H. J.; Brouwer, A. M.

   Photochem. Photobiol. Sci. **2003**, *2*, 995-1001. (c) Hviid, L.; Verhoeven, J.

   W.; Brouwer, A. M.; Paddon-Row, M. N.; Yang, J.; George, M. W.

   Photochem. Photobiol. Sci. **2004**, *3*, 246-251.

3. (a) Osyczka, A.; Moser, C. C.; Daldal, F.; Dutton, P. L. *Nature* **2004**, *427*,

   607-612. (b) Andreasson, J.; Kyrychenko, A.; Martensson, J.; Albinsson, B.

   Photochem. Photobiol. Sci. **2002**, *1*, 111-119. (c) Davis, W. B.; Ratner, M.

   A.; Wasielweski, M. R. *J. Am. Chem. Soc.* **2001**, *123*, 7877-7886.

4. Sinks, L. E.; Weiss, E. A.; Giairno, J. M.; Wasielewski, M. R. *Chem. Phys.*

   Lett. **2005**, *404*, 244-249.

5. (a) Tsukahara, K.; Ueda, R. *Bull. Chem. Soc. Jpn.* **2003**, *76*, 561-566. (b) Korchowiec, J. *Int. J. Quantum Chem.* **2005**, *101*, 714-721.

6. (a) Marcus, R. A.; Sutin, N. *Biochem. Biophys. Acta* **1985**, *811*, 265-322. (b) Marcus, R. A. *Angew. Chem., Int. Ed.* **1993**, *32*, 1111-1121.

7. (a) Fukuzumi, S. ; Ohkubo, K. ; Imahori, H. ; Shao, J. ; Ou, Z. ; Zheng, G. ; Chen, Y. ; Pandey, R. K. ; Fujitsuka, M. ; Ito, O. ; Kadish, K. M. *J. Am. Chem. Soc.* **2001**, *123*, 10676-10683. (b) Ohkubo, K. ; Imahori, H. ; Shao, J. ; Ou, Z. ; Kadish, K. M. ; Chen, Y. ; Zheng, G. ; Pandey, R. K. ; Fujitsuka, M. ; Ito, O. ; Fukuzumi, S. *J. Phys. Chem. A* **2002**, *106*, 10991-10998. (c) Kashiwagi, Y. ; Okhubo, K. ; McDonald, J. A. ; Blake, I. M. ; Crossley, M. J. ; Araki, Y. ; Ito, O. ; Imahori, H. ; Fukuzumi, S. *Org. Lett.* **2003**, *5*, 2719-2721. (d) Ohkubo, K.; Kotani, H.; Shao, J.; Ou, Z.; Kadish, K. M.; Li, G.; Pandey, R. K.; Fujitsuka, M.; Ito, O.; Imahori, H.; Fukuzumi, S. *Angew. Chem. Int. Ed.* **2004**, *43*, 853-855.

8. (a) Fukuzumi, S.; Kotani, H.; Ohkubo, K.; Ogo, S.; Tkachenko, N. V.; Lemmetyinen, H. *J. Am. Chem. Soc.* **2004**, *126*, 1600-1601. (b) Hasobe, T.; Hattori, S.; Kotani, H.; Ohkubo, K.; Hosomizu, K.; Imahori, H.; Kamat, P. V.; Fukuzumi, S. *Org. Lett.* **2004**, *6*, 3103-3106. (c) Kotani, H.; Ohkubo, K.; Fukuzumi, S. *J. Am. Chem. Soc.* **2004**, *126*, 15999-16006. (d) Fukuzumi, S.; Kotani, H.; Ohkubo, K. *Phys. Chem. Chem. Phys.* **2008**, *10*, 5159-5162. (e)

Okamoto, K. ; Hasobe, T. ; Tkachenko, N. V. ; Lemmetyinen, H. ; Kamat, P. V. ; Fukuzumi, S. *J. Phys. Chem. A* **2005**, *109*, 4662-4670.

9.   (a) Benniston, A. C.; Harriman, A.; Li, P.; Rostron, J. P.; Verhoeven, J. W. *Chem. Commun.* **2005**, 2701-2703. (b) Benniston, A. C., Harriman, A.; Li, P.; Rostron, J. P.; Ramesdonk, H. J.; Groeneveld, M. M.; Zhang, H.; Verhoeven, J. W. *J . Am. Chem. Soc.* **2005**, *127*, 16054-16064. (c) Verhoeven, J.; van Ramesdonk, H. J.; Zhang, H.; Groeneveld, M. M.; Benniston, A. C.; Harriman, A. *Int. J. Photoenergy* **2005**, *7*, 103-108. (d) van Ramesdonk, H. J.; Bakker, B. H.; Groeneveld, M. M.; Verhoeven, J. W.; Allen, B. D.; Rostron, J. P.; Harriman, A. *J. Phys. Chem. A* **2006**, *110*, 13145-13150. (e) Benniston, A. C.; Harriman, A.; Verhoeven, J. W. *Phys. Chem. Chem. Phys.* **2008**, *10*, 5156-5158. (f) Verhoeven, J. W.; van Ramesdonk, H. J.; Groeneveld, M. M.; Benniston, A. C.; Harriman, A. *ChemPhysChem.* **2005**, *6*, 2251-2260.

10. (a) Maulding, D. R.; Zweig, A. U.S. Patent 3729426, 1973. (b) Nakatsuji, S.; Matsuda, K.; Uesugi, Y.; Nakashima, K.; Akiyama, S.; Fabian, W. *J. Chem. Soc., Perkin Trans. 1* **1992**, 755-758. (c) Li, B.; Miao, W.; Cheng, L. *Dyes Pigm.* **2000**, *46*, 81-84.

11. Cicerone, M. T.; Blackburn, F. R.; Ediger, M.D. *J. Chem. Phys.* **1995**, *102*, 471-479.

12. Valentini, L.; Bagnis, D.; Marrocchi, A.; Seri, M.; Taticchi, A.; Kenney, J. M. *Chem. Mater.* **2008**, 20, 32-34.

13. Ishibashi, T. Eur. Pat. Appl. EP 1072668 A2 31, 2001.

14. (a) Swager, T. M.; Gil, D. J.; Wrighton, M. S. *J. Phys. Chem.***1995**, *99*, 4886-4893. (b) Ofer, D.; Swager, T. M.; Wrighton, M. S. *Chem. Mater.* **1995**, *7*, 418-425.

15. (a) Wiberg, J.; Guo, L.; Petterson, K.; Nilsson, D.; Ljungdahl, T.; Martensson, J.; Albinsson B. *J. Am. Chem. Soc.* **2007**, *129*, 155-163. (b) Pettersson, K.; Wiberg, J.; Ljungdahl, T.; Martensson, J.; Albinsson B. *J. Phys. Chem. A* **2006**, *110*, 319-326. (c) Winters, M. U.; Pettersson, K.; Martensson, J.; Albinsson B. *Chem. Eur. J.* **2005**, 11, 562-573. (d) Pettersson, K.; Kilsa, K.; Martensson, J.; Albinsson B. *J. Am. Chem. Soc.* **2004**, *126*, 6710-6719. (e) Kilsa, K.; Macpherson, A. N.; Gilbro, T.; Martensson, J.; Albinsson B. *Spectrochimica Acta A* **2001**, 57, 2213-2227. (f) Kilsa, K.; Kajanus, J.; Macpherson, A. N.; Martensson, J.; Albinsson B. *J. Am. Chem. Soc.* **2001**, *123*, 3069-3080.

16. (a) Moroi, M.; Braun, A. M.; Grätzel, M. *J. Am. Chem. Soc.* **1979**, *101*, 567-572. (b) Danielson, E.; Elliott, C. M.; Merkert, J. W.; Meyer, T. J. *J. Am. Chem. Soc.* **1987**, *109*, 2519-2520. (c) Chen, P.; Duesing, R.; Graff, D. K.; Meyer, T. J. *J. Phys. Chem.* **1991**, *95*, 5850-5858. (d) Klumpp, T.; Linsenmann, M.; Larson, S. L.; Limoges, B. R.; Bürssner, D.; Krissinel, E.

B.; Elliott, C. M.; Steiner, U. E. *J. Am. Chem. Soc.* **1999**, *121*, 1076-1087. (e) Ajayakumar, G.; Gopidas, K. R. *Photochem. Photobiol. Sci.* **2008**, *7*, 826-833.

17. Gimenez, R.; Pinol, M.; Serrano, J. L. *Chem. Mater.* **2004**, *16*, 1377-1383.

18. (a) Levitus, M.; Garcia-Garibay, M. A. *J. Phys. Chem. A* **2000**, *104*, 8632-8637. (b) Zhu, A.; White, J. O.; Drickamer, H. G. *J. Phys. Chem. A* **2002**, *106*, 9209-9212. (c) Beeby, A.; Findlay, K. S.; Goeta, A. E.; Porrès, L. Rutter, S. R.; Thompson, A. L. *Photochem. Photobiol. Sci.* **2007**, *6*, 982-986.

19. Lor, M.; Thielemans, J.; Viaene, L.; Cotlet, M.; Hofkens, J.; Well, T.; Hampell, C.; Mullen, K.; Verhoeven, J. W.; Auweraer, M. V; De Schryver, F. C. *J. Am. Chem. Soc.* **2002**, *124*, 9918-9925. (b) Thomas, K. R. J.; Thompson, A. L.; Sivakumar, A. V.; Bardeen, C. J.; Thayumanavan, S. *J. Am. Chem. Soc.* **2005**, *127*, 373-383.

20. Rehm, D.; Weller, A. *Ber. Bunsen-Ges. Phys. Chem.* **1969**, *73*, 834-839.

21. Fang, T.-S.; Lin, J.; Schneider, R.; Yamada, T.; Singer, L. A. *Chem. Phys. Lett.* **1982**, *92*, 283-287.

22. Gould, I. R.; Ege, D.; Moser, J. E.; Farid, S. *J. Am. Chem. Soc.* **1990**, *112*, 4290-4301.

23. Hayes, R. T.; Walsh, C. J.; Wasielewski, M. R. *J. Phys. Chem. A* **2004**, *108*, 2375-2381.

24. Borowicz, P.; Herbich, J.; Kapturkiewicz, A.; Opallo, M.; Nowacki, J. *Chem. Phys.* **1999**, *249*, 49-62.

25. (a) Wasielewski, M. R. *Chem. Rev.* **1992**, *92*, 435-461. (b) Suppan, P. In *Topics in Current Chemistry*, Mattay, J. Ed.; Springer Verlag: Berlin, 1992, Vol. 163, pp 95-130. (c) Gould, I.; Farid, S. *Acc. Chem. Res.* **1996**, *29*, 522-528.

26. (a) Smit, K. J.; Warman, J. M.; de Haas, M. P.; paddan-Row, M. N.; Oliver, A. M. *Chem. Phys. Lett.* **1988**, *152*, 177-182. (b) Liang, N.; Miller, J. R.; Closs, G. L. *J. Am. Chem. Soc.* **1990**, *112*, 5353-5354.

27. Murov, S. L.; Carmichael, I.; Hug, G. L. In *Handbook of Photochemistry*, 2nd ed.; Marcel Dekker: New York, 1993

28. Nguyen, P.; Todd, S.; Biggelaar, D. V.; Taylor, N. J.; Marder, T. B.; Wittmann, F.; Friend, R. H. *Synlett.* **1994**, 299-301.

29. Lutz, H.; Breheret, E.; Lindqvist, L. *J. Phys. Chem.* **1973**, *77*, 1758 -1762.

30. Bensasson, R.; Land, E. J. *Photochem. Photobiol. Rev.* **1978**, *3*, 163 -191.

31. Mondal, J. A.; Ghosh, H. N.; Mukherjee, T; Palit, D. K. *J. Phys. Chem. A* **2005**, *109*, 6836-6846.

Chapter 3

Long-lived Photoinduced Charge Separation in 9,10-Bis(phenylethynyl)anthracene Based Triads

3.1. Abstract

We have investigated the PET processes taking place in two molecular triads both of which had **BPEA** as sensitizer and light absorber and **PT** as donor. A nitrotoluene (**NT**) moiety was the acceptor in one of the triads and a pyromellitimide (**PI**) unit was the acceptor in the other. Fluorescence of the **BPEA** core was efficiently quenched and this was attributed to the electron transfer processes taking place in these triads. Two possible electron transfer pathways could be identified in these systems. Picosecond transient absorption studies suggested formation of a charge separated state directly from the singlet excited state of **BPEA** in both triads. Analysis of the picosecond transient absorption spectra suggested the involvement of the acceptor moiety (**NT** or **PI**) in the primary electron transfer step. Nanosecond flash photolysis experiments gave long-lived transient absorptions assignable to $PT^{•+}$ and $NT^{•-}$ or $PI^{•-}$. Assignments of radical ions were confirmed by oxygen quenching experiments. Analysis of the ΔG^0 and λ values suggested that the inverted region effect has no role in

stabilizing the final CS state. The relatively long lifetime of the final CS state is

attributed to the long distance separating the donor and acceptor components in

the CS state.

3.2. Introduction

In Chapter 1 of this thesis we described the use of triads, tetrads and other

higher assemblies that are designed with the aim of attaining long-lived

photoinduced charge separation. These higher order systems undergo sequential

electron transfer resulting in an increase in the charge separation distance. As the

distance between the ions increases, electron return becomes increasingly difficult,

resulting ultimately in long-lived charge separation. It is generally observed that

for photoinduced charge separation and thermal charge recombination reactions,

the rate constants display exponential distance dependence[1]

$$k_{et} = A \exp(-\beta \times \text{distance}) \qquad (3.1)$$

This equation is found to be valid irrespective of whether the distance is expressed

as the number of bonds separating the donor and acceptor moieties or as the

centre-to-centre distance, d_{cc}. β is called a damping factor and its value primarily

depends on the electronic structure and conducting nature of the bridging unit.

Bridging units which allows facile transfer of electron from donor to acceptor

moiety have low (≤ 0.5 Å^{-1}) β values.[2] β values for normal organic bridges lie in

the range $1.2 - 1.4$ Å^{-1}.

Let us consider PET reactions in the dyad $D-A_1$ and triad $D-A_1-A_2$, leading

to formation of the CS states $^{\bullet+}D-A_1^{\bullet-}$ and $^{\bullet+}D-A_1-A_2^{\bullet-}$, respectively. The centre-to-

centre distance (d_{cc}) in the triad is larger and hence BET would be slower in the

triad. $\Delta G^0{}_{BET}$ and λ are different in these systems and hence calculation of BET

rates using equation 3.1 is not straight forward. Depending on the values of $\Delta G^0{}_{BET}$

and λ, BET rates in triad systems can be higher than that in the dyad (ie., CS state

lifetime in triads can be lower compared to that in dyads). Such situations normally

arise if the CS state in the dyad is stabilized by the inverted region effects.[3] This

situation is illustrated in Scheme 3.1.
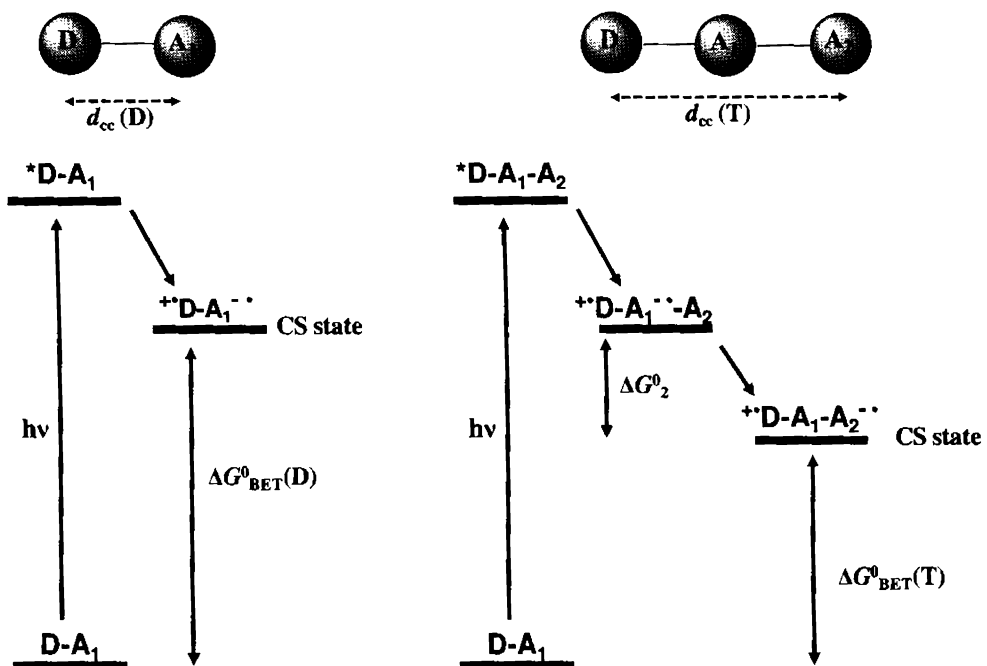
Scheme 3.1

Scheme 3.1 shows the photo processes taking place in the dyad and triad systems. In the dyad $|\Delta G^0{}_{BET}|$ is very large (indicated as $\Delta G^0{}_{BET}(D)$ in Scheme 3.1). Since the second electron transfer is exergonic by an amount $\Delta G^0{}_2$, $|\Delta G^0{}_{BET}|$ in the triad (indicated as $\Delta G^0{}_{BET}(T)$ in Scheme 3.1) is smaller by this amount. If we assume that D, A_1 and A_2 are rigid moieties then the inner shell reorganization energy component will be very small and the dominant factor contributing to the total reorganization would be the outer shell reorganization energy λ_o. The following equation is generally used to calculate λ_o (see chapter 2 for details).[4]

$$\lambda_o = \Delta e^2 \left(\frac{1}{2r_A} + \frac{1}{2r_D} - \frac{1}{d_{cc}} \right) \left(\frac{1}{\varepsilon_{op}} - \frac{1}{\varepsilon_s} \right) \qquad (3.2)$$

It can be seen from equation 3.2 that the centre-to-centre distance d_{cc} is a dominant factor in deciding the value of λ_o. If d_{cc} is large, λ_o is large and vice-versa.[5] Scheme 3.1 shows that d_{cc} in the triad is much larger than that in the dyad indicating that λ_o is much larger in the triad compared to that in the dyad. Thus, upon going from the dyad to triad, $\Delta G^0{}_{BET}$ decreases and λ_o increases.

The condition for the inverted region effect to operate is $-\Delta G^0{}_{BET} \gg \lambda$.[6] This condition is true in the dyad shown in Scheme 3.1. To maintain this condition in the triad, $|\Delta G^0{}_{BET}|$ be made larger and λ smaller. Upon going from the dyad to triad the opposite effect takes place, ie., $|\Delta G^0{}_{BET}|$ decreases and λ increases. Thus, from a condition of $-\Delta G^0{}_{BET} \gg \lambda$ operating in the dyad, a situation of $-\Delta G^0{}_{BET} \approx \lambda$ is attained in the triad. $-\Delta G^0{}_{BET} \approx \lambda$ actually corresponds to the top of the Marcus

parabola where the rate is maximum. Thus, if we consider the ΔG^0 and λ factors,

CS state lifetime would be smaller in a triad compared to that in the dyad. The

opposite is expected if the distance dependence of BET is the deciding factor.

There is only one report in the literature that addresses the above aspect.

Fukuzumi and co-workers have compared the CS state lifetimes in a formanilide-

anthraquinone (FA-AQ) dyad to that in a ferrocene-formanilide-anthraquinone

(Fc-FA-AQ) triad.[7] (Figure 3.1). FA-AQ gave an extremely long-lived CS state

(attributed to inverted region effects), which could be observed even at 900 μs after

laser excitation, whereas the CS state of Fc-FA-AQ was very short-lived (lifetime

20 ps). Fukuzumi et al. proposed that the reduction in CS state lifetime in the triad

compared to that in the dyad can be taken as yet another evidence for the inverted

region effect operating in the dyad. It is to be mentioned here that long-lived CS

state in FA-AQ is a controversial subject and the details were presented in Chapter

1 of this thesis.[8]

FA-AQ   **Fc-FA-AQ**
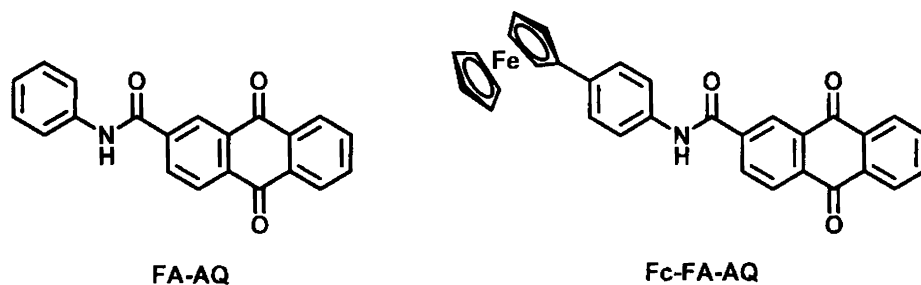
Figure 3.1

In Chapter 2 of this thesis we have studied the PET processes taking place in two bis(phenylethynyl)anthracene-phenothiazine (**BPEA-PT**) dyads. We observed a long-lived CS state in **BPEA-PT**, which was attributed to the inverted region effects. We were interested in knowing as to what would happen to the CS state lifetime if this dyad is converted to a triad by appending a suitable acceptor to it. Will the ΔG^0 and λ factors dominate leading to a reduction in the lifetime or will the distance factor dominate leading to long lifetime for the CS state. In order to answer this question we have designed and studied two triad systems, wherein the **BPEA-PT** dyad is appended to secondary acceptor units. In the triad designated as **NT-BPEA-PT**, a nitrotoluene acceptor unit is attached to the dyad system. In the second triad, **PI-BPEA-PT,** a pyromellitic diimide unit acts as the secondary acceptor. Structures of these molecules along with model systems are shown in Figure 3.2.

BPEA

BPEA-PT
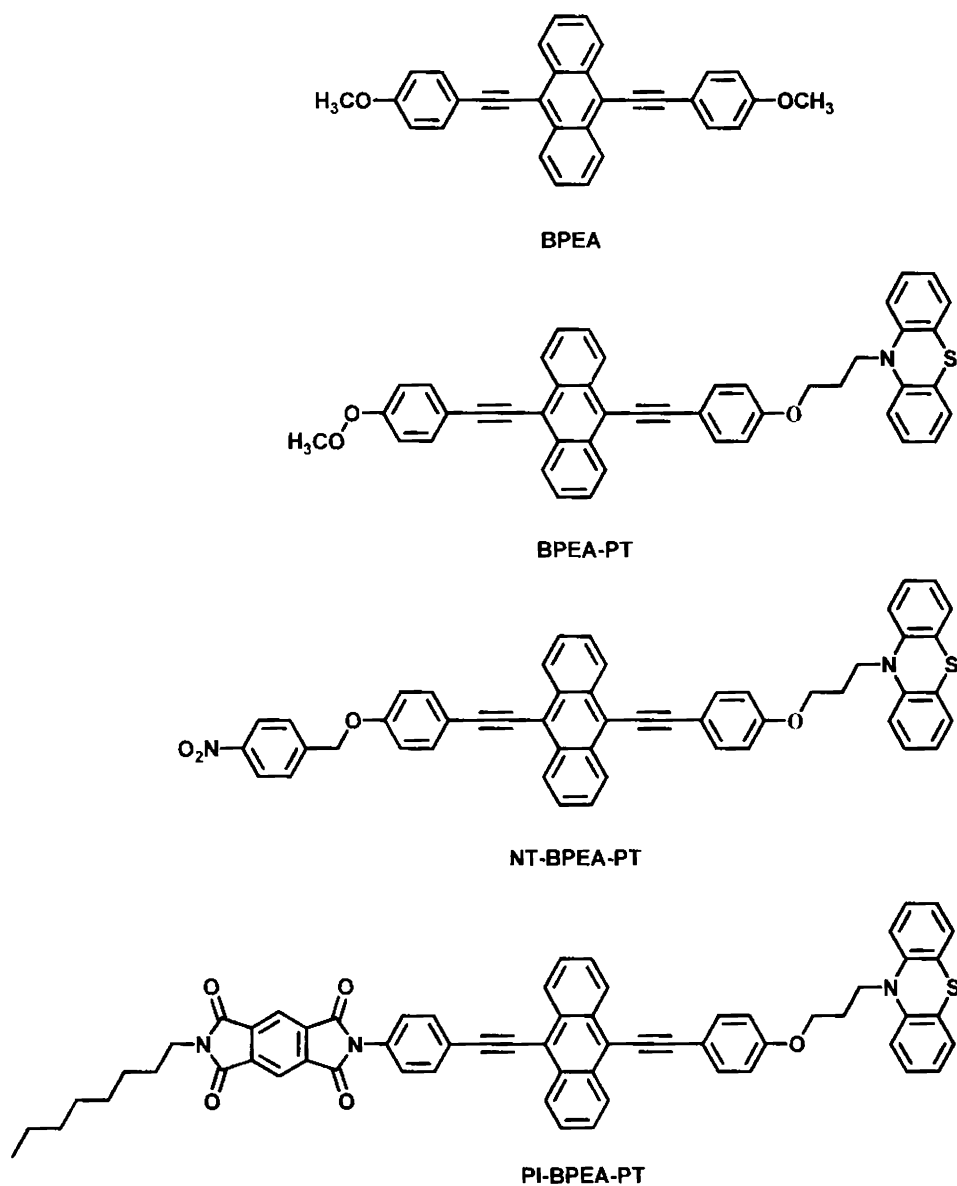
NT-BPEA-PT

PI-BPEA-PT

Figure 3.2. Structures of model compound **BPEA** and triads used in this study

3.3. Results and discussion

3.3.1. Synthesis and characterisation of BPEA, NT-BPEA-PT and PI-BPEA-PT

BPEA and **BPEA-PT** were synthesized as described in chapter 2. Compound **4** required for the synthesis of **NT-BPEA-PT** was prepared as shown in Scheme 3.2. **4** was prepared starting from **1**, which on reaction with 4-iodoanisole gave **2**. **2** on reaction with trimethylsilylacetylene under Sonogashira coupling condition gave **3**, which was converted to **4**, by deprotection with tertrabutylammoniun fluoride in THF.
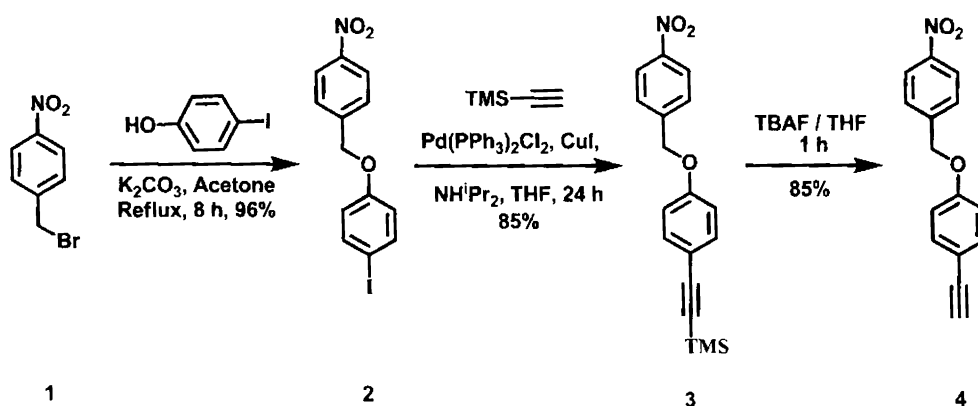
Scheme 3.2. Scheme for the synthesis of **4**

Compound **6**, which was the precursor for **NT-BPEA-PT**, was synthesized as shown in Scheme 3.3. **4** on Sonogashira coupling reaction with one equivalent of 9,10-dibromoanthracene (**5**) gave **6** in 35% yield.
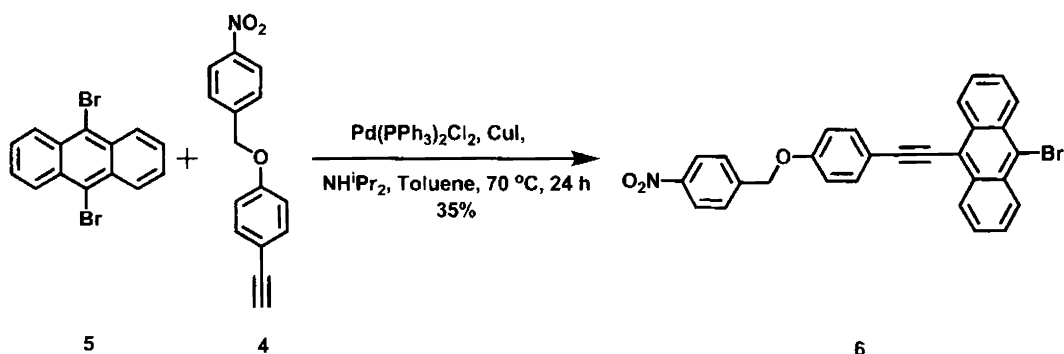
Scheme 3.3. Scheme for the synthesis of **6**

Reaction of **6** with one equivalent of **7** (see Chapter 2 for synthesis of **7**) under palladium catalysed reaction condition gave **NT-BPEA-PT** in 50% yield (Scheme 3.4).
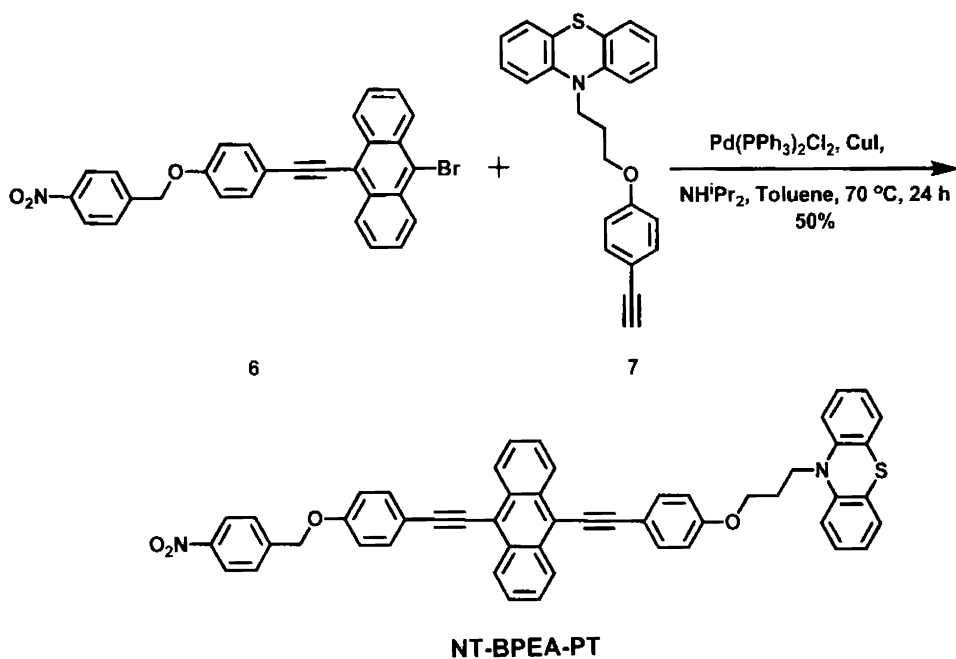
NT-BPEA-PT

Scheme 3.4. Scheme for the synthesis of **NT-BPEA-PT**

The precursor compound **10** of **PI-BPEA-PT** was synthesized as per Scheme 3.5. 4-nitroaniline was diazotised and then iodinated with potassium iodide to form 4-iodonitrobenzene(**8**).[9] **8** was reacted with trimethylsilylacetylene under palladium catalyzed reaction conditions to obtain **9**, which was deprotected with potassium carbonate to get **10**.[10]
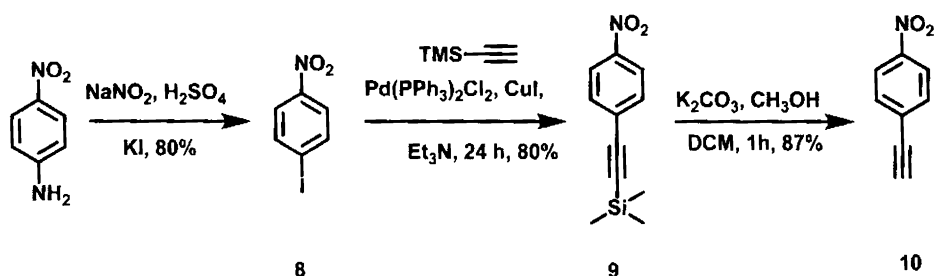
Scheme 3.5. Scheme for the synthesis of **10**

Another precursor **13**, required for the synthesis of **PI-BPEA-PT** was prepared as per Scheme 3.6. Sonogashira coupling reaction of **10** with 9,10-dibromoanthracene gave the compound **11** in 36% yield. **11** again on Sonogashira coupling reaction with **7** yielded **12**. **13** was prepared in 80% yield from **12** by reaction with stannous chloride in tetrahydrofuran in the presence of hydrochloric acid.
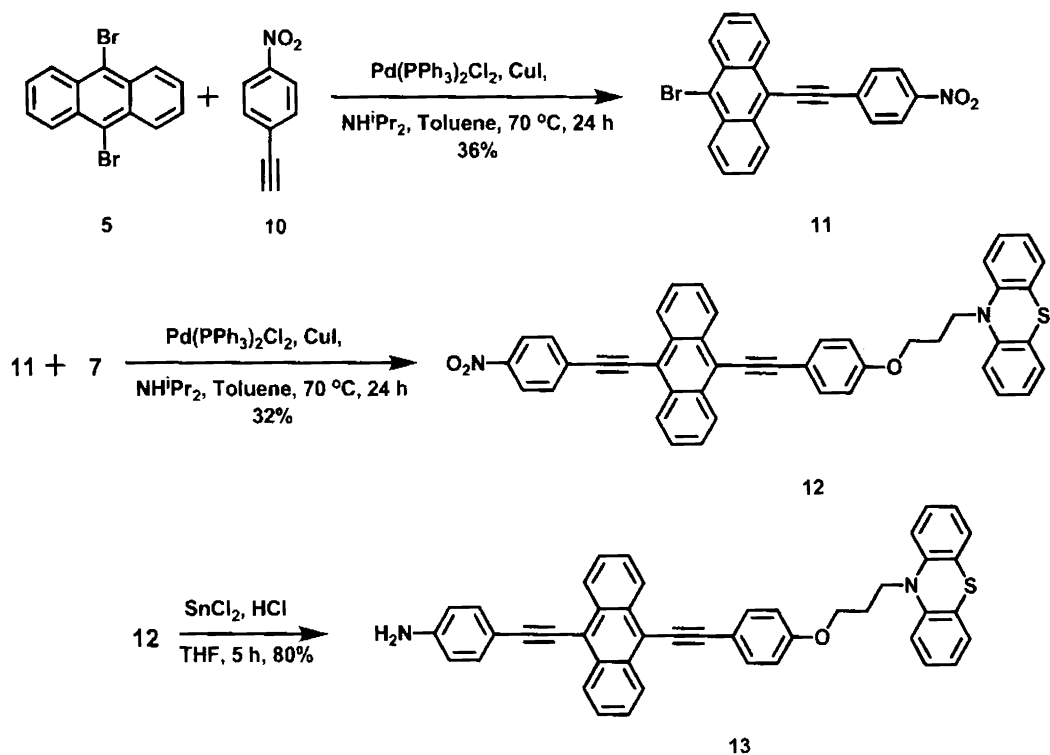
Scheme 3.6. Scheme for the synthesis of **13**

Finally **PI-BPEA-PT** was synthesized as shown in scheme 3.7. The precursor **14** was synthesized by the monoalkylation of pyromelliticdianhydride by slight modification of a reported procedure.[11] **13** on condensation reaction with **14** in DMF at 140 ^{0}C gave the triad compound **PI-BPEA-PT** in 50% yield.
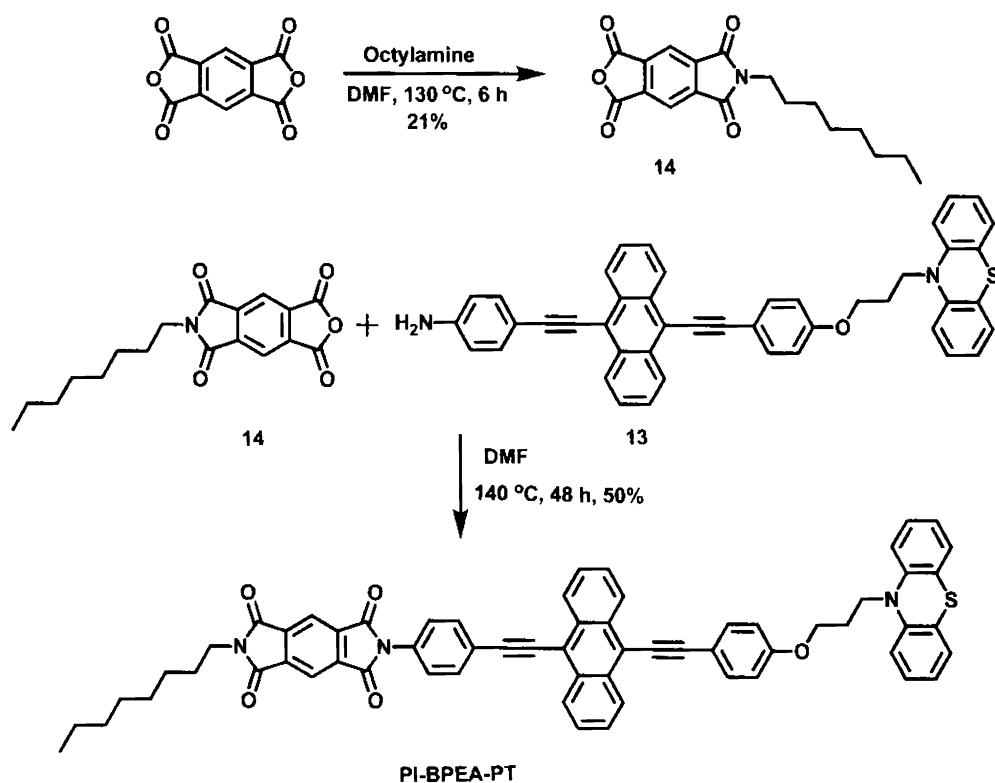
Scheme 3.7. Scheme for the synthesis of **PI-BPEA-PT**

Details of the synthetic procedures are given in the experimental section. The various intermediates and final products were characterized by analytical and spectroscopic techniques.

3.3.2. Photophysical and electrochemical studies

3.3.2.1. Photophysical and electrochemical studies of BPEA, BPEA-PT and NT-BPEA-PT

Although the absorption and emission spectra of **BPEA** and **BPEA-PT** were already presented in the previous chapter, these data are reproduced here for

comparison purposes. Absorption spectra of **BPEA**, **BPEA-PT** and **NT-BPEA-PT** are compared in Figure 3.3. The long wavelength absorption in **BPEA** occurs in the 400-500 nm region in DCM and attachment of **PT** and/or **NT** moieties did not result in any changes in its absorption above 400 nm. Absorption spectrum due to **BPEA-PT** can be obtained by adding the contributions due to **BPEA** and **PT**. In a similar manner, absorption spectrum of **NT-BPEA-PT** could be obtained by adding contributions due to **NT**, **BPEA** and **PT**, indicating that the constituents of the triad did not interact in the ground state. In these molecules the absorptions due to **PT** and **NT** occur at wavelengths below 350 nm. Therefore it can be safely assumed from Figure 3.3 that excitation above 350 nm populates only the **BPEA** excited states in these compounds.
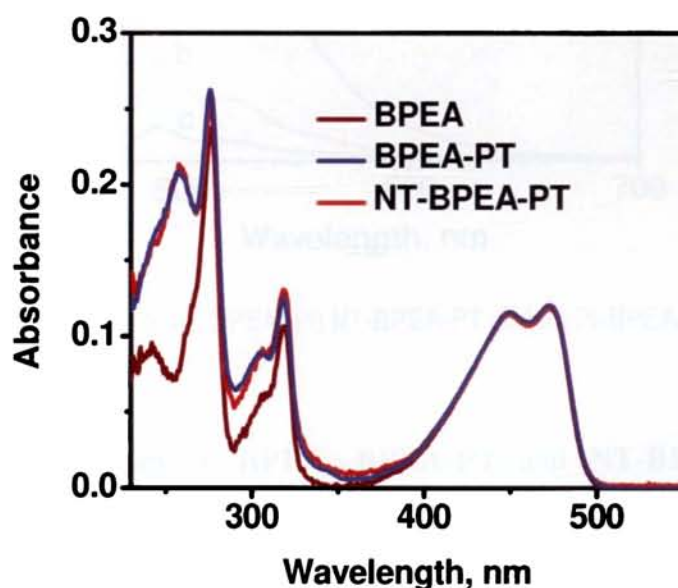
Figure 3.3. Absorption spectra of **BPEA**, **BPEA-PT** and **NT-BPEA-PT** in DCM

Fluorescence spectra of **BPEA-PT** and **NT-BPEA-PT** along with the model compound **BPEA** are compared in Figure 3.4. It was shown in Chapter 2 that substitution of **PT** lead to substantial quenching of the **BPEA** fluorescence. It is evident from Figure 3.4 that the fluorescence intensity in the triad is lower compared to that in **BPEA** and **BPEA-PT**. Fluorescence quantum yields were determined for these systems and the values obtained were 0.66, 0.15 and 0.05, respectively, for **BPEA**, **BPEA-PT** and **NT-BPEA-PT**.
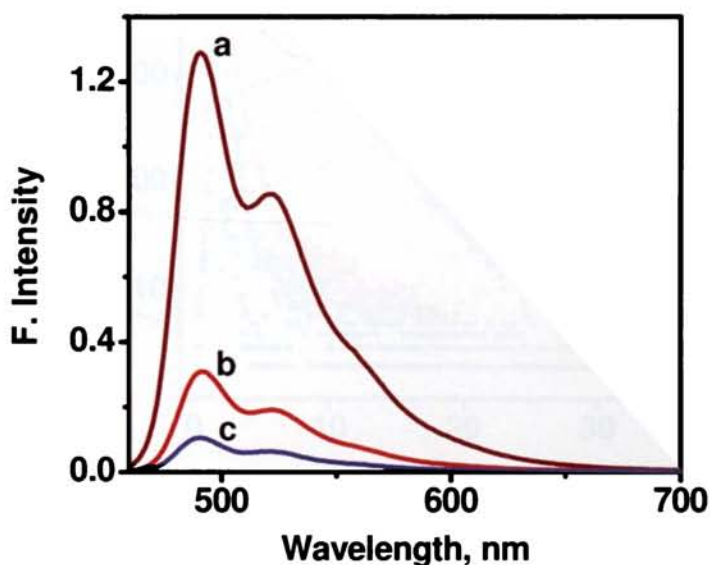
Figure 3.4. Fluorescence spectra of (a) **BPEA**, (b) **NT-BPEA-PT** and (c) **PI-BPEA-PT** in DCM. Excitation was at 440 nm

Fluorescence lifetimes of **BPEA**, **BPEA-PT** and **NT-BPEA-PT** were determined using single photon counting technique. The samples were excited using a 440 nm nanoLED excitation source. Decay profiles obtained are shown in Figure 3.5. For **BPEA-PT**, the decay was bi-exponential with $\tau_1 = 0.64$ ns (97%)

and $\tau_2 = 3.17$ ns (3%). Decay of **NT-BPEA-PT** fluorescence was bi-exponential

with components $\tau_1 = 0.25$ ns (97.6%) and $\tau_2 = 3.11$ ns (2.4%). The short-lived

component arises due to electron transfer involving the **BPEA** chromophore. The

long-lived component may arise from a small fraction of conformers in which PET

does not occur. From Figures 3.4 and 3.5 it is clear that attachment of **NT** leads to

further quenching of the fluorescence of **BPEA-PT**.
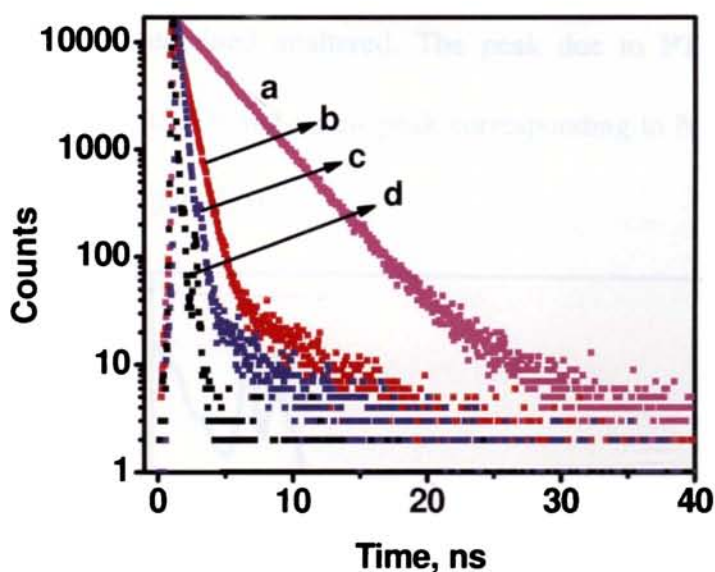
Figure 3.5. Fluorescence decay profiles of (a) **BPEA** (b) **BPEA-PT** and (c) **NT-BPEA-PT** in DCM. (d) Instrument profile. Excitation was at 440 nm

It is obvious from Figures 3.4 and 3.5 that **PT** and **NT** are efficient

quenchers of **BPEA** fluorescence. Since the absorptions due to **PT** and **NT** occur

at higher energy compared to **BPEA**, quenching of **BPEA** fluorescence by energy

transfer to these units is not possible and we can safely assume an electron transfer

mechanism for the fluorescence quenching in **NT-BPEA-PT**. The fast decay

components τ_1 in **BPEA-PT** and **NT-BPEA-PT** arises due to facile electron

transfer between **PT** and/or **NT** and **BPEA**.

Redox potentials of the compounds (vs SCE) were measured in DCM using

square wave voltammetry. Square wave voltammograms of **BPEA** and **BPEA-PT**

were given in chapter 2 (Figure 2.5). **BPEA** exhibited oxidation peak at 0.96 V and

reduction peak at -1.46 V. **BPEA-PT** exhibited an additional peak at 0.72 V

corresponding to **PT/PT•⁺** oxidation. In the case of **NT-BPEA-PT**, redox

potentials of **BPEA** remained unaltered. The peak due to **PT/PT•⁺** oxidation,

however, appeared at 0.75 V and a new peak corresponding to **NT/NT•⁻** reduction

appeared at -1.25 V (Figure 3.6).
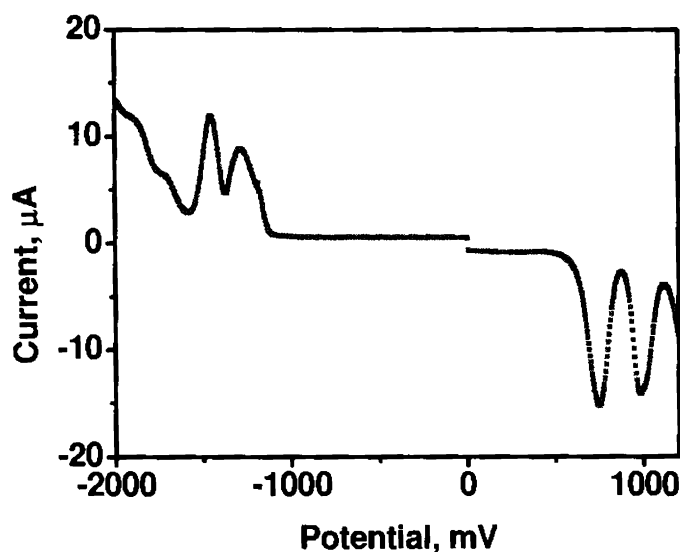
Figure 3.6. Squre wave voltammogram of **NT-BPEA-PT** in DCM

Thus, in **NT-BPEA-PT**, the lowest reduction is associated with the **NT** and the

lowest oxidation is associated with **PT**. Hence in this triad, **NT** is the final electron

acceptor and **PT** is the donor. Since **BPEA** is the light absorber and it can function as donor and acceptor, two PET pathways can be conceived as shown in Scheme 3.8, both of which ultimately result in the formation of $^\bullet$**NT-BPEA-PT**$^{\bullet+}$. In path A, the ^{1}**BPEA*** accepts an electron from **PT** (ΔG^0 = -0.36 eV) leading to the formation of **NT-**$^\bullet$**BPEA-PT**$^{\bullet+}$. Since **NT** is a better acceptor than **BPEA**, a second electron transfer can occur (ΔG^0 = -0.21 eV) to give the final CS state. In path B, ^{1}**BPEA*** is first involved in an oxidative electron transfer (ΔG^0 = -0.36 eV) resulting in the formation of $^\bullet$**NT-BPEA**$^{\bullet+}$**-PT**. Since **PT** is a better electron acceptor compared to **BPEA**, electron transfer can occur from **PT** to **BPEA**$^{\bullet+}$ (ΔG^0 = -0.21 eV) resulting in the formation of the final CS state. Since the two ET pathways involve steps with identical ΔG^0 values, it is difficult to predict which of the two pathways is actually followed in the PET reaction.

$$\text{NT-BPEA-PT} \xrightarrow{\ h\nu\ } \text{NT-}^1\text{BPEA}^*\text{-PT}$$

NT-^{1}BPEA*-PT

ΔG^0= -0.36 eV   Path A   Path B ΔG^0= -0.36 eV

NT-BPEA$^\bullet$-PT$^{\bullet+}$ NT$^\bullet$-BPEA$^{\bullet+}$-PT

ΔG^0= -0.21 eV ΔG^0= -0.21 eV
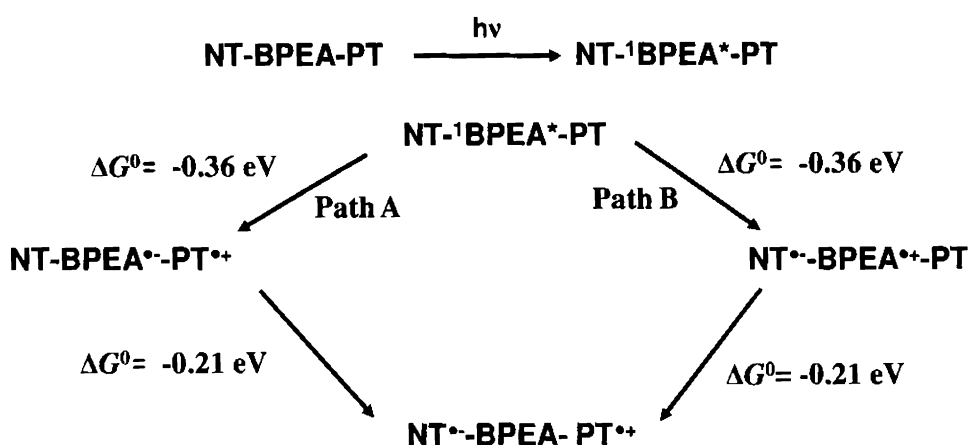
NT$^\bullet$-BPEA- PT$^{\bullet+}$

Scheme 3.8. Photophysical processes in **NT-BPEA-PT**

As mentioned in Chapter 2, rate constant for the PET process (k_{PET}) can be calculated either from the fluorescence quantum yields (equation 2.5) or from the fluorescence lifetimes (equation 2.6). k_{PET} values were calculated using both equations. The values obtained for **NT-BPEA-PT** were 4.09×10^9 s^{-1} and 3.67×10^9 s^{-1}, respectively using these two equations (the fast decay component was used for this calculation). Values obtained using the two equations did not differ very much and we took the average value ($= 3.88 \times 10^9$ s^{-1}) for calculating the quantum yield for PET ($\Phi_{et} = k_{PET}\tau_1 = 0.97$). Φ_{et} was very high which indicated that PET is very efficient in this system.

It may be noted that for **BPEA-PT** and **BPEA-PT$_2$** described in Chapter 2 of this thesis, PET rates obtained using fluorescence quenching experiments were 1.12×10^9 s^{-1}, and 2.38×10^9 s^{-1}, respectively. Since the ΔG^0 value for the first ET step in paths A and B are the same, one would expect the k_{PET} rates in **BPEA-PT$_2$** and **NT-BPEA-PT** to be nearly the same. The observed k_{PET} rate in **NT-BPEA-PT** is nearly twice as that in **BPEA-PT$_2$**. The difference arises most probably due to the smaller centre-to-centre distance between **BPEA** and **NT** moieties in the triad. The **BPEA** and **NT** moieties are separated by two bonds whereas the **BPEA** and **PT** moieties are separated by four bonds. Because of the shorter distance PET between the **BPEA** and **NT** moieties are expected to be faster than PET between **BPEA** and **PT** moieties, which explains the faster rate observed here. This suggests that path B is favored over path A.

3.3.2.2. Picosecond flash photolysis studies of NT-BPEA-PT

Results of the ultrafast flash photolysis investigations of **BPEA** were discussed in chapter 2 of this thesis. A transient having absorption in the 530-800 nm region with maximum at 570 nm was observed and this was assigned to the $S_1 \rightarrow S_n$ transition in **BPEA** (Figure 2.6). In Chapter 2 we also concluded that **BPEA** did not exhibit any tendency for ISC upon direct excitation.

In order to get a better understanding of the photophysical processes taking place in **NT-BPEA-PT**, picosecond flash photolysis was carried out and the results are presented in Figure 3.7. At the earliest timescale of 40 ps, transient absorptions with maxima at 570 and 710 nm were observed. At longer time scales formation of a species absorbing in the 500-550 nm region is also observed. Figure 3.7B shows the kinetic profiles of transients at 515, 570 and 710 nm (since the number of data points were limited, no attempt was made to fit the data to kinetic equations). Kinetic profiles of the 570 and 710 nm absorptions are similar and hence they can be assigned to the same species. Based on the results from chapter 2, this was identified as the $S_1 \rightarrow S_n$ absorption in **BPEA**. Based on our previous results the transient growth in the 510-550 nm region could be attributed to **PT**$^{\bullet+}$. Kinetic traces show that there is no match between the decay of the **BPEA** $S_1 \rightarrow S_n$ absorption and formation of the **PT**$^{\bullet+}$ absorption. In fact, **PT**$^{\bullet+}$ growth begins to appear after complete decay of the $S_1 \rightarrow S_n$ absorption, indicating that **PT**$^{\bullet+}$ is not formed directly from the 570 nm absorbing species. Most probably **PT**$^{\bullet+}$ arises

from the second electron transfer, suggesting that electron transfers in the triad **NT-BPEA-PT** proceed through path B shown in Scheme 3.8.
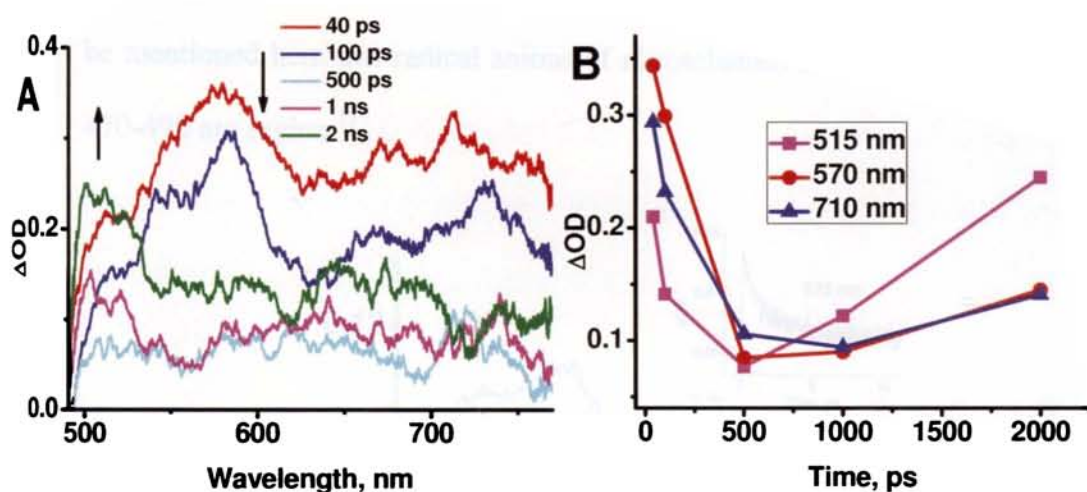
Figure 3.7. (A) Picosecond transient absorption spectra obtained in the flash photolysis of **NT-BPEA-PT** and (B) kinetic traces at 515, 570 and 710 nm

3.3.2.3. Nanosecond flash photolysis studies of NT-BPEA-PT

In order to see if any long-lived transient species are formed in the irradiation of **NT-BPEA-PT**, the molecule was subjected to nanosecond flash photolysis in DCM solution using the 355 nm light from a Nd-YAG laser. The transient absorption spectrum obtained exhibited maxima at 495 and 515 nm (Figure 3.8). In deaerated DCM both absorptions decayed at the same rate (see insets of Figure 3.8) and exhibited a lifetime of 3 μs. We have shown previously that excitation of **BPEA** did not lead to any transients in the nanosecond time scale. Hence the spectrum shown in Figure 3.8 can arise only from possible electron transfer pathways shown in Scheme 3.8. The final product of electron

transfer will have the radical cation on **PT** and the radical anion on **NT**. Based on

our previous results and literature reports,[12] the absorption at 515 nm can be

assigned to **PT**$^{\bullet+}$, and accordingly we assign the 495 nm absorption to **NT**$^{\bullet-}$. It is to

be mentioned here that radical anions of nitrotoluenes are known to absorb in the

470-490 nm region.[13]
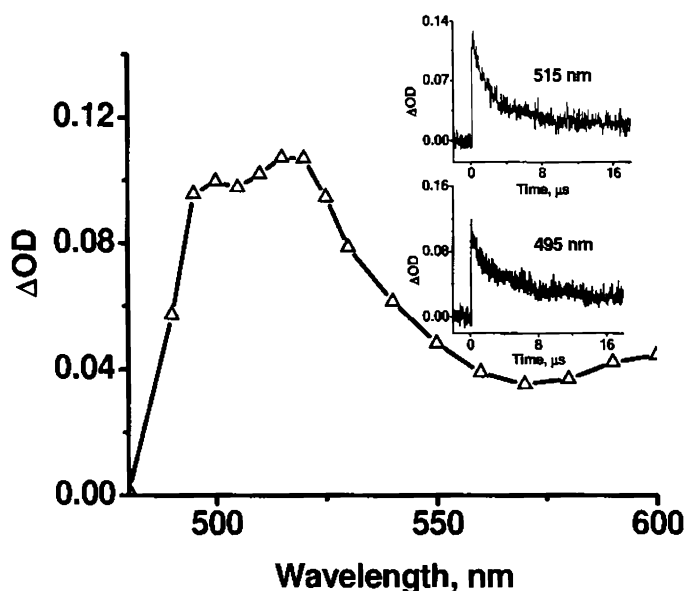
Figure 3.8. Transient absorption spectra of **NT-BPEA-PT** immediately after the laser pulse. The insets show decay profiles

To further confirm the assignment of the transient absorptions, we have

carried out the laser flash photolysis in the presence of oxygen. It is well known

that radical anions are quenched and radical cations are unaffected by oxygen. The

transient absorption spectrum obtained in the presence of oxygen along with the

kinetic traces at 495 and 515 nm are shown in Figure 3.9. It may be noted that the

peak at 495 nm is absent in the spectrum, which confirms our assignment that this peak was due to the radical anion NT$^{\bullet-}$. The kinetic traces at both wavelengths were similar and consisted of a very fast decay component attributable to quenching of the radical anion by oxygen and a very slow decay component due to the radical cation which is unaffected by oxygen. Because the absorption spectra due to the radical ions are very close and overlapping, the fast and slow components were seen in both kinetic traces.
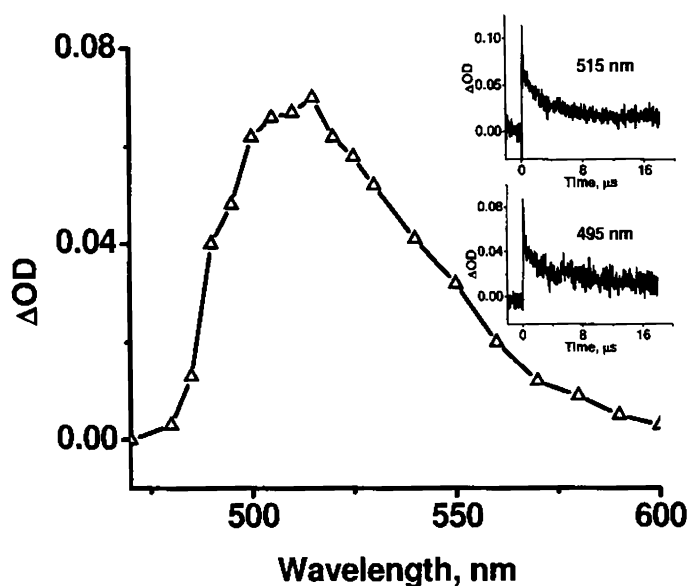
Figure 3.9. Transient absorption spectra of **NT-BPEA-PT** under oxygen saturated condition immediately after the laser pulse. The insets show decay profiles

The oxygen quenching experiments confirm the assignments of the transient absorptions. In the absence of oxygen the transients decay by back electron transfer (BET). From the measured lifetime, k_{BET} was obtained as 3.3×10^5 s^{-1}.

Thus the lifetime of the CS state in the **BPEA-PT** dyad (Chapter 2) is nearly ten times larger than that in **NT-BPEA-PT** triad.

The energy level diagram for the **NT-BPEA-PT** system is shown in Scheme 3.9. The triplet energy of **PT** in non-polar solvents is 2.62 eV [14] and that of **NT** is reported to be 2.73 eV.[15] The higher value of ^{3}**BPEA*** is reported to be at 1.74eV.[16] All other energy states were determined from our experiments.
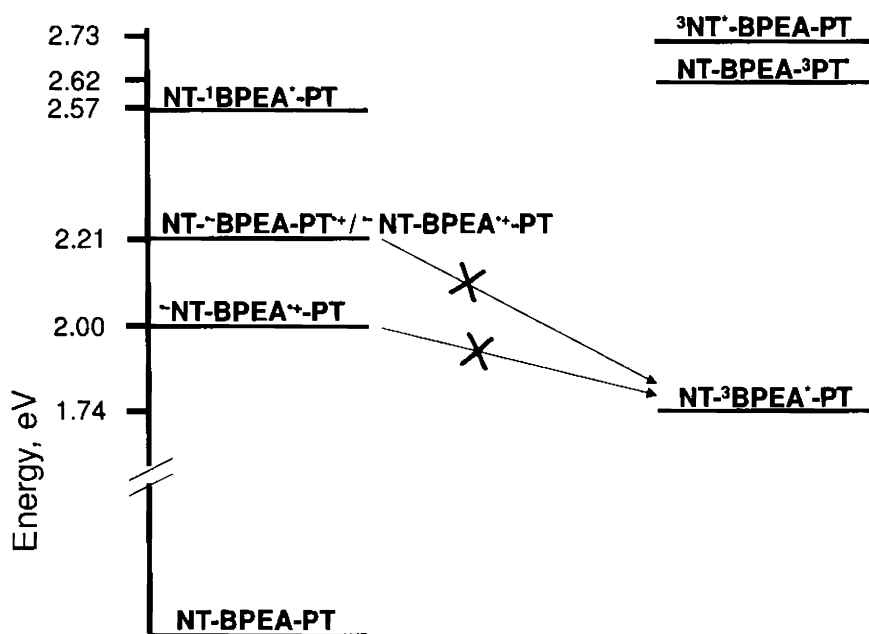
Scheme 3.9. Energy level diagram for **NT-BPEA-PT**

It can be seen from Scheme 3.9 that both the primary charge separated states and the final CS states lie above the local **BPEA** triplet level. However, the primary or final CS states do not show any tendency to decay to the low lying triplet level. This supports the conclusion we have drawn in Chapter 2 that the

forbidden nature of ISC in the **BPEA** chromophore exists in the CS states (involving **BPEA**) also.

3.3.2.4. Photophysical and electrochemical studies of PI-BPEA-PT

In Figure 3.10 we compare the absorption spectra due to **BPEA**, **BPEA-PT** and **PI-BPEA-PT**. It can be seen that appending **PI** to **BPEA-PT** leads to slight changes in the long-wavelength absorption due to **BPEA** chromophore. This could be due to two reasons. The **BPEA** chromophore in **PI-BPEA-PT** is slightly different in that it lacked the oxygen linker atom on the **PI** side. The second factor is the direct linkage between the **BPEA** and **PI** moieties, which could lead to charge transfer interactions between the two chromophores. It may be noted that the onset of absorption in **PI-BPEA-PT** is slightly shifted to the red which suggest a CT interaction between **BPEA** and **PI**. This interaction is, however, very small and is not expected to play a significant role in the photophysics of the triad.
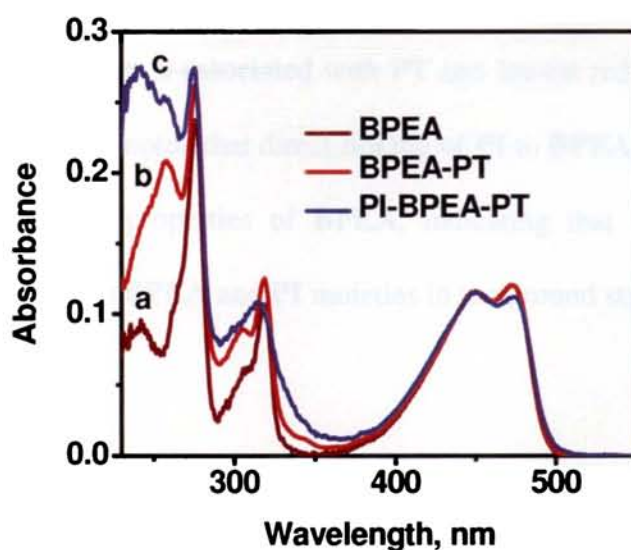
Figure 3.10. Absorption spectra of (a) **BPEA**, (b) **BPEA-PT** and (c) **NT-BPEA-PT** in DCM

The fluorescence from **PI-BPEA-PT** was extremely weak and could not be recorded under conditions comparable to those used for recording the spectra of **BPEA** and **BPEA-PT**. The fluorescence lifetime of **PI-BPEA-PT** also could not be obtained using single photon counting technique. Low fluorescence quantum yield and lifetime in **PI-BPEA-PT** is due to PET occurring in the triad. Under these circumstances we assume a low value of 0.001 for the fluorescence quantum yield of **PI-BPEA-PT** and using this value k_{PET} was calculated employing equation 2.5. In this way we obtained $k_{PET} \approx 2 \times 10^{11}$ s^{-1}.

Redox potentials of **PI-BPEA-PT** (vs SCE) were measured in DCM using square wave voltammetry and the voltammogram is shown in Figure 3.11. The voltammogram exhibited oxidation peaks at 0.75 V (corresponding to **PT** → **PT$^{•+}$**) and 0.96 V (corresponding to **BPEA** → **BPEA$^{•+}$**). The reduction peak at -1.46 V is due to **BPEA** → **BPEA$^{•-}$**. The additional peaks seen at -0.89 V and -1.6 V are due to the first and second reductions, respectively, of **PI**. Thus in the triad **PI-BPEA-PT**, the lowest oxidation is associated with **PT** and lowest reduction is associated with **PI**. It may also be noted that direct linking of **PI** to **BPEA** did not lead to any changes in the redox properties of **BPEA**, indicating that there is very little interaction between the **BPEA** and **PI** moieties in the ground state.
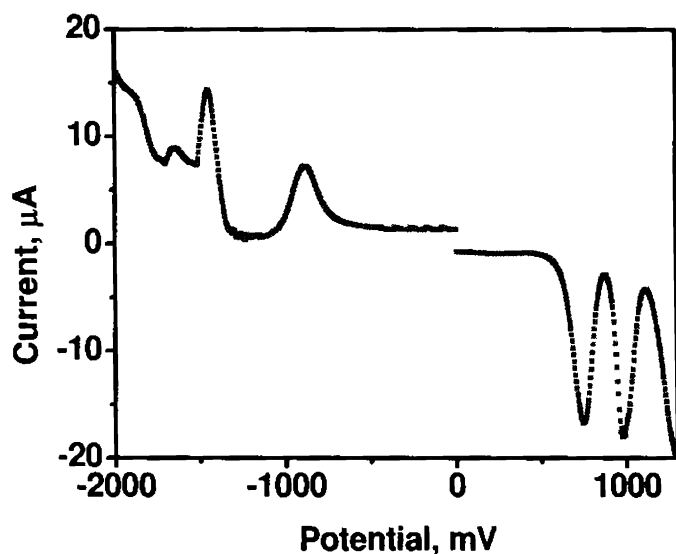
Figure 3.11. Squre wave voltammogram of **PI-BPEA-PT** in DCM

Since **BPEA** is the light absorber and it can act as donor and acceptor, excitation of **BPEA** can lead to probable electron transfer pathways shown in Scheme 3.10. Path A involves electron transfer from **PT** to ^{1}**BPEA*** as the first step (ΔG^0 = -0.36 eV) to give **PI-•BPEA-PT•+**. This step is followed by a second electron transfer from **BPEA•+** to **PI** (ΔG^0 = -0.57 eV) leading to the final CS state. In path B the first electron transfer occurs between ^{1}**BPEA*** and **PI** (ΔG^0 = -0.72 eV) to give **•PI-BPEA•+-PT**. This is followed by a second electron transfer from **PT** to **BPEA•+** (ΔG^0 = -0.21 eV), to give the final CS state. Since the free energy change in the first step of path B is much larger than that in path A, it is reasonable to assume that path B is more favored over path A. The very short distance between the **BPEA** and **PI** moieties is also expected to favors path B.

PI-BPEA-PT $\xrightarrow{\text{h}\nu}$ PI-^{1}BPEA*-PT

PT-^{1}BPEA*-PT

$\Delta G^0 = -0.43$ eV

PI-BPEA$^{\bullet-}$-PT$^{\bullet+}$

Path A

$\Delta G^0 = -0.72$ eV

Path B

$\Delta G^0 = -0.57$ eV

PI$^{\bullet-}$-BPEA$^{\bullet+}$-PT

$\Delta G^0 = -0.21$ eV
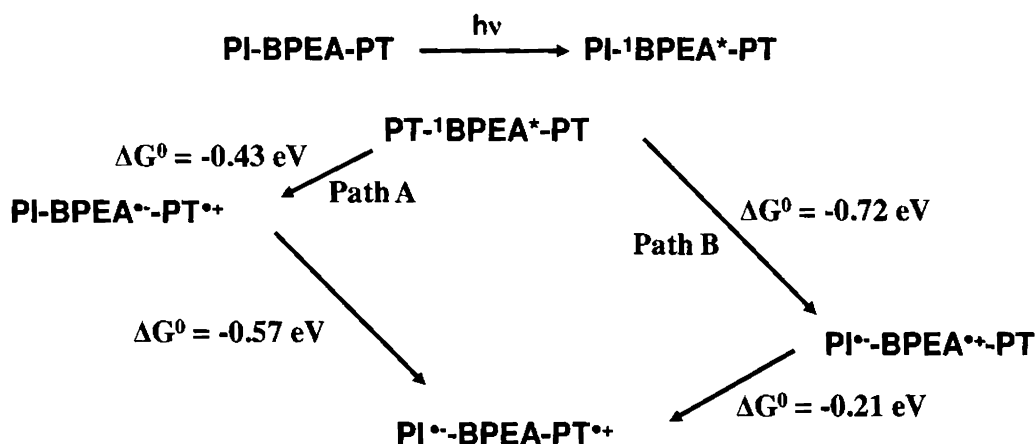
PI$^{\bullet-}$-BPEA-PT$^{\bullet+}$

Scheme 3.10. Photophysical processes in **PI-BPEA-PT**

3.3.2.5. Picosecond flash photolysis studies of PI-BPEA-PT

Picosecond transient absorption studies were carried out on **PI-BPEA-PT** to obtain a detailed understanding of the photophysical processes occurring in the triad. Figure 3.12 shows the picosecond transient absorption spectrum of **PI-BPEA-PT** immediately after and 2 ns following the laser flash. The most notable feature in the spectrum taken at the shortest possible time scale is the absence of the absorption at 570 nm due to the $S_1 \rightarrow S_n$ transition. This indicates that ^{1}**BPEA*** is extremely short-lived in the triad due to the ultrafast electron transfer. The spectrum taken immediately after the laser flash exhibited absorption maxima at 515 and 720 nm. These absorptions can be assigned to **PT**$^{\bullet+}$ and **PI**$^{\bullet-}$, respectively, based on literature reports and our own studies.[12,17]
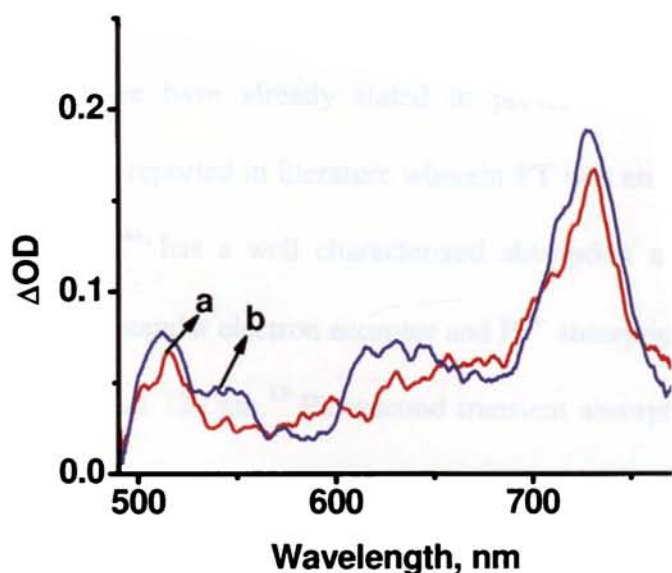
Figure 3.12. Picosecond transient absorption spectra obtained in the flash photolysis of **NT-BPEA-PT** (a) immediately and (b) 2 ns after the laser excitation

3.3.2.6. Nanosecond flash photolysis studies of PI-BPEA-PT

The transient spectrum obtained in the nanosecond laser flash photolysis of **PI-BPEA-PT** is shown in Figure 3.13. The spectrum exhibited maxima at 515 and 720 nm, as in the case of the picosecond spectrum. Under deaerated conditions decays of both the absorptions were similar and exhibited a lifetime of 25 μs (see insets in Figure 3.13). According to Scheme 3.9, excitation of the **BPEA** chromophore in **PI-BPEA-PT (PT-BPEA-PI)** can initiate electron transfer from either **PT** to ¹**BPEA*** leading to formation of **PT**$^{•+}$- **BPEA**$^{•-}$-**PI** or from ¹**BPEA*** to PI leading to the formation of **PT- BPEA**$^{•+}$-**PI**$^{•-}$. Our observations suggest that both these states were too short-lived to observe with the picosecond or nanosecond laser flash photolysis techniques. The spectrum observed in the

picosecond and nanosecond time scales correspond to the final CS state, **PT**$^{\bullet+}$-**BPEA-PI**$^{\bullet-}$. As we have already stated in previous chapter there are many molecular systems reported in literature wherein **PT** was employed as the electron donor and the **PT**$^{\bullet+}$ has a well characterized absorption maximum around 515 nm.[12] **PI** is a very popular electron acceptor and **PI**$^{\bullet-}$ absorption is known to exhibit a sharp peak around 720 nm.[17] Picosecond transient absorption studies indicated the very fast formation of transient absorptions at 515 and 720 nm and the same transients survived even in the microsecond time scale. These transients are very long-lived (τ = 25 μs) and decay by BET process, for which we obtained a rate constant (k_{BET} = 1/τ) of 4 × 10^4 s^{-1}. The lifetime of the CS state in **PI-BPEA-PT** triad is comparable to that observed for the **BPEA-PT** dyad.
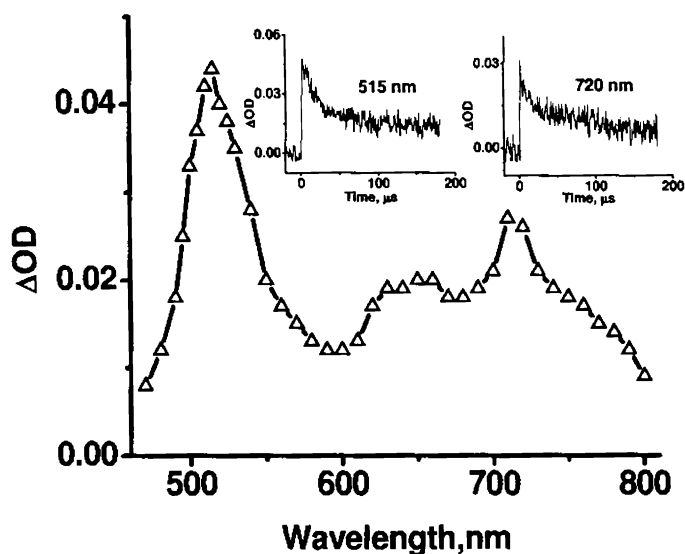
Figure 3.13. Transient absorption spectra of **PI-BPEA-PT** immediately after the laser pulse. The insets show decay profiles

In order to further confirm the assignment of the transient absorptions, we have carried out the nanosecond flash photolysis of **PI-BPEA-PT** in the presence of oxygen. The transient absorption spectrum along with the kinetic traces obtained at 515 and 720 nm are shown in Figure 3.14. It can be seen that the decay behaviors of the two transients are very different in the presence of oxygen. The decay of the 515 nm transient is not much affected and the 720 nm transient disappeared almost completely in the presence of oxygen. This result suggested that the absorptions at 515 nm is due to radical cation and that at 720 nm is due to radical anion. The spectrum taken in the presence of oxygen did not show any absorption in the 700 nm region.
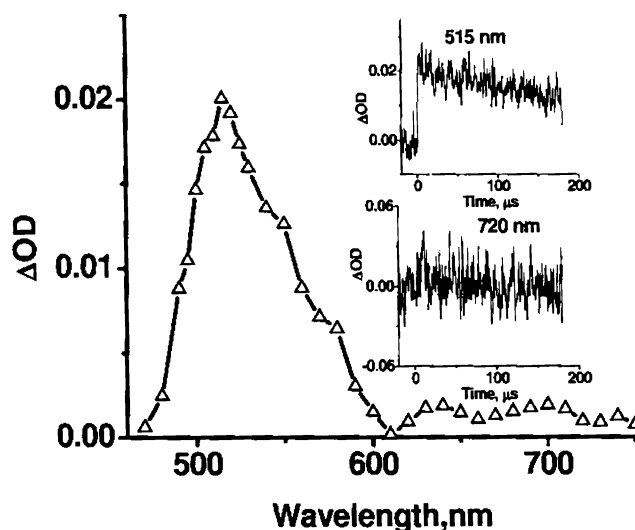
Figure 3.14. Transient absorption spectra of **PI-BPEA-PT** under oxygen saturated condition immediately after the laser pulse. The insets show decay profiles

Based on our results and literature reports, the following energy level diagram is proposed for **PI-BPEA-PT** (Scheme 3.11). The triplet energy of **PT** in

non-polar solvents is 2.62 eV[14] and that of **PI** is reported to be 2.45 eV.[17(f)] Albinsson and co-workers have reported the higher value of ^{3}**BPEA*** to be at 1.74eV.[16] All other energy states were determined from our experiments.
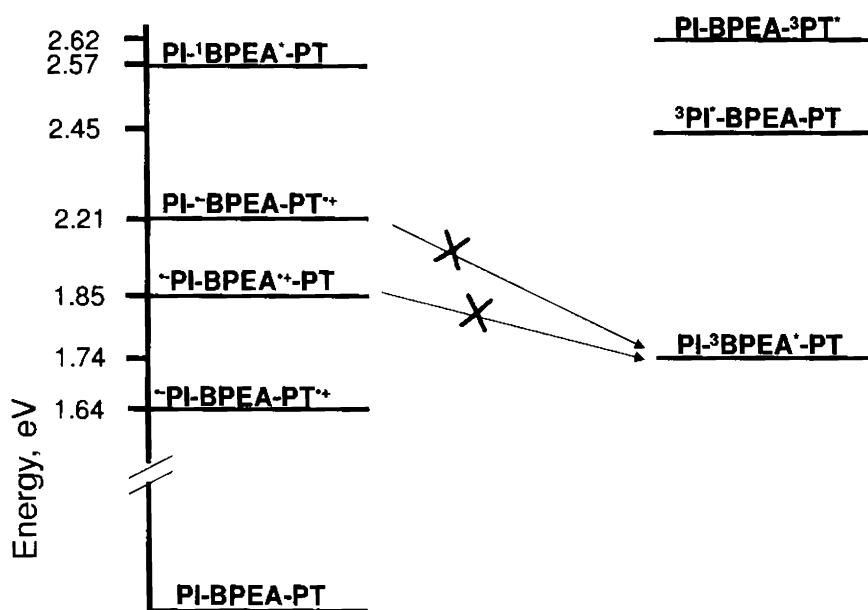
Scheme 3.11. Energy level diagram for **PI-BPEA-PT**

The energy level diagram for **PI-BPEA-PT** is different from that of **NT-BPEA-PT** in that the final CS state is lower in energy compared to the local **BPEA** triplet level. So once the final CS state is formed it cannot decay to any local triplet levels. The primary CS states, however, are higher in energy compared to the local **BPEA** triplet, but formation of the triplet is not observed in the flash photolysis experiments. We would like to point out that ISC from the primary CS states to the

local **BPEA** triplet level seems to be forbidden in this system as well and this is attributed to the forbidden nature of ISC in the parent **BPEA** chromophore.

3.3.3. Inverted region effect vs distance dependent electron transfer in BPEA based triads.

We have examined the photoinduced electron transfer processes in two **BPEA** based triads, **NT-BPEA-PT** and **PI-BPEA-PT**, and observed that in both systems reasonably long-lived CS states are formed. Lifetimes of the final CS states in these triads were, however, lower than the **BPEA-PT** dyads studied in Chapter 2. In the beginning of this chapter we have discussed the opposing nature of the distance dependence of ET and inverted region effects and in this section we try to analyze these factors quantitatively.

The inverted region effects operate when $-\Delta G^0 \gg \lambda$. As stated previously $\lambda = \lambda_i + \lambda_o$, where λ_i stands for the inner shell reorganization energy and λ_o stands for the outer shell reorganization energy. Inner shell reorganization energy for BET from the final CS states will have contributions due to $\mathbf{PT^{•+}} \rightarrow \mathbf{PT}$ reduction and $\mathbf{NT^{•-}} \rightarrow \mathbf{NT}$ or $\mathbf{PI^{•-}} \rightarrow \mathbf{PI}$ reduction. In Chapter 2 we stated that the inner shell reorganization energy associated with phenothiazine redox process is 0.2 –0.27 eV. **NT** and **PI** are rigid systems and we can assume a low value of 0.1 eV for the inner shell reorganization in these systems. Thus the total inner shell reorganization energy for BET in these triad systems is about 0.37 eV.

Outer shell reorganization energy in these triads could be calculated using equation 3.2. For **NT-BPEA-PT** we used values of r_A = 2.49 Å, r_D = 3.34 Å and d_{cc} = 29.13 Å (all values obtained from molecular models assuming linear configuration) and obtained λ_o = 1.73 eV. For the triad **PI-BPEA-PT**, we obtained λ_o = 1.4 eV (r_A = 3.52 Å, r_D = 3.34 Å and d_{cc} = 28.53 Å). Thus the total reorganization energy in **NT-BPEA-PT** is 2.1 eV and that in **PI-BPEA-PT** is 1.77 eV. $-\Delta G^0$ values in the two systems were 2.0 eV and 1.64 eV, respectively. Thus for the BET reactions in these triads $-\Delta G^0 \leq \lambda$. In other words BET processes in these triads fall in the normal region near the top of the Marcus parabola where the rates are expected to be maximum. Hence it is certain that the inverted region effect is not responsible for the slow BET processes in **NT-BPEA-PT** and **PI-BPEA-PT** triads. The observed long lifetime of the CS states in these molecules is thus attributed to the large distance between the donor and acceptor components in the final CS state. It is to be noted however, that inverted region effects may be operating in these triads in the first electron transfer stage. This would reduce BET at the primary ET stage and result in high yield of the final CS state.

3.4. Conclusions

In this chapter we have investigated the PET processes in two **BPEA** based triads, namely **NT-BPEA-PT** and **PI-BPEA-PT**. Fluorescence of the **BPEA** chromophore in both systems were highly quenched due to PET processes. Two possible electron transfer pathways could be identified in these systems and the

picosecond transient absorption studies suggested PET between the **BPEA** and acceptor **NT** or **PI** units as the first step. Nanosecond laser flash photolysis experiments confirmed formation of long-lived CS states in both cases. Analysis of the ΔG^0 and λ values suggested that the inverted region effect has no role in stabilizing the final CS state. Hence the long lifetime of the final CS state is attributed to the long distance separating the donor and acceptor components in the CS state.

3.5. Experimental section

3.5.1. General

Melting points were determined on a Mel-Temp II melting point apparatus and are uncorrected. Proton NMR data were obtained from either a 300 MHz Bruker Avance DPX spectrometer or a 500 MHz Bruker Avance DPX spectrometer .^{13}CNMR spectra were recorded using a 500 MHz Bruker Avance DPX spectrometer. FT-IR spectra were recorded on a Shimadzu IR Prestige 21 spectrometer. High-resolution mass spectra were obtained by using a JOEL JMS600 mass spectrometer. Absorption spectra were obtained using a Shimadzu 3101PC UV/Vis-NIR scanning spectrophotometer. Steady state fluorescence experiments were performed with a SPEX Fluorolog F112X spectrofluorimeter by using optically dilute solutions. The fluorescence quantum yields in dichloromethane were determined with relative method employing an optically

matched solution of **BPEA** in chloroform as reference (Φ_R = 0.64).[18] The following equation was used,

$$\Phi_F = \Phi_R \frac{A \; OD_R \; n^2}{A_R \; OD \; n_R^2} \qquad (3.5)$$

where, the subscript R refers to the reference, OD is the optical density at the excitation wavelength (OD $\approx$ 0.1 at 440 nm for both reference and standard), n is the refractive index of the solvent and A is the area under the fluorescence spectrum. Electrochemical experiments were performed by using a BAS 50W voltammetric analyser. Solutions of the compounds (1 $\times$ 10^{-3} M) in dichloromethane containing 0.1 M tetra-n-butylammonium hexafluorophosphate were thoroughly deaerated and used for CV experiments. Time-resolved fluorescence experiments were performed by using an IBH picosecond single-photon counting system employing a 440 nm Nano-LED excitation source and a Hamamatsu C4878-02 micro channel plate (MCP) detector. Nanosecond laser flash photolysis experiments were performed by using an Applied Photophysics Model LKS-60 laser kinetic spectrometer by using the third harmonic (355 nm) from an INDI-40-10-HG Quanta Ray Nd:YAG laser. The analysing and laser beams were fixed at right angles to each other. Solutions for laser flash photolysis studies were deaerated by purging with argon for 20 min before experiments. Picosecond transient absorption experiments were carried out using Mode-Locked

Nd:YAG laser system PY61C-10, (532 nm, 5 mj/pulse, FWHM 35 ps, 10 Hz

repetition rate). The white light probe was generated by focusing fundamental laser

output (1064 nm) on to a 10 mm quartz cuvette containing 10 ml water and 10 ml

D_2O mixture. The optical delay line provided a pump beam time window of 2.45

ns and a step resolution of 3.33 ps. The scattered 532 nm laser beam was filtered

using a band pass filter. The reflected probe light was focused on a 200 µm core

fibre connected to an Ocean Optics SD2000 UV-Vis CCD spectrophotometer (400

nm to 800 nm). Typically 100 excitation pulses were averaged to obtain the

transient absorption at the set delay time. All the experiments were conducted at

room temperature.

3.5.2. Synthesis and characterization

Synthesis of 2: 4-iodophenol (2.24 g, 10.18 mmol) was dissolved in dry acetone

(20 mL). Potassium carbonate (2.42 g, 18.52 mmol) and 4-nitrobenzyl bromide (2

g, 9.26 mmol) in dry acetone (20 mL) were added and the mixture refluxed under

argon for 24 h. It was poured into water and extracted with dichloromethane. The

extract was washed with 20% sodium hydroxide solution and then with water. The

organic layer was dried and evaporated at reduced pressure to get **2**, (3.16 g, 96%).

mp 139-140 °C. Mass (GC-MS): calcd. for $C_{13}H_{10}INO_3$: 355; found: 355. ^1H NMR

(CDCl$_3$, 500 MHz) δ: 5.06 (s, 2H), 6.66 (d, 2H), 7.50 (m, 4H), 8.16 (d, 2H).

Synthesis of 3: **2** (1.55g, 4.36 mmol), dichlorobis(triphenylphosphine) palladium(II) (123 mg, 0.17 mmol) and copper(I) iodide (83 mg, 0.44 mmol) were dissolved in dry THF (50 mL). Dry diisopropylamine (10 mL) and trimethylsilylacetylene (555 mg, 5.66 mmol) were added under argon and the mixture stirred for 24 h. Solvent was removed and residue was purified by column chromatography on silica using chloroform/hexane (20:80) to get **3**. (1.2 g, 85%). mp 95-96 °C. Mass (GC-MS): calcd. for $C_{18}H_{19}NO_3Si$: 325; found: 325. ^1H NMR (CDCl$_3$, 500 MHz) δ: 0.258 (s, 9H), 5.17 (s, 2H), 6.89 (d, 2H), 7.44 (d, 2H), 7.60 (d, 2 H), 8.25 (d, 2H).

Synthesis of 4: **3** (1.36 g, 4.19 mmol) was dissolved in THF (20 mL). The solution was cooled to 0 °C and TBAF (1M in THF, 4.2 mL) added. The mixture was then stirred for 2 h at RT, poured into ice-cold water and extracted with dichloromethane. The solvent was removed and residue was purified over alumina column using chloroform/hexane (20:80) to obtain **4**. (900 mg, 85%). mp 151-152 °C. Mass (GC-MS): calcd. for $C_{15}H_{11}NO_3$: 253; found: 253. ^1H NMR (CDCl$_3$, 500 MHz) δ: 3.01 (s, 1H), 5.17 (s, 2H), 6.91 (d, 2H), 7.44 (d, 2H), 7.60 (d, 2H), 8.24 (d, 2 H).

Synthesis of 6: To an argon degassed RB flask, 9, 10-dibromoanthracene (300 mg, 0.89 mmol), dichlorobis(triphenylphosphine)palladium(II) (19 mg, 0.026 mmol), copper(I) iodide (5 mg, 0.026 mmol), dry toluene (60 mL) and dry diisopropylamine (15 mL) were added. **4** (270 mg, 1.07 mmol) in dry toluene (10

mL) was added drop wise to it and the reaction mixture was stirred for 24 h at 70

°C under argon. Solvent was removed and the residue obtained was purified by

column chromatography over silica gel using chloroform/hexane (3:7) to obtain **6**,

(158 mg, 35%). mp 178-179 °C. FAB-MS (M^+) calcd. for $C_{29}H_{18}BrNO_3$: 508.36;

found: 508.79. ^{1}H NMR (CDCl$_3$, 300 MHz) δ: 5.17 (s, 2H), 6.92 (d, 2H), 7.44 (m,

6H), 7.60 (d, 2H), 8.24 (d, 2H), 8.55 (d, 2 H), 8.68 (d, 2H).

Synthesis of NT-BPEA-PT: To an argon degassed RB flask, **6** (100 mg, 0.19

mmol), dichlorobis(triphenylphosphine)palladium(II) (5 mg, 0.006 mmol),

copper(I) iodide (2 mg, 0.009 mmol), dry toluene (25 mL) and dry

diisopropylamine (5 mL) were added. **7** (85 mg, 0.23 mmol) in dry toluene (10

mL) was added and the reaction mixture stirred for 24 h at 70 °C under argon.

Solvent was removed and the residue obtained was purified by column

chromatography over silica gel using chloroform/hexane (3:1) to obtain **NT-**

BPEA-PT, (75 mg, 50%). Decomposed above 250 °C. IR (KBr) v_{max}: 529, 571,

638, 758, 829, 1051, 1107, 1171, 1248, 1288, 1344, 1462, 1510, 1601, 2191, 3055

cm^{-1}. ^{1}H NMR (CDCl$_3$, 500 MHz) δ = 2.31 (m, 2H), 4.14 (m, 4H), 5.19 (s, 2H),

6.76 (d, 2H), 6.94 (m, 8H), 7.05 (d, 2H), 7.19 (m, 6H), 7.66 (m, 4 H), 7.73 (d, 2H),

8.28 (d, 2H), 8.67 (m, 2H). ^{13}C NMR (CDCl$_3$, 125 MHz) δ: 26.73, 43.79, 70.44,

85.33, 102.47, 114.31, 114.93, 118.45, 119.73 122.62, 123.83, 127.23, 127.99,

129.47, 133.27, 135.39, 142.81, 145.14, 146.93, 159.21. FAB-MS (M^+) calcd. for

$C_{52}H_{36}N_2O_4S$: 784.92; found: 785.26.

Synthesis of 8 (1-iodo-4-nitrobenzene):[9] A mixture of 4-nitroaniline (10 g, 72 mmol), concentrated sulphuric acid (8 mL) and water (60 mL) was stirred for 1 hour. The mixture was cooled to 0-5 °C, and diazotised with a solution of sodium nitrite (5 g, 72 mmol) in water (15 mL). The cold solution was filtered and added to a solution of potassium iodide (20 g, 120 mmol) in water (60 mL). The precipitated product was suction filtered and recrystallised from ethanol to obtain 8 (14.5 g, 80%). mp 171-172 °C. Mass (GC-MS): calcd. for $C_6H_4INO_2$: 249; found: 249. ^{1}H NMR (CDCl$_3$, 300 MHz) δ: 7.94 (m, 4H).

Synthesis of 9:[10] To a 100 mL RB flask was added 1-iodo-4-nitrobenzene (1.06 g, 4.04 mmol), dichlorobis(triphenylphosphine)palladium(II) (0.029 g, 0.0411 mmol), and copper (I) iodide (7.7 mg, 0.0404 mmol). After purging the flask with argon for 10 minutes, triethylamine (40 mL) was added via syringe and the reaction stirred for 10 minutes under a constant flow of argon. The argon flow was stopped and of trimethylsilylacetylene (1.20 mL, 0.834 g, 8.49 mmol) was added via syringe. Argon was allowed to flow briefly while the septum was replaced with a ground glass stopper and the flask sealed and heated slightly while stirring for 22 h. The reaction was cooled to room temperature and filtered to remove the inorganic catalysts. The precipitate was washed with ethyl acetate and the filtrates combined and evaporated to leave behind brown oil which crystallized upon standing. The oil was chromatographed through silica gel with a solvent system of hexane/ethyl acetate (90:10) and the product was isolated as a yellow liquid which

solidified under vacuum drying (0.704 g, 80%), mp 77-78 °C. Mass (GC-MS): calcd. for $C_{11}H_{13}NO_2Si$: 219; found: 219. ^{1}HNMR (CDCl$_3$, 300 MHz) δ: 0.28 (s, 9H), δ 7.60 (d, 2H), 8.17 (d, 2H).

Synthesis of 10:[10] To a 100 mL round-bottomed flask was added **9** (0.500 g, 2.28mmol) and dichloromethane (20 mL). Next was added a suspension of potassium carbonate (0.477 g, 3.45 mmol) in methanol (70 mL). The suspension was stirred under a positive pressure of argon for 1 hour. The reaction was filtered and evaporated to leave behind a solid which was chromatographed through a plug of silica gel with a solvent system of hexane/ethyl acetate (90:10). The product was dried under vacuum (0.29 g, 87%), mp 151-152 °C. Mass (GC-MS): calcd. for $C_8H_5NO_2$: 147; found: 147. ^{1}HNMR (CDCl3, 500 MHz) δ: 3.36 (s, 1H), 7.64 (d, 2H,) 8.20 (d, 2H).

Synthesis of 11: To an argon degassed RB flask, 9, 10-dibromoanthracene (300 mg, 0.89 mmol), dichlorobis(triphenylphosphine) palladium(II) (19 mg, 0.026 mmol), copper(I) iodide (5 mg, 0.026 mmol), dry toluene (60 mL) and dry diisopropylamine (15 mL) were added. **10** (157 mg, 1.07 mmol) in dry toluene (10 mL) was added drop wise to it and the reaction mixture was stirred for 24 h at 70 °C under argon. Solvent was removed and the residue obtained was purified by column chromatography over silica gel using chloroform/hexane (1:1) to obtain **6**, (130 mg, 36%). mp 215-216 °C. FAB-MS (M$^+$) calcd. for $C_{22}H_{12}BrNO_2$: 402.24;

found: 402.65.^{1}H NMR (CDCl$_3$, 300 MHz) δ: 7.68 (m, 4H), 7.90 (d, 2H), 8.32 (d, 2H), 8.62 (m, 4H).

Synthesis of 12: To an argon degassed RB flask, **11** (100 mg, 0.25 mmol), dichlorobis(triphenylphosphine)palladium(II) (7 mg, 0.01 mmol), copper(I) iodide (3 mg, 0.012 mmol), dry toluene (30 mL) and dry diisopropylamine (5 mL) were added. **7** (105 mg, 0.3 mmol) in dry toluene (10 mL) was added and the reaction mixture stirred for 24 h at 70 °C under argon. Solvent was removed and the residue obtained was purified by column chromatography over silica gel using chloroform/ hexane (3:1) to obtain **12**, (54 mg, 32%). mp 193-194 °C. FAB-MS (M$^+$) calcd. for C$_{45}$H$_{30}$N$_2$O$_3$S: 678.80; found: 678.26. ^{1}H NMR (CDCl$_3$, 300 MHz) δ: 2.32 (t, 2H), 4.17 (m, 4H), 6.94 (m, 6H), 7.18 (m, 4H), 7.67 (m, 6H), 7.89 (d, 2H), 8.32 (d, 2H), 8.62 (d, 2H), 8.70 (d, 2H).

Synthesis of 13: **12** (30 mg, 0.044 mmol), SnCl$_2$ (H2O)$_2$ (180 mg, 0.79 mmol), were added to THF (15 mL) with 4 drops 37% HCl and stirred under reflux condition for 5 h. The reaction mixture was diluted with 50 mL of DCM and washed once with 0.1 M sodium bicarbonate and two times with water. The organic solvent was removed on a rotary evaporator and the crude product was purified by filteration through an alumina pad using DCM as the eluent to afford **13** (23 mg, 80%). mp 182-183 °C. FAB-MS (M$^+$) calcd. for C$_{45}$H$_{32}$N$_2$OS: 648.81; found: 648.42. ^{1}H NMR (CDCl$_3$, 300 MHz) δ: 2.32(t, 2H), 3.92 (s, 2H), 4.15 (m, 4H), 6.73 (d, 2H), 6.94 (m, 6H), 7.18 (m, 4H), 7.61 (m, 8H), 8.68 (m, 4H).

Synthesis of 14: Pyromellitic dianhydride (8.72 g, 40 mmol) is added to dry DMF

(100 mL) in a 250 mL round-bottom flask. 1-Octanamine (5.16 g, 40.2 mmol) is

added, and the mixture was heated to 130 °C overnight. The DMF is cooled in the

refrigerator, and the solid formed (the bisimide) is suction-filtered. The DMF is

evaporated on a rotary evaporator. The residue is taken up in chloroform and

washed with water to remove the dianhydride starting material. The organic layer

is dried over anhydrous sodium sulphate, and the solvent is removed on a rotary

evaporator to obtain **14** (3.9 g, 30%). FAB-MS (M$^+$) calcd. for $C_{18}H_{19}NO_5$: 329.35;

found: 330.13. ^{1}H NMR (DMSO (d$_6$), 300 MHz) δ: 0.81(t, 3H), 1.22 (m, 10H),

1.57 (m, 2H), 3.56 (t, 2H), 8.23 (s, 2H).

Synthesis of PI-BPEA-PT: **13** (15 mg, 0.023 mmol) and **14** (12 mg, 0.035 mmol)

was dissolved in dry DMF (10 mL) in a 25 mL RB flask. The reaction mixture was

heated at 140 °C for 48 hours under argon atmosphere. The DMF was removed

evaporation under reduced pressure. The residue was chromatographed on a silica

gel column using chloroform as eluent to obtain **PI-BPEA-PT** (11 mg, 50%).

Decomposed above 200 °C. IR (KBr) v_{max}: 528, 571, 638, 748, 825, 1083, 1173,

1246, 1364, 1466, 1512, 1719, 2851, 2922 cm^{-1}. ^{1}H NMR (CDCl$_3$, 300 MHz)δ:

0.88(t, 3H), 1.26 (m, 12H), 2.33 (t, 2H), 3.7 (t, 2H), 4.17 (m, 4H), 6.95 (m, 6H),

7.18 (m, 4H), 7.65 (m, 8H), 7.86 (d, 2H), 8.17 (s, 2H), 8.65 (4H). ^{13}C NMR

(CDCl$_3$, 125 MHz) δ: 14.23, 22.63, 26.71, 29.36, 31.94, 40.17, 43.78, 73.34,

85.31, 102.45, 111.41, 114.32, 114.93, 118.45, 119.73 122.67, 123.81, 125.46,

127.26, 128.11, 129.17, 130.92, 132.41, 133.22, 135.36, 144.81, 159.19, 167.13, 167.96. FAB-MS (M^+) calcd. for $C_{63}H_{49}N_3O_5S$: 960.15; found: 960.71.

3.6. References

1. (a) Verhoeven, J. W. in *Electron Transfer- From Isolated Molecules to Biomolecules, Part I*; Jortner, J., Bixon, M., Prigogine, i., Rice, S. A. Eds.; john Wiley and Sons, Inc.: London, 1999; p 603. (b) McLendon, G. *Acc. Chem. Res.* **1988**, *21*, 160-167. (c) Jordan, K. D.; Paddon-Row, M. N. *Chem. Rev.* **1992**, *92*, 395-410. (d) Davis, W. B.; Svec, W. A.; Ratner, M. A.; Wasielewski, M. R. *Nature* **1998**, *396*, 60-63. (e) Yonemoto, E. H.; Saupe, G. B.; Schmehl, R. H.; Hubig, S. M.; Riley, R. l.; Iverson, B. L.; Mallouk, T. E. *J. Am. Chem. Soc.* **1994**, *116*, 10557-10563. (f) Isied, S. S.; Ogawa, M. Y.; Wishart, J. F. *Chem. Rev.* **1992**, *92*, 381-394. (g) Shuster, G. B. *Acc. Chem. Res.* **2000**, *33*, 253-260. (h) Smitha, M. A.; Prasad, E.; Gopidas, K. R. *J. Am. Chem. Soc.* **2001**, *123*, 1159-1165.

2. Heiler, D.; Mc.Lendon, G.; Rogalskyj, P. *J. Am. Chem. Soc.* **1987**, *109*, 604-606.

3. (a) Fukuzumi, S. *Bull. Chem. Soc. Jpn.* **2006**, *79*, 177-195. (b) Fukuzumi, S. *Phys. Chem. Chem. Phys.* **2008**, *10*, 2283-2297.

4. (a) Kavarnos, G. J. *Fundamentals of Photoinduced Electron Transfer*, VCH, New York, 1993; p 315. (b) Marcus, R. A. *J. Chem. Phys.* **1956**, *24*, 966-978.

(c) Marcus, R. A. *Annu. Rev. Phys. Chem.* **1964**, *15*, 155-196. (d) Barbara, P. F.; Meyer, T. J.; Ratner, M. A. *J. Phys. Chem.* **1996**, *100*, 13148-13168.

5.   (a) Ohkubo, K.; Kotani, H.; Shao, J.; Ou, Z.; Kadish, K. M.; Li, G.; Pandey, R. K.; Fujitsuka, M.; Ito, O.; Imahori, H.; Fukuzumi, S. *Angew. Chem. Int. Ed.* **2004**, *43*, 853-856. (b) Fukuzumi, S.; Kotani, H.; Ohkubo, K.; Ogo, S.; Tkachenko, N. V.; Lemmetyinen, H. *J. Am. Chem. Soc.* **2004**, *126*, 1600-1601.

6.   (a) Marcus, R. A.; Sutin, N. *Biochim. Biophys. Acta* **1985**, *811*, 265-322 (b) Marcus, R. A. *Angew. Chem., Int. Ed.* **1993**, *32*, 1111-1121.

7.   Okamoto, K. ; Hasobe, T. ; Tkachenko, N. V. ; Lemmetyinen, H. ; Kamat, P. V. ; Fukuzumi, S. *J. Phys. Chem. A* **2005**, *109*, 4662-4670.

8.   van Ramesdonk, H. J.; Bakker, B. H.; Groeneveld, M. M.; Verhoeven, J. W.; Allen, B. D.; Rostron, J. P.; Harriman, A. *J. Phys. Chem. A* **2006**, *110*, 13145-13150.

9.   Furniss, B. S.; Hannaford, A.J.; Smith, P. W. G.; Tatchell, A. R. *Vogel's Text Book of Practical Organic Chemistry*, Pearson Education, Singapore, 2004; p 930.

10.   Serwinski, P. R.; Lahti, P. M. *Org. Lett.* **2003**, *5*, 2099-2102.

11.   Wiederrecht, G. P.; Svec, W. A.; Niemczyk, M. P.; Wasielewski, M. R. *J. Phys. Chem.* **1995**, *99*, 8918-8926.

12. (a) Moroi, M.; Braun, A. M.; Grätzel, M. *J. Am. Chem. Soc.* **1979**, *101*, 567-572. (b) Danielson, E.; Elliott, C. M.; Merkert, J. W.; Meyer, T. J. *J. Am. Chem. Soc.* **1987**, *109*, 2519-2520. (c) Chen, P.; Duesing, R.; Graff, D. K.; Meyer, T. J. *J. Phys. Chem.* **1991**, *95*, 5850-5858. (d) Klumpp, T.; Linsenmann, M.; Larson, S. L.; Limoges, B. R.; Bürssner, D.; Krissinel, E. B.; Elliott, C. M.; Steiner, U. E. *J. Am. Chem. Soc.* **1999**, *121*, 1076-1087. (e) Ajayakumar, G.; Gopidas, K. R. *Photochem. Photobiol. Sci.* **2008**, *7*, 826-833.

13. Shida, T.; Iwata, S. *J. Phys. Chem.* **1971**, *75*, 2591-2602.

14. Murov, S. L.; Carmichael, I.; Hug, G. L. In *Handbook of Photochemistry*, 2nd ed.; Marcel Dekker: New York, 1993

15. Takezaki, M.; Hirota, N.; Terazima, M. *J. Phys. Chem. A* **1997**, *101*, 3443-3448.

16. Kilsa, K.; Macpherson, A. N.; Gilbro, T.; Martensson, J.; Albinsson B. *Spectrochimica Acta A* **2001**, 57, 2213-2227.

17. (a) Hayes, R. T.; Walsh, C. J.; Wasielewski, M. R. *J. Phys. Chem. A* **2004**, *108*, 2375-2381. (b) Gosztola, D.; Niemczyk, M. P.; Svec, W.; Lukas, A. S.; Wasielewski, M. R. *J. Phys. Chem. A* **2000**, *104*, 6545-6551. (c) Harada, K.; Fujitsuka, M.; Sugimoto, A.; Majima, T. *J. Phys. Chem. A*, **2007**, *111*,

11430–11436. (d) Osuka, A.; Nakajima, S.; Maruyama, K.; Mataga, N.; Asahi, T. *Chem. Lett.* **1991**, 1003-1006. (e) Redmore, N. P.; Rubtsov, I. V.; Therien, M. J. *Inorg. Chem.* **2002**, *41*, 566-570. (f) Balan, B.; Gopidas. K. R. *Chem. Eur. J.* **2007**, *13*, 5173-5185.

18. Nguyen, P.; Todd, S.; Biggelaar, D. V.; Taylor, N. J.; Marder, T. B.; Wittmann, F.; Friend, R. H. *Synlett.* **1994**, 299-301.

Long-lived Photoinduced Charge Separation in 1,6-Bis(phenylethynyl)pyrene – Phenothiazine Dyads

4.1. Abstract

*A strategy for the design of donor-acceptor dyads, wherein decay of the charge separated (CS) state to low lying local triplet levels could possibly be prevented, is proposed. In order to examine this strategy, a linked donor-acceptor dyad **BPEP-PT** with bis(phenylethynyl)pyrene (**BPEP**) as the light absorber and acceptor and phenothiazine (**PT**) as donor was designed and photoinduced electron transfer in the dyad investigated. Absorption spectra of the dyad can be obtained by adding contributions due to the **BPEP** and **PT** moieties indicating that the constituents do not interact in the ground state. Fluorescence of the **BPEP** moiety was efficiently quenched by the **PT** donor and this was attributed to electron transfer from **PT** to **BPEP**. Picosecond transient absorption studies suggested formation of a charge separated state directly from the singlet excited state of **BPEP**. Nanosecond flash photolysis experiments gave long-lived transient absorptions assignable to **PT** radical cation and **BPEP** radical anion. These assignments were confirmed by oxygen quenching studies and secondary electron transfer experiments. Based on*

*the available data, energy level diagram for **BPEP-PT** was constructed. The long lifetime of the charge separated state was attributed to the inverted region effects. The CS state did not undergo decay to low lying **BPEP** triplet indicating the success of our strategy.*

4.2. Introduction

In the second chapter of this thesis we discussed the generation of long-lived CS states in 9,10-bis(phenylethynyl)anthracene-phenothiazine (**BPEA-PT**) dyads. Observations of long-lived charge separation in these dyads were attributed to 'inverted region effects'. In Chapter 1 of this thesis we have given a detailed account of the arguments both in favor and against the inverted region effect as being responsible for the generation of long-lived charge separation in simple dyads. Proponents of the inverted region effect argue that components of the D-A dyads could be selected in such a manner that $-\Delta G^0_{PET} \leq \lambda$ and $-\Delta G^0_{BET} >> \lambda$. In such cases k_{PET} would fall in the normal region and k_{BET} would be in the deep inverted region of the Marcus parabola.[1] Under these circumstances $k_{PET} >> k_{BET}$, leading to formation of long-lived CS state.[2] The argument against the inverted region effect is that when $-\Delta G^0_{BET}$ is very large, other deactivation channels such as jumps to low lying local triplet levels may prevail over charge recombination to the ground state.[3] Nuclear tunneling also may become very important and it is suggested that the Marcus equation may not adequately describe electron transfer

in the deep inverted region.[4] Observation of long-lived CS state in **BPEA-PT** systems supports the arguments favoring inverted region effects.

As mentioned in Chapter 1 of this thesis, arguments against the inverted region effects also merit attention. The energy level diagram for **BPEA-PT** showed the presence of a **BPEA** based triplet below the CS state (Chapter 2) and it is not clear as to why the CS state does not cross over to the local triplet level. We proposed that inter system crossing (ISC) from ^{1}**BPEA*** to ^{3}**BPEA*** is forbidden and this forbidden-ness exists even in the ^{1}($^\bullet$**BPEA-PT**$^{\bullet+}$) CS state also. If our proposal is correct, then it would be possible to design dyads capable of long-lived charge separation, even if low-lying local triplet levels exist in these dyads. Scheme 4.1 can form the basis of such a design.
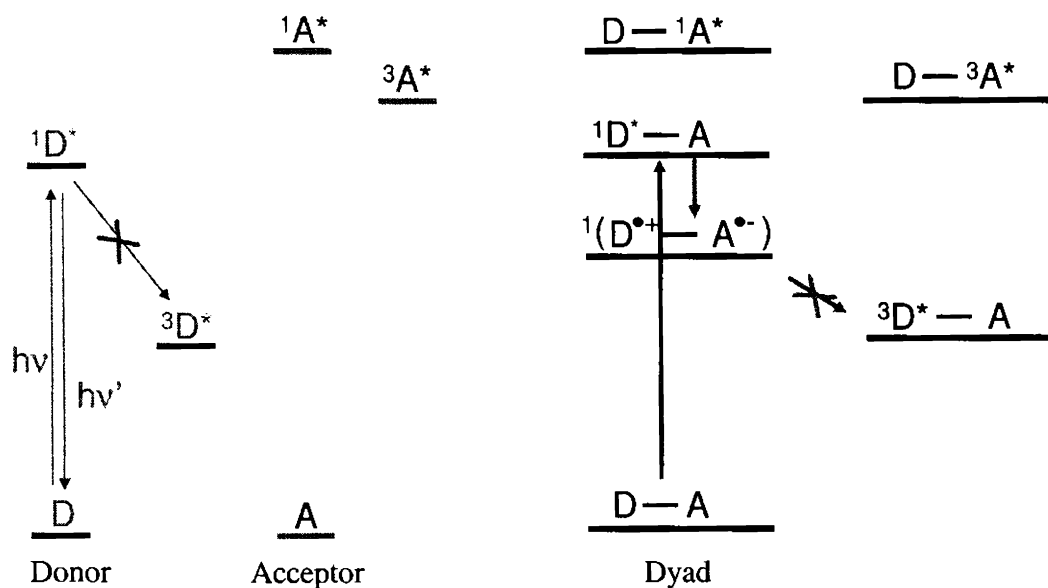
Scheme 4.1. Scheme proposed for the design of dyads with long-lived CS state

In Scheme 4.1, D is the light absorber and donor. Excitation of D would result in the formation of $^1D^*$, which exhibits very high fluorescence quantum yield. $^1D^*$ does not exhibit any tendency to undergo ISC to $^3D^*$. The acceptor A is selected such that both $^1A^*$ and $^3A^*$ are placed above $^1D^*$. Under these conditions the only local triplet state below the CS state would be the $^3D^*$-A state. If our proposal is correct, $^{+\bullet}D\text{-}A^{\bullet-}$ would not cross over to ^3D-A because of the negligible efficiency of the $^1D^* \rightarrow {}^3D^*$ transition. In Scheme 4.1 the light absorber acts as the donor. A similar scheme can be drawn for chromophores acting as acceptor.

In this chapter we try to provide more support for our proposal. This study required a chromophore with low ISC efficiency. Chromophores with very high fluorescence quantum yields normally have low ISC efficiencies. It is generally observed that fluorescence quantum yields of arenes are considerably improved upon substitution with phenylethynyl groups. This has been shown for naphthalene,[5] anthracene, tetracene,[6] pyrene,[7] and perylene.[8] Hence the ISC ability and population of the triplet state is expected to be considerably less in phenylethynyl arenes compared to their parent arenes. In this study we selected pyrene and attached phenylethynyl groups at its 1 and 6 positions to obtain a chromophore with very high fluorescence quantum yield.

Pyrene and its derivatives have been extensively applied to photonic devices[9] and biological probes like nucleic acids[10] and proteins[11] by virtue of their inherent and novel photophysical characteristics. However, a few serious

drawbacks exist in the photophysical properties of pyrene, which include the relatively short absorption wavelength, substantial quenching of its fluorescence by the presence of oxygen,[12] and the low fluorescence quantum yield.[13] Recently it has been shown by Inouye *et. al.* and Berlin *et. al.* that introduction of ethynyl groups into pyrene nuclei induced effective extension of π-conjugation and a large increase of fluorescence quantum yield compared to parent pyrene.[14] Also, the ethynylpyrenes maintain most of their fluorescence intensities even under aerated conditions, making them useful candidates for practical uses. Due to these peculiar fluorescence properties, bis(phenylethynyl)pyrene and its derivatives have been used in various applications such as optoelectronic devices,[15] electroluminescent devices,[16] two photon absorption dyes,[17] labelling of biomolecules[18] and detection of proteins.[19] Use of bis(phenylethynyl)pyrenes as PET probes, however, has not been explored.

In this chapter we report the photoinduced electron transfer processes in a dyad wherein 1,6-bis(methoxyphenylethynyl)pyrene (**BPEP**) serve as light absorber and acceptor and phenothiazine (**PT**) units serve as electron donor. The **BPEP** core is connected to the **PT** moieties through a short alkyl chain. Photoprocesses in the dyad **BPEP -PT** are compared with a model **BPEP** system. Structures of the model system and dyad are shown in Figure 4.1. We have probed the photoinduced charge separation in the **BPEP-PT** dyad using fluorescence

lifetime measurements. Picosecond and nanosecond laser flash photolysis

techniques confirmed the formation of a long-lived CS state in the dyad.
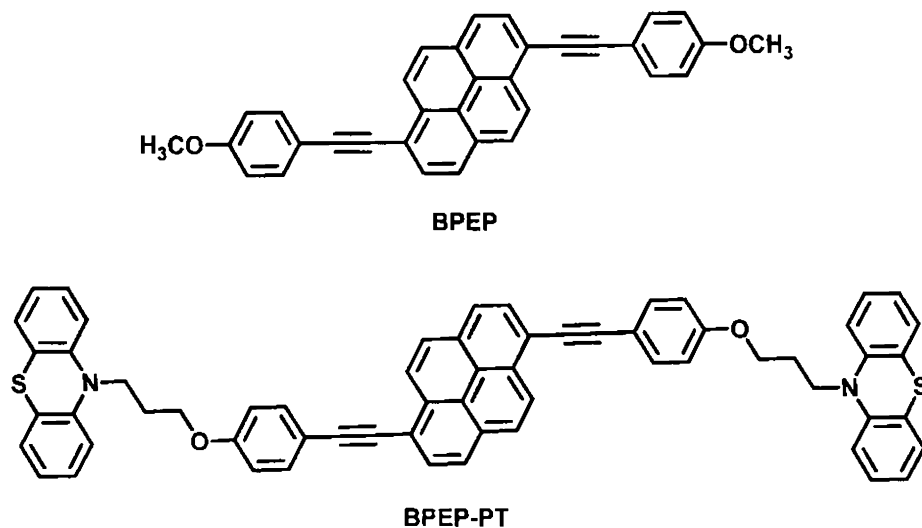

Figure 4.1. Structures of model compound **BPEP** and dyad **BPEP-PT** used in this study

4.3. Results and discussion

4.3.1. Synthesis and characterisation of BPEP and BPEP-PT

The model compound **BPEP** was synthesized as shown in scheme 4.2.

4-iodoanisole was reacted with trimethylsilylacetylene in the presence of Pd

catalyst to give **2** in 91% yield. **2** was desilylated using tetrabutylammonium

fluoride in THF to yield 4-methoxyphenylacetylene (**3**). Sonogashira reaction

between 1,6-dibromopyrene and **3** gave the model compound **BPEP** in 68% yield.

The dyad **BPEP-PT** was prepared as per Scheme 4.3. Synthesis of the **PT**-

appended phenylacetylene derivative **8** was presented in Chapter 2 of this thesis.

Dyad **BPEP-PT** was prepared in 51% yield by the Sonogashira reaction between

1,6-dibromopyrene and **8**.
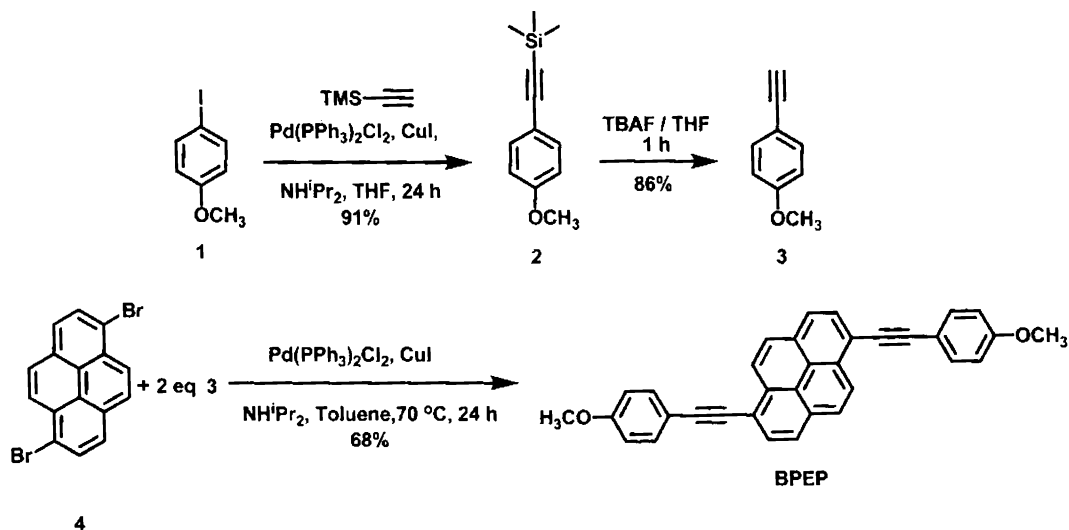
Scheme 4.2. Scheme for the synthesis of **BPEP**
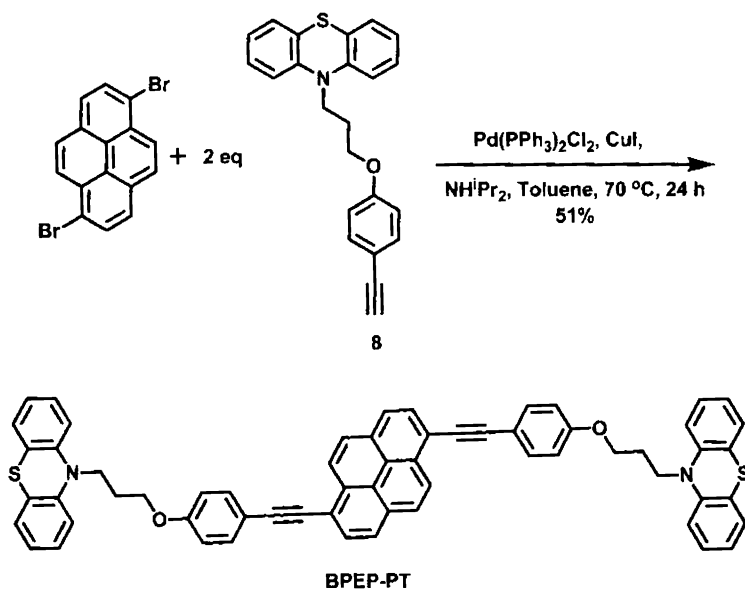
Scheme 4.3. Scheme for the synthesis of **BPEP-PT**

Details of the synthetic procedures are given in the experimental section. The various intermediates and final products were characterized thoroughly by analytical and spectroscopic techniques.

4.3.2. Photophysical and electrochemical studies

The absorption spectrum of **BPEP** is considerably red shifted when compared with that of the parent pyrene. The long wavelength absorption due to **BPEP** in dichloromethane (DCM) occurs in the 350-450 nm region (Figure 4.2). The long wavelength absorption in **BPEP-PT** is nearly identical to that in **BPEP** suggesting that the donor and acceptor moieties did not exhibit any electronic interaction in the ground state. The absorption due to the **PT** moieties in the dyad appeared at 250 and 300 nm. It can be safely assumed from Figure 4.2 that excitation above 350 nm populates only the **BPEP** excited states in the dyad.
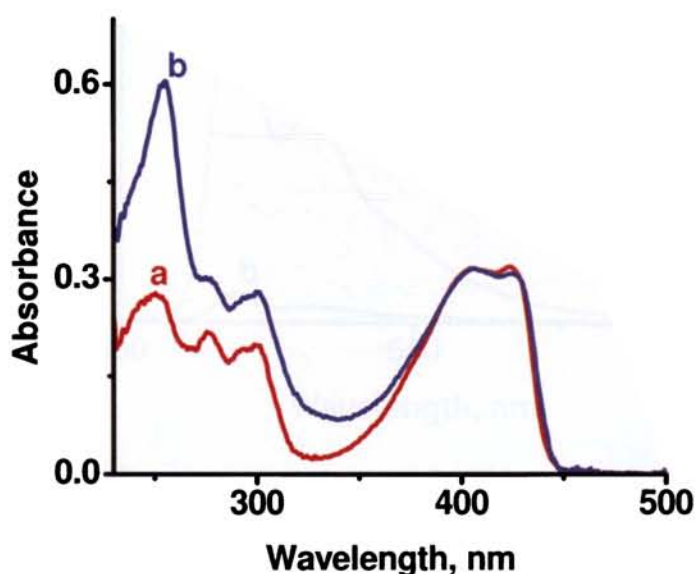

Figure 4.2. Absorption spectra of (a) **BPEP** and (b) **BPEP-PT** in DCM

Fluorescence spectrum of the model compound **BPEP** is shown in Figure 4.3a. The emission maximum occurs at 438 nm. The Stokes shift observed is very small (810 cm^{-1}) suggesting similar geometry for the S_0 and S_1 states of **BPEP**. Using the absorption and emission spectra, the excitation energy (E_{00}) was calculated and the value obtained was 2.86 eV. Fluorescence quantum yield (Φ_{BPEP} = 0.93) was very high for **BPEP**. Substitution of **PT** leads to considerable quenching of the fluorescence intensity as is evident from a comparison of the fluorescence spectra of **BPEP** and **BPEP-PT** shown in Figure 4.3. Spectra 4.3a and 4.3b were recorded under identical conditions and optical densities were matched at 390 nm. Fluorescence quantum yield for **BPEP-PT** ($\Phi_{BPEP-PT}$) was 0.1.
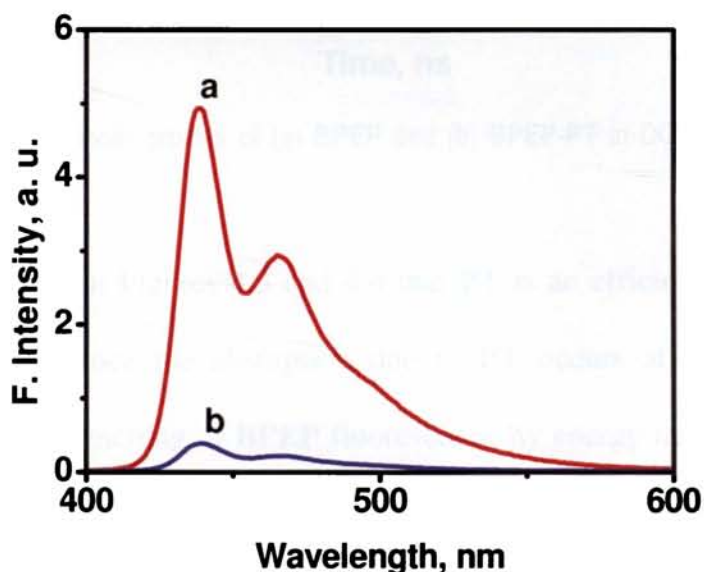

Figure 4.3. Fluorescence spectra of (a) **BPEP** and (b) **BPEP-PT** in DCM

Fluorescence lifetimes of **BPEP** and **BPEP-PT** were determined using single photon counting technique. The samples were excited using a 401 nm

nanoLED excitation source. **BPEP** exhibited monoexponential decay with a lifetime (τ_0) of 1.3 ns. **BPEP-PT** exhibited biexponential decay with $\tau_1 = 0.17$ ns (97.2%) and $\tau_2 = 1.25$ ns (2.8%). Decay profiles of **BPEP** and **BPEP-PT** along with the instrument function are presented in Figure 4.4.
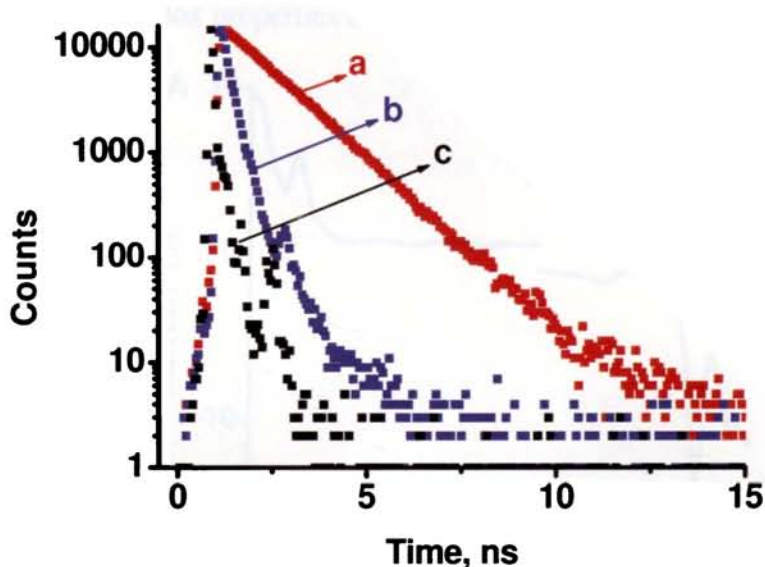
Figure 4.4. Fluorescence decay profiles of (a) **BPEP** and (b) **BPEP-PT** in DCM. (c) Instrument profile

It is obvious from Figures 4.3 and 4.4 that **PT** is an efficient quencher of **BPEP** fluorescence. Since the absorption due to **PT** occurs at higher energy compared to **BPEP**, quenching of **BPEP** fluorescence by energy transfer to **PT** is not possible and we can safely assume an electron transfer mechanism for the quenching. The reduced fluorescence quantum yield and lifetime of **BPEP-PT** are due to facile electron transfer from **PT** to the $^1S^*$ state of **BPEP** moiety in the dyad.

Redox potentials of the compounds (vs SCE) were measured in DCM using square wave voltammetry. Figure 4.5A shows the square wave voltammogram of

BPEP. The voltammogram exhibited oxidation peak at 1.10 V and reduction peak

at -1.68 V, vs SCE. Square wave voltammogarm of **BPEP-PT** shown in Figure

4.5B exhibited the above peaks and an additional oxidation peak at 0.72 V vs SCE

corresponding to the **PT/PT$^{•+}$** oxidation. It may be noted that linking **PT** to **BPEP**
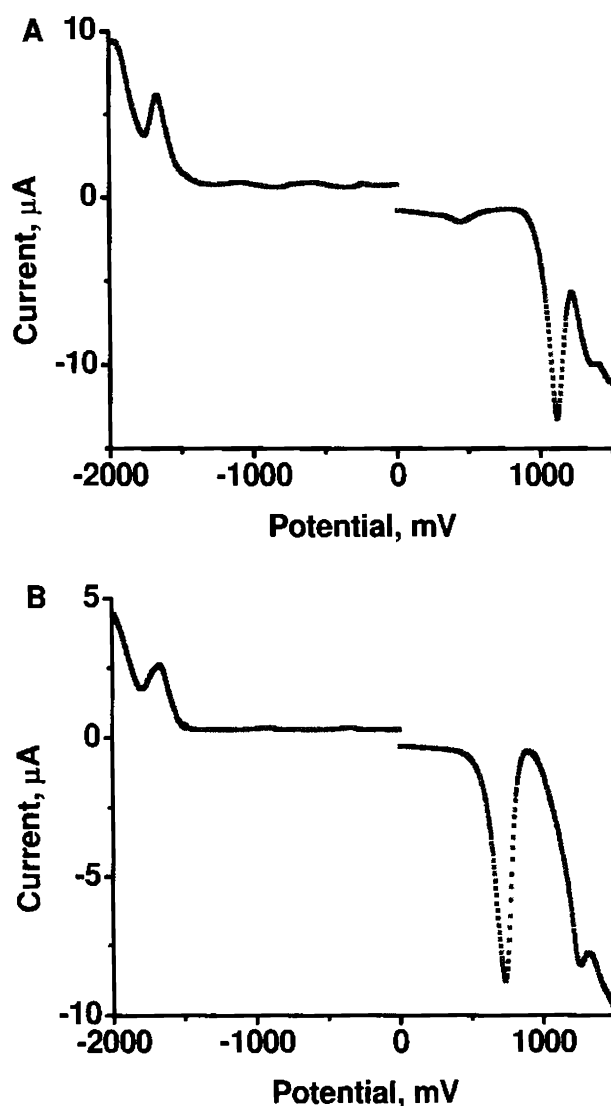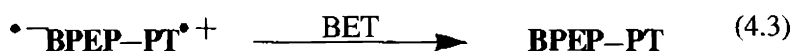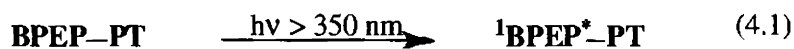
did not alter the redox properties of **BPEP**.

Figure 4.5. Squre wave voltammogram of (A) **BPEP** (B) **BPEP-PT** in DCM

Thus, in **BPEP-PT**, the lowest reduction is associated with the **BPEP** chromophore and the lowest oxidation is associated with **PT**. Hence in the **BPEP-PT** dyad, **BPEP** is the acceptor and **PT** is the donor. The free energy change associated with the electron transfer from **PT** to the $^1S^*$ state of **BPEP** can be calculated using the Weller equation[20] (see equation 2.1). Since the centre-to-centre distance d_{cc} is very large in **BPEP-PT**, the coulombic term in the equation was neglected and we obtained ΔG_{PET} = -0.46 eV. Thus PET is exergonic in **BPEP-PT** dyad and upon excitation to the lowest energy band we expect the following processes to take place.

$$\textbf{BPEP-PT} \xrightarrow{\text{hv} > 350 \text{ nm}} \, ^1\textbf{BPEP}^*\textbf{-PT} \qquad (4.1)$$

$$^1\textbf{BPEP}^*\textbf{-PT} \xrightarrow{\text{ET}} \, ^{\bullet-}\textbf{BPEP-PT}^{\bullet+} \qquad (4.2)$$

$$^{\bullet-}\textbf{BPEP-PT}^{\bullet+} \xrightarrow{\text{BET}} \textbf{BPEP-PT} \qquad (4.3)$$

As mentioned in Chapter 2, rate constant for the PET process (k_{PET}) can be calculated either from the fluorescence quantum yields (equation 2.5) or from the fluorescence lifetimes (equation 2.6). k_{PET} values were calculated using both equations and the values obtained were 6.38×10^9 s^{-1} and 5.1×10^9 s^{-1}, respectively (the fast decay component was used for this calculation). Values obtained using the two equations did not differ very much. Quantum yield for PET was calculated using the k_{et} values ($\Phi_{et} = k_{PET}\tau_1$) and we obtained value of 0.97 for

BPEP-PT, which indicated that PET is very efficient in this system (the average value of the k_{PET} was used for this calculation).

4.3.3. Picosecond flash photolysis studies

In order to gain a deeper understanding of the excited state processes, **BPEP** and **BPEP-PT** were subjected to picosecond flash photolysis in deaerated DCM solution. The transient absorption spectra obtained in the picosecond flash photolysis of **BPEP** in the 40 ps – 2.3 ns range are shown in Figure 4.6. The spectra taken at very short times after the laser flash showed absorption around 730 nm and bleaching below 500 nm. At longer times (1.5 ns – 2.3 ns), formation of a transient that absorbs in the entire visible region with a maximum at 690 nm is indicated. Inset of Figure 4.6 (A, B, C) show the ΔOD vs time profiles at 600, 690 and 730 nm. It can be seen that the 730 nm absorption exhibited a fast decay followed by a slow decay. The profile for the 690 nm absorption was complex initially, but showed a growth at later times. At 600 nm no decay or growth was observed in the 40 – 850 ps range, but a clear growth was observed thereafter.

We assign the 730 nm absorption to the $S_1 \rightarrow S_n$ absorption of **BPEP**. Note that in chapter 2 of this thesis, the transient absorption observed for **BPEA** in the femtosecond time scale was assigned to the $S_1 \rightarrow S_n$ absorption of **BPEA**. A probable candidate for the 690 nm absorption is the triplet state of **BPEP**. Such an assignment, however, is not supported by the experiment. If the 690 nm species is due to ^{3}**BPEP***, its formation should match the decay of the $S_1 \rightarrow S_n$ absorption at

730 nm. It is clear from insets of Figure 4.6 that this is not the case. The 690 nm species in fact is formed after an initial delay, which clearly indicates that this species did not form from the S_1 state of **BPEP** directly. Our conclusion is that data obtained from the picosecond absorption studies is insufficient to identify the 690 nm absorbing species.

Figure 4.6. Picosecond transient absorption spectra obtained in flash photolysis of **BPEP** in DCM. (a) 40ps, (b) 350 ps, (c) 500 ps, (d) 850 ps, (e) 1.5 ns and (f) 2.3 ns. Inset shows decay and growth of the transients at 730 nm, 690 nm and 600 nm

Figure 4.7 shows the transient absorption spectra obtained in the picosecond flash photolysis of **BPEP-PT**. At short time scales the absorption due to the 730 nm species (which we assign to the $S_1 \rightarrow S_n$ absorption of **BPEP**) is dominant. This absorption decays within the observation window with concomitant formation of new absorptions at 600 and 515 nm. Inset of Figure 4.7 show the decay at 730 nm

and matching growth at 600 nm, indicating that the 600 nm species is formed directly from the $^1S^*$ of **BPEP**. Since the number of data points was limited, the decay and growth rates could not be calculated accurately from the inset in Figure 4.7. Since the enhanced fluorescence decay in **BPEP-PT** is attributed to electron transfer from **PT** to ^{1}**BPEP*** (equation 4.2), the transient absorptions arising from the decay of the ^{1}**BPEP*** absorption can be attributed to products of this electron transfer reaction.
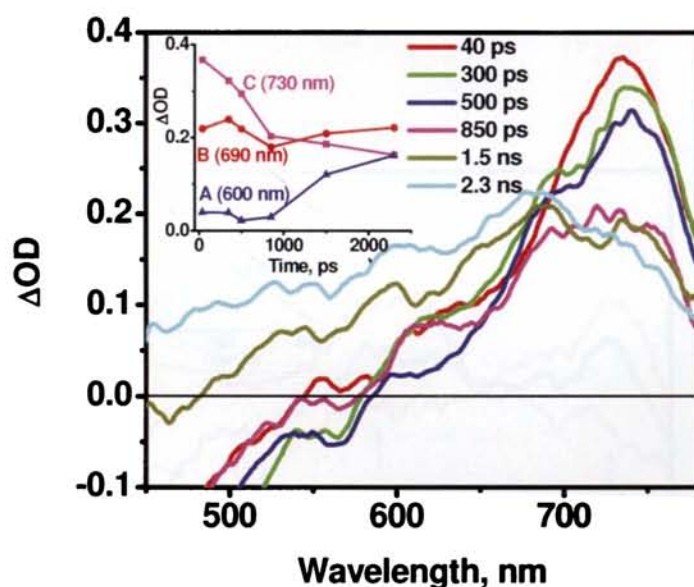

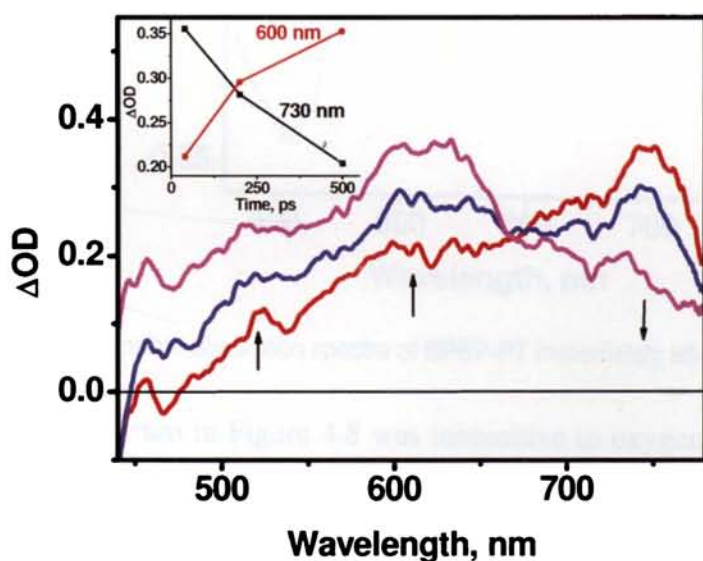**Figure 4.7.** Picosecond transient absorption spectra obtained in the flash photolysis of **BPEP-PT** in DCM. (a) 40 ps, (b) 200 ps, and (c) 500 ps. Inset shows decay of the transient at 730 nm and growth at 730 nm

4.3.4. Nanosecond flash photolysis studies

Nanosecond transient absorption studies were performed on both **BPEP** and **BPEP-PT** in deaerated DCM solution. Upon excitation using 355 nm (Nd-YAG,

3rd harmonic) light, **BPEP** exhibited a transient absorption with a maximum

around 690 nm as shown in Figure 4.8. This species appears to be the same as that

observed at longer time scales (850 ps -2.3 ns) in the picosecond flash photolysis

of **BPEP** (Figure 4.6).
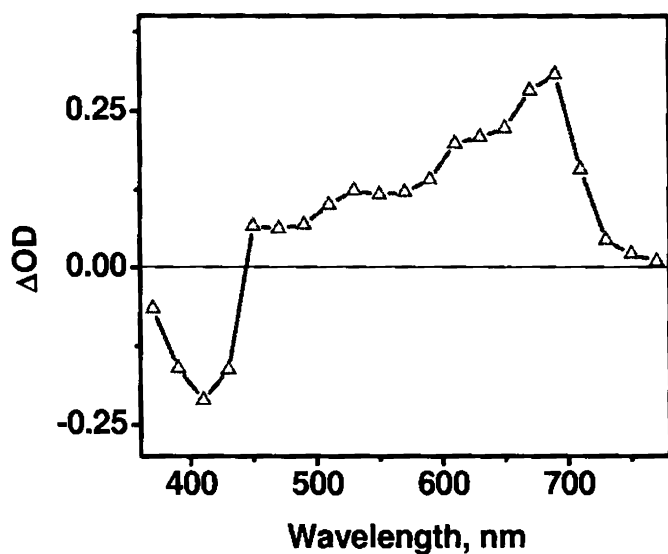
Figure 4.8. Transient absorption spectra of **BPEP-PT** immediately after the laser pulse

The transient spectrum in Figure 4.8 was insensitive to oxygen. Nanosecond laser

flash photolysis in the presence of oxygen also gave same spectra as shown in

Figure 4.8. Kinetic traces at 690 nm obtained under argon saturated and oxygen

saturated conditions are shown in Figure 4.9, and these are very similar. It is well

known that the transient absorptions due to triplet excited states will be quenched

by molecular oxygen. Since the transient absorption observed in the nanosecond

time scale is unaffected by oxygen, we can conclude that this absorption is not due

to ^{3}**BPEP***. One may also conclude that this absorption did not arise from a triplet precursor.
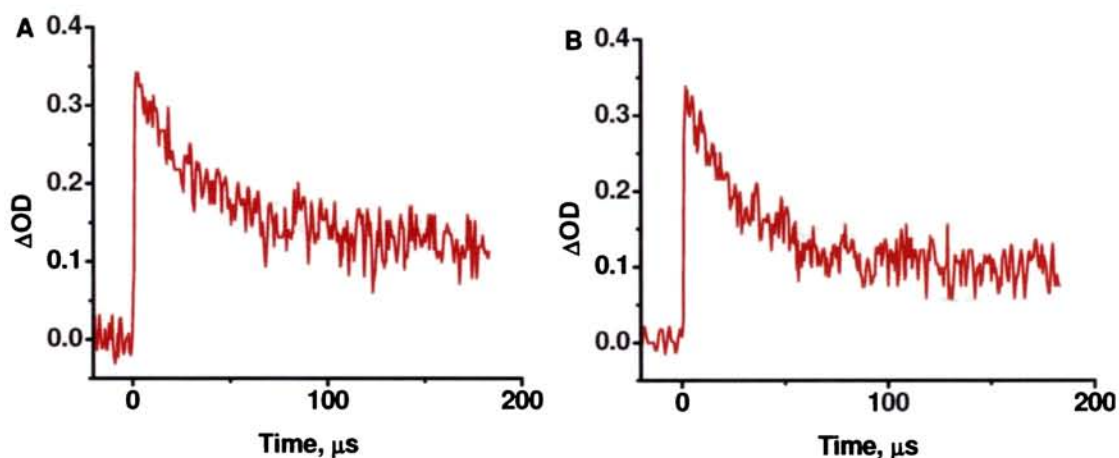
Figure 4.9. Kinetic traces at 690 nm in the (A) argon and in the (B) oxygen saturated condition

The kinetic traces shown in Figure 4.9 exhibited considerable amount of residual absorption indicating formation of stable products. We observed that continuous laser irradiation leads to decomposition of **BPEP**. We attribute the transient in Figure 4.8 to photoionization products of **BPEP**. It may be stated here that pyrene derivatives are known to undergo photoionisation.[21]

The fluorescence quantum yield of **BPEP** is very high at 93%. The maximum ISC yield would be 7% and hence good transient absorption attributable to ^{3}**BPEP*** was actually not expected upon direct excitation. The ^{3}**BPEP*** can in principle be obtained through sensitization experiments. We have tried to generate ^{3}**BPEP*** by energy transfer from the MLCT state of $[Ru(bpy)_3]^{2+}$. A solution of $[Ru(bpy)_3]$ $2PF_6$ in DCM was flash photolyzed in the presence of excess **BPEP**

using the 532 nm light from a Nd-YAG laser. Under the experimental conditions all the light is absorbed by $[Ru(bpy)_3]^{2+}$ (**BPEP** has no absorption at 532 nm) to form its MLCT triplet state which undergo energy transfer to **BPEP** to generate ^{3}**BPEP***. The triplet-triplet absorption spectrum of $Ru(bpy)_3$ is well characterized by a strong absorption around 370 nm, bleaching around 450 nm and emission from the MLCT state in the 600-750 nm region. In the presence of **BPEP** the above transient absorptions and bleaching disappear and the new spectrum shown in Figure 4.10 is obtained. The transient absorption exhibited maximum at 600 nm and decayed without leaving any residual absorption. Since the transient was formed from a triplet state, we assign it to ^{3}**BPEP***.
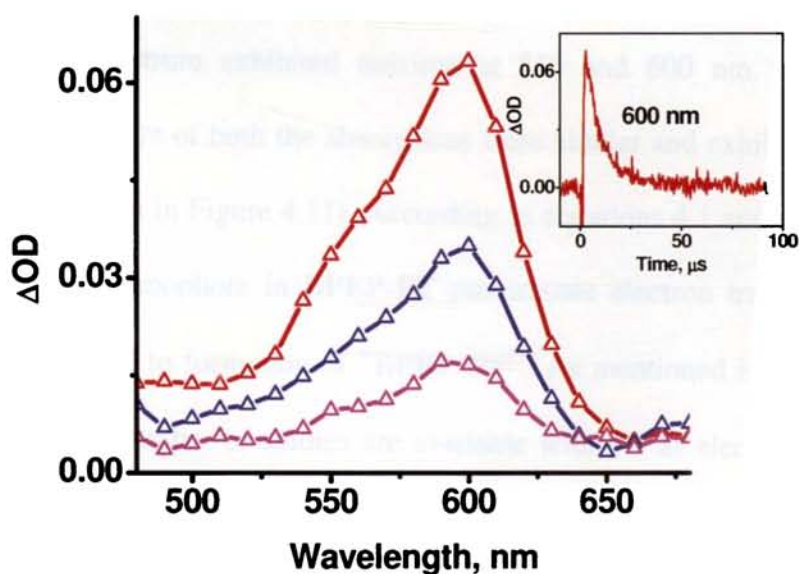

Figure 4.10. Transient absorption spectra obtained upon excitation of $[Ru(bpy)_3]$ $2PF_6$ in the presence of **BPEP** (a) 3 μs, (b) 8 μs and (c) 14 μs after the laser irradiation. Inset shows the kinetic trace at 600 nm

It may be noted that the transient absorption spectrum obtained in the

sensitization experiment (Figure 4.10) is different from the one obtained by direct

excitation of **BPEP** (Figure 4.8). The lifetimes of the transients were also different.

All these observations suggest that the transient species observed at nanosecond

time scale in the direct excitation of **BPEP** is not due to ^{3}**BPEP***. Therefore we

conclude that ISC to the triplet state is not a significant process in the photophysics

of **BPEP**. Since ^{3}**BPEP*** can be obtained readily by energy transfer from

^{3}[Ru(bpy)$_3$]*, energy of the ^{3}**BPEP*** state must be lower than that of ^{3}[Ru(bpy)$_3$]*

state. This puts an upper limit for the ^{3}**BPEP*** state at 2.1 eV.

BPEP-PT was also subjected to nanosecond flash photolysis in deaerated

DCM and the transient spectrum obtained is shown in Figure 4.11. The transient

absorption spectrum exhibited maxima at 515 and 600 nm. Under deaerated

conditions decays of both the absorptions were similar and exhibited a lifetime of

30 μs (see insets in Figure 4.11). According to equations 4.1 and 4.2, excitation of

the **BPEP** chromophore in **BPEP-PT** can initiate electron transfer from **PT** to

^{1}**BPEP*** leading to formation of $^•$**BPEP-PT**$^{•+}$. As mentioned in Chapter 2 of this

thesis a large number of studies are available with **PT** as electron donor and the

PT$^{•+}$ is known to have absorption maximum around 515 nm region.[22] The **BPEP**$^{•-}$

is not known in the literature. To the best of our knowledge, there are no reports on

the photochemical or electrochemical reduction of bis(phenylethynyl)pyrene in the

literature. Our attempts to generate **BPEP**$^{•-}$ through spectroelectrochemistry were

also not successful. Since electron transfer from **PT** to ^{1}**BPEP*** is implicated and

the 515 nm absorption can be assigned to **PT**$^{\bullet+}$, the 600 nm absorption is assigned

to **BPEP**$^{\bullet-}$. In fact picosecond transient absorption studies also indicated formation

of transient absorptions at 515 and 600 nm directly from the singlet excited state of

the **BPEP** moiety. The results indicated that the same transients are seen in the

picosecond – microsecond time scale. These transients are very long-lived ($\tau = 30$

μs) and decay by BET process, for which we obtained a rate constant ($k_{BET} = 1/\tau$)

of 3.34×10^4 s^{-1}.
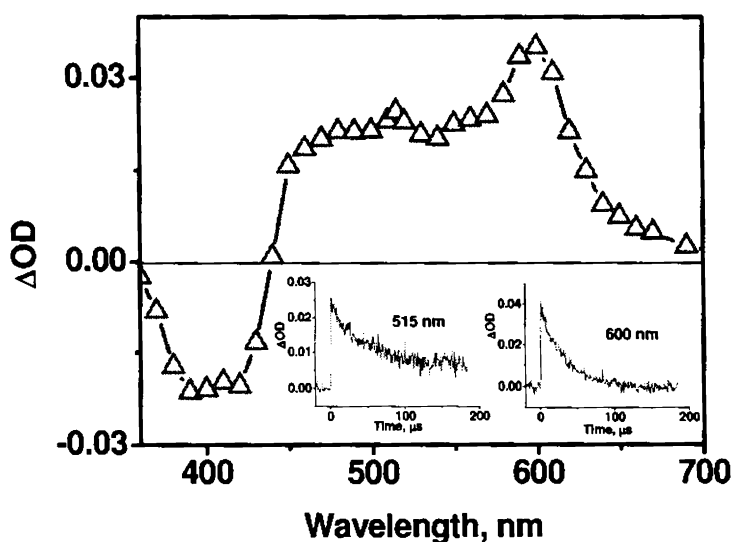

Figure 4.11. Transient absorption spectra of **BPEP-PT** immediately after the laser pulse. The insets show decay profiles at 515 and 600 nm

In order to further confirm the assignment of the transient absorptions, we

have carried out the nanosecond flash photolysis of **BPEP-PT** in the presence of

oxygen. The transient absorption spectra along with the kinetic traces obtained at

515 and 600 nm are shown in Figure 4.12. It can be seen that the decay behaviors

of the two transients are very different in the presence of oxygen. The decay of the

515 nm transient has become somewhat slower and the 600 nm transient

disappeared completely in the presence of oxygen. This result suggested that the

absorptions at 515 and 600 nm are due to different species. It is well known that

radical anions are quenched efficiently by oxygen whereas radical cations are

relatively unaffected. Disappearance of the 600 nm transient in the presence of

oxygen confirms our assignment of this species to a radical anion.

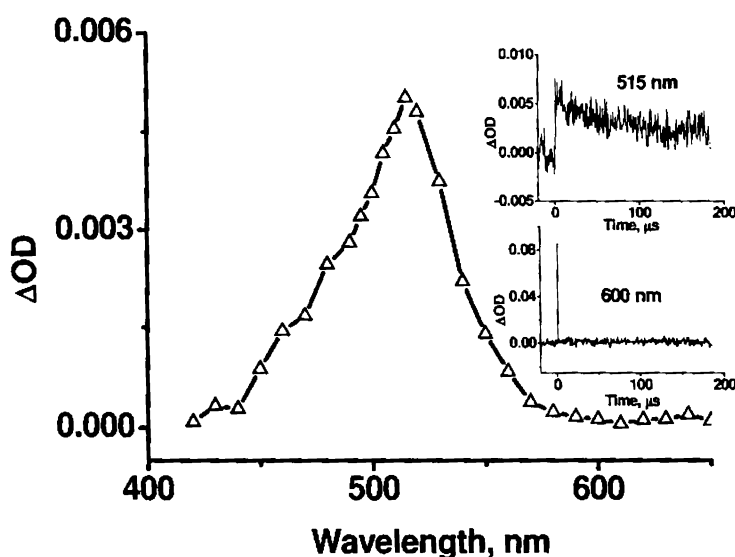**Figure 4.12.** Transient absorption spectra of **BPEP-PT** under oxygen saturated condition immediately after the laser pulse. The insets show decay profiles

It is to be mentioned here that laser irradiation in the absence of oxygen did

not lead to any decomposition in **BPEP-PT**. Absorption spectra of **BPEP-PT** (3

mL, 10^{-4} M) was taken before and after laser irradiation (100 laser shots) and

identical spectra were obtained. This is in contrast to the model **BPEP** which exhibited significant decomposition under these conditions.

In order to further confirm the transient absorptions in Figure 4.11 to the CS state of the **BPEP-PT** dyad, we have carried out secondary electron transfer experiments. As shown in Chapter 2, when the CS state is long-lived, they can be involved in exergonic electron transfer reactions with better donors or acceptors. In Chapter 2 we showed that the CS state of **BPEA-PT** could undergo secondary electron transfer with tris(4-methoxyphenyl)amine (**TMPA**), leading to the formation of **TMPA**$^{•+}$. A similar experiment was carried out in the case of **BPEP-PT**. A solution of **BPEP-PT** was flash photolyzed in the presence of **TMPA** in DCM solution and the transient spectra obtained at different times following the laser flash are shown in Figure 4.13. The spectrum at short time scales is similar to that in Figure 4.11 and is assigned to **$^{•-}$BPEP-PT$^{•+}$**. At longer times the absorption due to **PT**$^{•+}$ at 515 nm decays with concomitant formation of absorption at 715 nm, which is assigned to **TMPA**$^{•+}$.[23] The inset shows the decay of the transient at 515 nm and formation of absorption at 720 nm. Since **TMPA** is a better electron donor (E_{ox} = 0.57 V vs SCE in DCM) compared to **PT** (E_{ox} = 0.75 V vs SCE), secondary electron transfer as shown in equation 4.4 is expected to take place. From the oxidation potentials of the **PT** and **TMPA** moieties, ΔG^0 for reaction 4.4 was obtained as -0.18 eV.

$$\bullet^{-}BPEA-PT^{\bullet+} + TMPA \xrightarrow{\quad ET \quad} \bullet^{-}BPEA-PT + TMPA^{\bullet+} \qquad (4.4)$$

This experiment further confirmed the assignment of the transients in Figure 4.11 to the long-lived CS state of **BPEP-PT**.
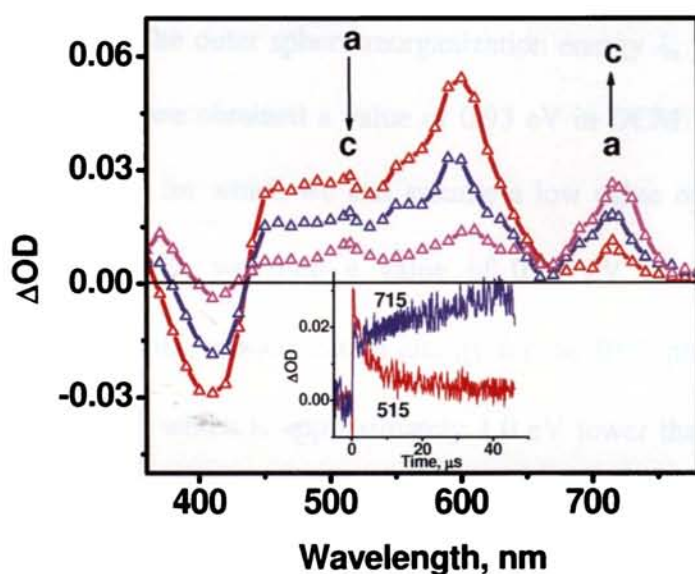
Figure 4.13. Transient absorption spectra of **BPEP-PT** in the presence of **TMPA** (2×10^{-4} M) in deaerated DCM solution, (a) 1.5, (b) 4, and (c) 8 μs after excitation

In **BPEP-PT** dyad, the forward electron transfer rate constant, $k_{PET} = 5.74 \times 10^9$ s^{-1}. The BET rate constant obtained from nanosecond flash photolysis studies is 3.34×10^4 s^{-1}. Thus $k_{PET}/k_{BET} = 2 \times 10^5$, which is very large compared to most of the reported systems. Since $k_{PET}/k_{BET} \gg 5000$, and since the same transients are observed in the entire picosecond – microsecond time range, **BPEP-PT** qualifies to be known as a dyad with 'unusually long-lived' CS state as per the criteria put forward by Harriman and Verhoeven.[24]

We attribute the long lifetime of the CS state to inverted region effects. This aspect was discussed in detail in previous chapters of this thesis. The inverted region effects operate when $-\Delta G^0 \gg \lambda$. For the BET reaction between **BPEP•‾** and **PT•+** the ΔG^0 value is highly negative at -2.4 eV. The reorganization energy λ is the sum of λ_o and λ_i. The outer sphere reorganization energy λ_o was calculated as per equation 2.10 and we obtained a value of 0.93 eV in DCM. **BPEP** is a very rigid organic molecule for which we can assume a low value of $\lambda_i = 0.1$ eV. As mentioned in Chapter 2, we used a value of 0.27 eV as λ_i for **PT→PT•+** oxidation.[25] Thus the total reorganization energy for the BET process in **•‾BPEP-PT•+** would be 1.3 eV, which is approximately 1.0 eV lower than $-\Delta G^0$, pushing the system into the deep inverted region.

The energy level diagram of **BPEP-PT**, constructed on the basis of available information is given in Scheme 4.4. The S_1 state in **BPEP-PT** is placed at 2.86 eV, based on the positions of the absorption and emission bands. Based on electrochemical studies energy of the CS state in **BPEP-PT** is placed at 2.4 eV. Based on literature reports the triplet energy of **PT** in non-polar solvents is placed at 2.62 eV.[26] For **BPEP** the triplet energy level (E_T) is not known in the literature. Our attempts to obtain a phosphorescence spectrum for **BPEP** also failed. We generated the **BPEP** triplet by sensitization experiments using $[Ru(bpy)_3]^{2+}$, which indicated that the triplet energy of **BPEP** is lower than that of $[Ru(bpy)_3]^{2+}$. Energy

of the MLCT state of $[Ru(bpy)_3]^{2+}$ is 2.1 eV.[26] In Scheme 4.4 we placed ^{3}**BPEP*** at

this value, which is a higher limit.

Based on Scheme 4.4, the photo processes taking place in **BPEP-PT** can be

summarized as follows. Excitation of the **BPEP** chromophore leads to ^{1}**BPEP***-

PT, where the excitation is localized on **BPEP**. The excited chromophore can

undergo fluorescence decay to the ground state or accept an electron from **PT** to

generate the ^{1}CS state, **˙BPEP-PT˙⁺**. Energy transfer from ^{1}**BPEP***-**PT** to **BPEP-**

^{1}**PT*** will be endergonic and hence ruled out. Although **BPEP-**^{3}**PT*** lies 0.24 eV

lower than ^{1}**BPEP***-**PT**, formation of **BPEP-**^{3}**PT*** is spin-forbidden. Our studies

showed that ^{1}**BPEP*** do not undergo ISC to ^{3}**BPEP***. Hence we do not expect

^{1}**BPEP***-**PT** also to undergo ISC to ^{3}**BPEP***-**PT**. The CS state, **˙BPEP-PT˙⁺**, thus

generated has two options. It can undergo a spin-allowed BET to generate either

the ground singlet state (indicated by green arrow) or a spin-forbidden BET to

generate ^{3}**BPEP***-**PT** (indicated by red arrow). If the latter process is happening,

then it would be possible to observe the ^{3}**BPEP*** in the nanosecond flash photolysis

experiments. Since ^{3}**BPEP*** is not observed this pathway is ruled out. All these

observations support BET to the ground state. As stated previously, this process is

slow because of the inverted region effects.
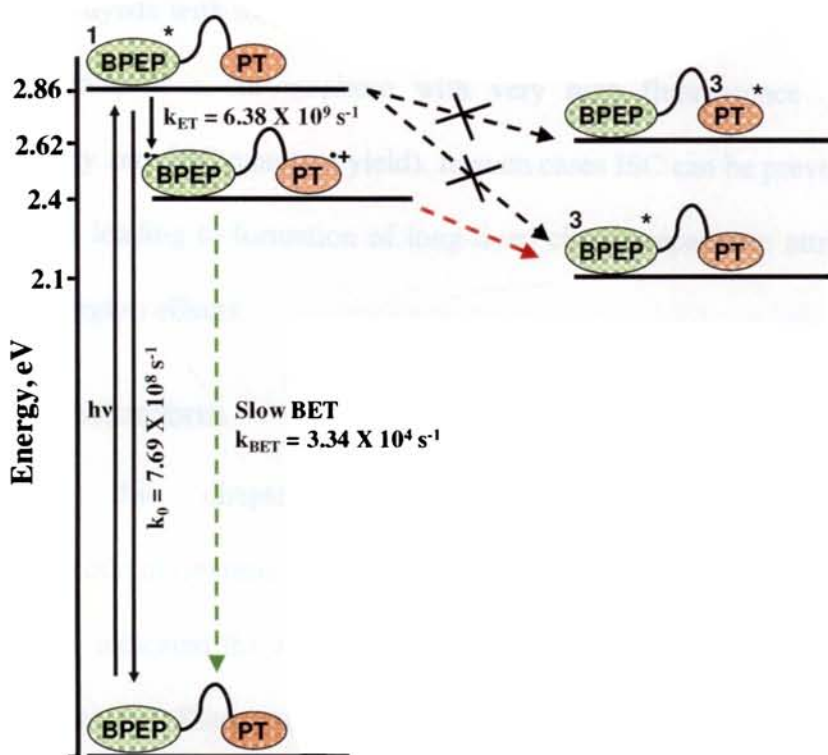
Scheme 4.4. Schematic representation of various photophysical processes in **BPEP-PT**

Since electron transfer occurs in the singlet manifold, the CS state produced is present in the singlet state, $^1(^\bullet\text{BPEP-PT}^{\bullet+})$. This state can also undergo ISC to $^3(^\bullet\text{BPEP-PT}^{\bullet+})$. The singlet – triplet splitting within radical ion pairs is given by the magnitude of the spin-spin exchange interaction $2J$, which actually is a very small value. If the $^3(^\bullet\text{BPEP-PT}^{\bullet+})$ state is actually formed, it will also be placed above the $^3\text{BPEP}^*\text{-PT}$ level. In such a situation, $^3\text{BPEP}^*\text{-PT}$ will be formed easily from $^3(^\bullet\text{BPEP-PT}^{\bullet+})$. Since triplet state of **BPEP** was not detected at all, assignment of the long-lived CS state to $^3(^\bullet\text{BPEP-PT}^{\bullet+})$ can also be ruled out. This conclusion overwhelmingly supports our proposal (Scheme 4.1) for the

design of dyads with long CS state lifetimes. Most crucial aspect in the design is the selection of a chromophore with very high fluorescence quantum yield (practically zero ISC quantum yield). In such cases ISC can be prevented in the CS state also, leading to formation of long-lived charge separation attributable to the inverted region effects.

4.4. Conclusions

In this chapter we report the PET processes in the bis(phenylethynyl)pyrene-phenothaiazine dyad, **BPEP-PT**. Absorption spectra of **BPEP-PT** indicated the absence of any ground state interactions between **BPEP** and **PT** moieties. Fluorescence of the **BPEP** moiety is highly quenched in the dyad due to facile electron transfer from the **PT** unit. The rate constants and quantum yields of the PET process were determined from the steady state and time resolved fluorescence studies. Picosecond and nanosecond transient absorption studies suggested formation of a long-lived CS state in **BPEP-PT**. Oxygen quenching studies and secondary electron transfer experiments confirmed the assignment of the long-lived transient to the CS state. Based on available data a scheme summarizing the dynamics and energetics of the probable photophysical processes in the dyad was constructed. Based on the data obtained the long-lifetime of the CS state in **BPEP-PT** was attributed to inverted region effects. The results supports the proposal outlined in this chapter for the design of long-lived CS states.

4.5. Experimental section

4.5.1. General

Melting points were determined on a Mel-Temp II melting point apparatus and are uncorrected. Proton NMR data were obtained from either a 300 MHz Bruker Avance DPX spectrometer or a 500 MHz Bruker Avance DPX spectrometer .^{13}CNMR spectra were recorded using a 500 MHz Bruker Avance DPX spectrometer. FT-IR spectra were recorded on a Shimadzu IR Prestige 21 spectrometer. High-resolution mass spectra were obtained by using a JOEL JMS600 mass spectrometer. Absorption spectra were obtained using a Shimadzu 3101PC UV/Vis-NIR scanning spectrophotometer. Steady state fluorescence experiments were performed with a SPEX Fluorolog F112X spectrofluorimeter by using optically dilute solutions. The fluorescence quantum yields in dichloromethane were determined with relative method employing an optically matched solution of 9,10-diphenylanthracene in ethanol as reference ($\Phi_R = 0.95$).[27] The following equation was used,

$$\Phi_F = \Phi_R \ \frac{A \ OD_R \ n^2}{A_R \ OD \ n_R^2} \qquad (4.5)$$

where, the subscript R refers to the reference, OD is the optical density at the excitation wavelength (OD $\approx$ 0.1 at 390 nm for both reference and standard), n is the refractive index of the solvent and A is the area under the fluorescence spectrum. Electrochemical experiments were performed by using a BAS 50W

voltammetric analyser. Solutions of the compounds (1×10^{-3} M) in dichloromethane containing 0.1 M tetra-*n*-butylammonium hexafluorophosphate were thoroughly deaerated and used for CV experiments. Time-resolved fluorescence experiments were performed by using an IBH picosecond single-photon counting system employing a 401 nm Nano-LED excitation source and a Hamamatsu C4878-02 micro channel plate (MCP) detector. Nanosecond laser flash photolysis experiments were either performed by using an Applied Photophysics Model LKS-20 laser kinetic spectrometer by using the third harmonic (355 nm) from an GCR-12 series Quanta Ray Nd:YAG laser or by using an Applied Photophysics Model LKS-60 laser kinetic spectrometer by using the third harmonic (355 nm) from an INDI-40-10-HG Quanta Ray Nd:YAG laser. The analysing and laser beams were fixed at right angles to each other. Solutions for laser flash photolysis studies were deaerated by purging with argon for 20 min before experiments. Picosecond transient absorption experiments were carried out using Mode-Locked Nd:YAG laser system PY61C-10, (532 nm, 5 mj/pulse, FWHM 35 ps, 10 Hz repetition rate). The white light probe was generated by focusing fundamental laser output (1064 nm) on to a 10 mm quartz cuvette containing 10 ml water and 10 ml D_2O mixture. The optical delay line provided a pump beam time window of 2.45 ns and step resolution of 3.33 ps. The scattered 532 nm laser beam was filtered using band pass filter. The reflected probe light was focused on a 200 μm core fibre connected to an Ocean Optics SD2000 UV-

Vis CCD spectrophotometer (400 nm to 800 nm). Typically 100 excitation pulses were averaged to obtain the transient absorption at the set delay time. All the experiments were conducted at room temperature.

4.5.2. Synthesis and characterization

Synthesis of 2: 4-iodoanisole (5g, 21.36 mmol), dichlorobis(triphenylphosphine) palladium(II) (600 mg, 0.85 mmol) and copper(I) iodide (160 mg, 0.85 mmol) were dissolved in dry THF (50 mL). Dry diisopropylamine (10 mL) and trimethylsilylacetylene (3.15 g, 32.1 mmol) were added under argon and the mixture stirred for 24 h. Solvent was removed and residue was purified by column chromatography on alumina using chloroform/hexane (1:9) mixture to get **2** (3.97 g, 91%). Mass (GC-MS): calcd. for $C_{12}H_{16}OSi$: 204; found: 204. ^{1}H NMR (CDCl$_3$, 300 MHz) δ: 0.27 (s, 9H), 3.58 (s, 3H), 6.62 (d, 2H), 7.19 (d, 2H).

Synthesis of 3: **2** (2 g, 9.8 mmol) was dissolved in THF (20 mL). The solution was cooled to 0 °C and TBAF (1M in THF, 12 mL) added. The mixture was then stirred for 2 h at RT, poured into ice-cold water and extracted with dichloromethane. The solvent was removed and residue was purified over alumina column using chloroform/hexane (1:9) to obtain **3** (1.1 g, 86%). Mass (GC-MS): calcd. for C_9H_8O: 132; found: 132. ^{1}H NMR (CDCl$_3$, 300 MHz) δ: 2.99 (s, 1H), 3.76 (s, 3H), 6.83 (d, 2 H), 7.43 (d, 2H).

Synthesis of BPEP: To an argon degassed RB flask, 1,6-dibromoanthracene (500 mg, 1.38 mmol), dichlorobis(triphenylphosphine)palladium(II) (42 mg, 0.06

mmol), copper(I) iodide (12 mg, 0.06 mmol), dry toluene (35 mL) and dry

diisopropylamine (10 mL) were added. **3** (395 mg, 3.12 mmol) in dry toluene (10

mL) was added and the reaction mixture stirred for 24 h at 70 °C under argon.

Solvent was removed and the residue obtained was purified by column

chromatography over silica gel using chloroform/hexane (3:7) to obtain **BPEP**,

(435 mg, 68%). mp 261-262 °C. IR (KBr) v_{max}: 530, 631, 723, 812, 831, 852,

1028, 1105, 1165, 1178, 1250, 1290, 1447, 1460, 1510, 1597, 2199, 2549, 2839,

3005 cm^{-1}. ^{1}H NMR (CDCl$_3$, 500 MHz) δ: 3.88 (s, 6H), 6.97 (d, 4H), 7.66 (d, 4H),

8.16 (m, 4H), 8.20 (d, 2H), 8.67 d, 2H). ^{13}C NMR (CDCl$_3$, 125 MHz) δ: 55.42,

92.42, 102.57, 114.22, 115.21, 118.44, 126.52, 127.52, 131.97, 133.17, 157.94.

FAB-MS (M$^+$) calcd. for C$_{34}$H$_{22}$O$_2$: 462.54; found: 462.38.

Synthesis of BPEP-PT: To an argon degassed RB flask, 1, 6-dibromoanthracene

(500 mg, 1.38 mmol), dichlorobis(triphenylphosphine)palladium(II) (42 mg, 0.06

mmol), copper(I) iodide (12 mg, 0.06 mmol), dry toluene (40 mL) and dry

diisopropylamine (10 mL) were added. A solution of Compound **8** (1.15 g, 3.1

mmol) in dry toluene (15 mL) was added and the mixture was refluxed for 24 h at

70 °C under argon. The solvent was removed and residue was purified by column

chromatography over silica using chloroform/hexane (1:1) to obtain **BPEP-PT**

(645 mg, 51%). Decomposed at 215 °C. IR (KBr) v_{max}: 530, 741, 835, 851, 960,

1059, 1238, 1248, 1288, 1375, 1465, 1510, 1597, 2201, 2965 cm^{-1}. ^{1}H NMR

(CDCl$_3$, 500 MHz) δ: 2.31 (m, 4 H), 4.15 (m, 8 H), 6.89 (d, 2 H), 6.93 (m, 8 H),

7.17 (m, 8 H), 7.60 (d, 4 H), 8.15 (m, 6 H), 8.66 (d, 2 H). ^{13}C NMR (CDCl$_3$, 125 MHz) δ: 26.79, 43.88, 65.42, 92.41, 102.59, 114.27, 115.14, 118.43, 122.77, 125.32, 126.51, 127.19, 127.50, 129.88, 132.00, 133.22, 146.16, 157.98. FAB-MS (M$^+$) calcd. for C$_{62}$H$_{44}$N$_2$O$_2$S$_2$ = 912.28; found: 912.29.

4.6. References

1. (a) Marcus, R. A.; Sutin, N. *Biochim. Biophys. Acta* **1985**, *811*, 265-322 (b) Marcus, R. A. *Angew. Chem., Int. Ed.* **1993**, *32*, 1111-1121.

2. (a) Fukuzumi, S. *Bull. Chem. Soc. Jpn.* **2006**, *79*, 177-195. (b) Fukuzumi, S. *Phys. Chem. Chem. Phys.* **2008**, *10*, 2283-2297.

3. Verhoeven, J. W.; van Ramesdonk, H. J.; Groeneveld, M. M.; Benniston, A. C.; Harriman, A. *ChemPhysChem* **2005**, *6*, 2251-2260. (b) Verhoeven, J. W. *J. Photochem. Photobiol. C* **2006**, *7*, 40-60.

4. (a) Smit, K. J.; Warman, J. M.; de Haas, M. P.; Paddan-Row, M. N.; Oliver, A. M. *Chem. Phys. Lett.* **1988**, *152*, 177-182. (b) Liang, N.; Miller, J. R.; Closs, G. L. *J. Am. Chem. Soc.* **1990**, *112*, 5353-5354.

5. Bazyl, O. K.; Majer, G. V.; Kopylova, T. N.; Danilova, V. I.; Chajkovsky, V. K. *Zh. Prikl. Spektroskopii* **1981**, *35*, 261-267.

6. (a) Hanhela, P. J.; Paul, D. B. *Aust. J. Chem.* **1981**, *34*, 1669-1685. (b) Hanhela, P. J.; Paul, D. B. *Aust. J. Chem.* **1981**, *34*, 1687-1700. (c) Hanhela,

P. J.; Paul, D. B. *Aust. J. Chem.* **1981**, *34*, 1701-1717. (d) Hanhela, P. J.; Paul, D. B. *Aust. J. Chem.* **1984**, *37*, 553-559.

7.   Bazyl, O. K.; Majer, G. V.; Kopylova, T. N.; Danilova, V. I. *Zh. Prikl. Spektroskopii* **1982**, *37*, 80-86.

8.   (a) Devadoss, C.; Bharathi, P.; Moore, J. S. *J. Am. Chem. Soc.* **1996**, *118*, 9635-9644. (b) Pan, Y.; Lu, M.; Peng, Z.; Melinger, J. S. *J. Org. Chem.* **2003**, *68*, 6952-6958.

9.   (a) Otsubo, T.; Aso, Y.; Takamiya. K. *J. Mater. Chem.* **2002**, *12*, 2565-2575. (b) Ohshita, J.; Yoshimoto, K.; Tada, Y.; Harima, Y.; Kunai, A.; Kunugi, Y.; Yamashita, K. *J. Organomet. Chem.* **2003**, *678*, 33-38. Jia, W.-L.; McCormick, T.; Liu, Q.-D.; Fukutani, H.; Motala, M.; Wang, R.-Y.; Tao, Y.; Wang, S. *J. Mater. Chem.* **2004**, *14*, 3344-3350. (d) Tang, C.; Liu, F.; Xia, Y.-J.; Lin, J.; Xie, L.-H.; Zhong, G.-Y.; Fan, Q.-L.; Huang, W. *Org. Electron.* **2006**, *7*, 155-162.

10. (a) Paris, P. L.; Langenhan, J. M.; Kool, E. T. *Nucleic Acids Res.* **1998**, *26*, 3789-3793. (b) Masuko, M.; Ohtani, H.; Ebata, K.; Shimadzu, A. *Nucleic Acids Res.* **1998**, *26*, 5409-5416. (c) Yamana, K.; Iwai, T.; Ohtani, Y.; Sato, S.; Nakamura, M.; Nakano, H. *Bioconjugate Chem.* **2002**, *13*, 1266-1273. (d) Okamoto, A.; Kanatani, K.; Saito, I. *J. Am. Chem. Soc.* **2004**, *126*, 4820-4827. (e) Fujimoto, K.; Shimizu, H.; Inouye, M. *J. Org. Chem.* **2004**, *69*, 3271-3275

11. (a) Han, M. K.; Lin, P.; Paek, D.; Harvey, J. J.; Fuior, E.; Knutson, J. R. *Biochemistry* **2002**, *41*, 3468-3476. (b) West, J. M.; Tsuruta, H.; Kantrowitz, E. R. *J. Biol. Chem.* **2004**, *279*, 945-951. (c) Drury, J.; Narayanaswami, V. *J. Biol. Chem.* **2005**, *280*, 14605-14610. (d) Yang, C. J.; Jockusch, S.; Vicens, M.; Turro, N. J.; Tan, W. *Proc. Natl. Acad. Sci. U.S.A.* **2005**, *102*, 17278-17283. (e) Maeda, H.; Maeda, T.; Mizuno, K.; Fujimoto, K.; Shimizu, H.; Inouye, M. *Chem. Eur. J.* **2006**, *12*, 824-831.

12. Valeur, B. *Molecular Fluorescence*; Wiley-VCH: Weinheim, 2002; pp 46-48.

13. (a) Kalyanasundaram, K.; Thomas, J. K. *J. Am. Chem. Soc.* **1977**, *99*, 2039-2044. (b) Kalyanasundaram, K.; Thomas, J. K. *J. Phys. Chem.* **1977**, *81*, 2176-2180. (c) Kusumoto, Y.; Takeshita, Y.; Kurawaki, J.; Satake, I. *Chem. Lett.* **1997**, 349-350. (d) Oton, J. M.; Acuna, A. U. *J. Photochem.* **1980**, *14*, 341-343. (e) Silva, M. A. D. R.; da Silva, D. C.; Machado, V. G.; Longhinotti, E.; Frescura, V. L. A. *J. Phys. Chem. A* **2002**, *106*, 8820-8826.

14. (a) Malakhov, A. D.; Skorobogatyi, M. V.; Prokhorenko, I. A.; Gontarev, S. V.; Kozhich, D. T.; Stetsenko, D. A.; Stepanova, I. A.; Shenkarev, Z. O.; Berlin, Y. A.; Korshun, V. A. *Eur. J. Org. Chem.* **2004**, 1298-1307. (b) Maeda, H.; Maeda, T.; Mizuno, K.; Fujimoto, K.; Shimizu, H.; Inouye, M. *Chem. Eur. J.* **2006**, *12*, 824 – 831.

15. Diring, S.; Camerel, F.; Donnio, B.; Dintzer, T.; Toffanin, S.; Capelli, R.; Muccini, M.; Ziessel R. *J. Am. Chem. Soc.* **2009**, *131*, 18177-18185.

16. Oh, J. W.; Lee, Y. O.; Kim, T. H.; Ko, K. C.; Lee, J. Y. Kim, H.; Kim, J. S. *Angew. Chem. Int. Ed.* **2008**, *47*, 1-4.

17. Kim, H. M.; Lee, Y. O.; Lim, C. S.; Kim, J. S.; Cho, B. R. *J. Org. Chem.* **2008**, *73*, 5127 – 5130.

18. Astakhova, I. V.; Korshun, V. A.; Wengel J. *Chem. Eur. J.* **2008**, *14*, 11010-11026.

19. Shinmori, H.; Furukawa, H.; Fujimoto, K.; Shimizu, H.; Inouye, M.; Takeuchi, T. *Chem. Lett.* **2009**, *38*, 84-85.

20. Rehm, D.; Weller, A. *Ber. Bunsen-Ges. Phys. Chem.* **1969**, *73*, 834-839.

21. (a) Grellmann, K. H.; Watkins, A. R. *J. Am. Chem. Soc.* **1973**, *95*, 983-985.
    (b) Watkins, A. R. *J. Phys. Chem.* **1976**, *80*, 713-717.

22. (a) Moroi, M.; Braun, A. M.; Grätzel, M. *J. Am. Chem. Soc.* **1979**, *101*, 567-572. (b) Danielson, E.; Elliott, C. M.; Merkert, J. W.; Meyer, T. J. *J. Am. Chem. Soc.* **1987**, *109*, 2519-2520. (c) Chen, P.; Duesing, R.; Graff, D. K.; Meyer, T. J. *J. Phys. Chem.* **1991**, *95*, 5850-5858. (d) Klumpp, T.; Linsenmann, M.; Larson, S. L.; Limoges, B. R.; Bürssner, D.; Krissinel, E. B.; Elliott, C. M.; Steiner, U. E. *J. Am. Chem. Soc.* **1999**, *121*, 1076-1087. (e) Ajayakumar, G.; Gopidas, K. R. *Photochem. Photobiol. Sci.* **2008**, *7*, 826-833.

23. Gould, I. R.; Ege, D.; Moser, J. E.; Farid, S. *J. Am. Chem. Soc.* **1990**, *112*, 4290-4301.

24. van Ramesdonk, H. J.; Bakker, B. H.; Groeneveld, M. M.; Verhoeven, J. W.; Allen, B. D.; Rostron, J. P.; Harriman, A. *J. Phys. Chem. A* **2006**, *110*, 13145-13150.

25. Borowicz, P.; Herbich, J.; Kapturkiewicz, A.; Opallo, M.; Nowacki, J. *Chem. Phys.* **1999**, *249*, 49-62.

26. Murov, S. L.; Carmichael, I.; Hug, G. L. In *Handbook of Photochemistry*, 2nd ed.; Marcel Dekker: New York, 1993.

27. Morris, J. V.; Mahaney, M. A.; Huber, J. R. *J. Phys. Chem.* **1976**, *80*, 969-974.

List of Publications

1. Long-lived Photoinduced Charge Separation in 9,10(Bisphenylethynyl) anthracene – Phenothiazine Dyads.
   Suneesh, C. V.; Gopidas, K. R. *J. Phys. Chem. C* **2009**, *113*, 1606-1614.

2. Generation of Triarylamine Radical Cations Through Reaction of Triarylamines with Cu(II) in Acetonitrile. A Kinetic Investigation.
   Sreenath, K.; **Suneesh, C. V.**; Gopidas, K. R.; Flowers, R. A. II *J. Phys. Chem. A* **2009**, *113*, 6477-6483.

3. Cu(II)-Mediated Generation of Triarylamine Radical Cations and Their Dimerization. An Easy Route to Tetraarylbenzidines.
   Sreenath, K.; **Suneesh, C. V.**; Ratheesh Kumar, V. K.; Gopidas, K. R. *J. Org. Chem.* **2008**, *73*, 3245-3251.

Papers presented at conferences

1. Long-Lived Photoinduced Charge Separation in 9,10(Bisphenylethynyl) anthracene – Phenothiazine Dyads.
   Suneesh, C. V.; Gopidas, K. R. in the *National Symposium on Radiation and Photochemistry*, Kumaun University, Nainital, India, 2009, March 12-14 **(Adjudged best poster)**.

2. Generation of Aromatic amine Radical Cations by Reaction of Aromatic amines with Cu^{2+}: Kinetic and Spectroscopic Studies and Synthetic Applications.
   Sreenath, K.; **Suneesh, C. V.**; Gopidas, K. R. in the *11th CRSI National Symposium in Chemistry*, National Chemical Laboratory, Pune, India, 2009, February. 5-8.